Environment Canada Environnement Canada
0050393J DEST PVM EXCH COPY 03
TP 360 E5613
VOL ISS 147
ENFOR PROJECT C

ENFOR Project C-147

Ultrapyrolysis of Cellulose and Wood Components

by

The University of Western Ontario

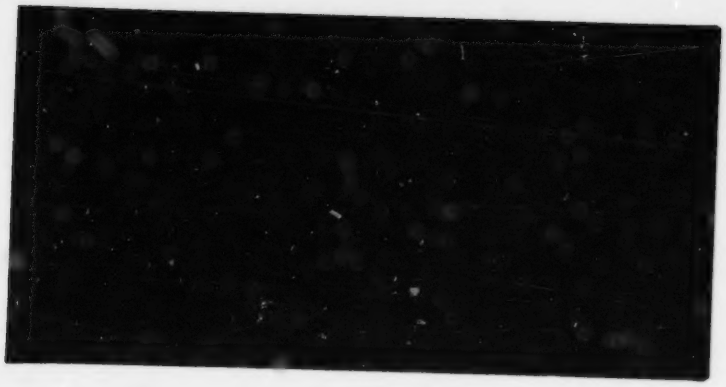

Contractor's Final Report 1/
DSS Contract 47SS.KL229-0-4118

ENFOR Project C-147

Ultrapyrolysis of Cellulose and Wood Components

by

The University of Western Ontario

Contractor: The University of Western Ontario
Faculty of Engineering Science
London, Ontario
N6A 5B9

Science Authority:

Dr. D.P.C. Fung
CANMET
Energy, Mines and Resources Canada
555 Booth Street
Ottawa, Ontario
K1A 0G1

1/ This report has been reviewed by the Canadian Forestry Service and approved for distribution. Approval does not necessarily signify that the contents reflect the views and policies of the Canadian Forestry Service. Mention of trade names or commercial products does not constitute recommendation or endorsement for use.

October 1983

ABSTRACT

A fast pyrolysis process, termed **ULTRAPYROLYSIS** , has been developed at the University of Western Ontario in order to exploit the high heating rates, short residence times, high temperatures and rapid quenching, which are required to produce valuable non-equilibrium chemical intermediates from biomass. The equipment evolved considerably from the first concept to the final design with the aid of extensive cold model testing. Hot solids (**THERMOFOR**) are used to carry and transfer heat to biomass particles in a very turbulent vortical contactor (**THERMOVORTACTOR**) . This turbulence creates an ideal environment for fast thorough mixing and extremely rapid heat transfer. Cold solids (**CRYOFOR**) are used to quickly quench the products. Trials with cellulose, lignin and wood flour were conducted at temperatures between 750 and 900°C and residence times between 250 and 450 milliseconds. Maximum ethylene yields, expressed as a mass fraction of the product gas, were 8.2, 7.3 and 6.3 percent for cellulose, wood and lignin trials, respectively at 900°C. Total hydrocarbon yields, also expressed as a mass fraction of the product gas, were 18.8, 19.4 and 23.9 percent for cellulose, lignin and wood, respectively, at 900°C.

TABLE OF CONTENTS

	Page
LIST OF TABLES	iv
LIST OF FIGURES	vi
1.0 INTRODUCTION	1
2.0 PROJECT OBJECTIVES	2
3.0 FAST PYROLYSIS THEORY	3
4.0 ULTRAPYROLYSIS APPROACH	11
4.1 Novel Reactor Concept	11
4.1.1 Recent Trends in The Petroleum Cracking Industry	11
4.1.2 Advantages Associated with Ultra-Rapid Fluidization (URF)	13
4.1.3 The Application of Ultra-Rapid Fluidization (URF) to Fast Pyrolysis Processes	16
4.2 General ULTRAPYROLYSIS Concept	18
4.3 Process Highlights	21
4.4 Commercial Significance	23
4.5 General Accomplishments	25
4.6 Future Imperatives for ULTRAPYROLYSIS Research	27
5.0 ULTRAPYROLYSIS DESIGN	29
5.1 Chronology of the General Design	29
5.2 Laboratory Flow Scheme	33
5.3 Safety Design Features	35
5.4 Equipment Design	36
5.4.1 VORTACTORS	36
5.4.1.1 THERMOVORTACTOR	36
5.4.1.2 CRYOVORTACTOR	40
5.4.2 Feeders	43
5.4.2.1 THERMOFOR Feeder	43
5.4.2.2 CRYOFOR Feeder	48
5.4.2.3 Biomass Feeder	52
5.4.3 Heat Transfer Coils	55
5.4.3.1 Preheater Coil	57
5.4.3.2 Cooling Coil	57

TABLE OF CONTENTS (continued)

		Page
5.4.4	Entrained Bed Reactor	60
5.4.5	Furnaces	60
5.4.5.1	Preheater Furnace	62
5.4.5.2	Injector Furnace	62
5.4.5.3	THERMOVORTACTOR Furnace	63
5.4.5.4	Reactor Furnace	67
5.4.5	Filters	67
5.4.6.1	Mass Balance Filter	67
5.4.6.2	Bypass Filter	70
5.4.7	Vortical Splitter	70
5.4.8	Gas Sampling Bags	72
5.4.9	Gas Collection Vessel	75
6.0	BIOMASS FEEDSTOCKS AND SOLID HEAT CARRIERS	77
6.1	Biomass Feedstocks	77
6.1.1	Cellulose	77
6.1.2	Lignin	79
6.1.3	Wood	79
6.2	Solid Heat Carriers	80
7.0	COLD MODELLING STUDIES	84
7.1	VORTACTOR	84
7.1.1	VORTACTOR Mark I	84
7.1.2	VORTACTOR Mark II	86
7.1.3	VORTACTOR Mark III	88
7.1.4	VORTACTOR Mixing Studies	90
7.2	CRYOFOR Spitter	90
7.3	General Feeder Studies	101
7.4	Wood Feeder Studies	107
7.5	Load Cell Testing	114
8.0	EXPERIMENTAL PROCEDURE	117
9.0	RESULTS	120
9.1	Overview	120
9.2	Residence Time Determination	123
9.3	Mass Balance	126

TABLE OF CONTENTS (continued)

		Page
10.0	DISCUSSION	127
10.1	Product Yields for Cellulose	128
10.2	Comparison of Product Gas Yields for Various Feedstocks	131
10.2.1	Carbon Monoxide	134
10.2.2	Carbon Dioxide	137
10.2.3	Ethylene	139
10.2.4	Ethane	139
10.2.5	Acetylene	141
10.2.6	Methane	141
10.2.7	Propylene	143
10.2.8	Hydrogen	144
10.3	Molar Ratio of Product Gases	145
10.3.1	Carbon Monoxide to Carbon Dioxide	145
10.3.2	Hydrogen to Carbon Monoxide	145
10.3.3	Ethylene to Ethane	147
10.3.4	Acetylene to Ethane	150
10.3.5	Propylene to Ethane	150
10.3.6	C_2's to Methane	152
10.3.7	Ethylene to C_2's	154
10.4	Hydrocarbons	154
10.5	Heating Value of the Product Gas	165
10.6	Molecular Weight of the Product Gas	167
11.0	CONCLUSIONS	169
12.0	ACKNOWLEDGEMENTS	171
13.0	REFERENCES	172
14.0	APPENDIX. Summary of Initial Experiments Using Silica Sand as the THERMOFOR	177

LIST OF TABLES

		Page
1.	THERMOVORTACTOR Design Parameters	39
2.	CRYOVORTACTOR Design Parameters	42
3.	THERMOFOR Feeder Design Parameters	46
4.	CRYOFOR Feeder Design Parameters	51
5.	Biomass Feeder Design Parameters	56
6.	Preheater Coil Design Parameters	59
7.	Cooling Coil Design Parameters	61
8.	THERMOVORTACTOR Furnace Design Parameters	66
9.	Mass Balance Filter Design Parameters	69
10.	Bypass Filter Design Parameters	72
11.	Vortical Splitter Design Parameters	74
12.	Biomass Feedstock Analysis	78
13.	THERMOFOR (Silica Sand) Analysis	82
14.	Results of Splitting Experiments Using a Horizontal Polypropylene Y Connector	95
15.	Results of Splitting Experiments Using a Vertical Polypropylene Y Connector	96
16.	Results of Splitting Experiments Using a Horizontal Machined Plexiglass Y Device	97
17.	Results of Splitting Experiments Using a Horizontal Commercial Ducon T Device	98
18.	Results of Splitting Experiments Using a Horizontal Machined Plexiglass Y Device with Adjusting Screws	99
19.	Results of Splitting Experiments Using the VORTACTOR and Vertical Machined Plexiglas Y Assembly	100

LIST OF TABLES (continued)

		Page
20.	ULTRAPYROLYSIS Product Gas Distribution (Mole Percent)	121
21.	ULTRAPYROLYSIS Product Gas Distribution (Mass Percent).....	122
22.	Cellulose ULTRAPYROLYSIS Product Yields and Mass Balance.....	124
23.	Elemental Balance, Empirical Formula and Gas Higher Heating Value of the Cellulose ULTRAPYROLYSIS Product Gas.....	125
24.	Results of Initial Cellulose Experiments Using Silica Sand as the THERMOFOR.....	178

LIST OF FIGURES Page

1. Reactions Competing With Fast Pyrolysis Reactions 6
2. ULTRAPYROLYSIS Flow Scheme 19
3. THERMOVORTACTOR 37
4. CRYOVORTACTOR 41
5. THERMOFOR Feeder 45
6. CRYOFOR Feeder 49
7. CRYOFOR Feeding Assembly 50
8. Biomass Feeder 53
9. Biomass Feeder Support Assembly 54
10. THERMOFOR Preheater Coil Assembly (Double Coil) 58
11. THERMOVORTACTOR Furnace 65
12. Mass Balance Filter 68
13. Vortical Splitter 73
14. VORTACTOR Mark I 85
15. VORTACTOR Mark II 87
16. VORTACTOR Mark III 89
17. Mixing Experiment Apparatus 91
18. THERMOFOR Feeder Test Results: Solids Loading vs Coil Gas Superficial Velocity at Constant Feeder Pressure 102
19. THERMOFOR Feeder Test Results: Solids Mass Flowrate vs Coil Gas Superficial Velocity at Constant Feeder Pressure 103
20. THERMOFOR Feeder Test Results: Solids Loading vs Feeder Pressure at Constant Coil Gas Superficial Velocity 105

LIST OF FIGURES (continued) Page

21. THERMOFOR Feeder Test Results: Solids Mass Flowrate vs Feeder Pressure at Constant Coil Gas Superficial Velocity 106
22. Biomass Feeder Test Results: Solids Loading vs Coil Gas Superficial Velocity at Constant Feeder Pressure 108
23. Spouted Bed Wood Feeder 110
24. Downflow Wood Feeder 111
25. Ring Wood Feeder 113
26. Load Cell Test Results: Load Cell Reading vs Balance Reading 116
27. Cellulose Pyrolysis Product Yields at Various Temperatures 129
28. Gas Product Distribution for Cellulose at Various Temperatures 132
29. Gas Product Distribution for Lignin at Various Temperatures 133
30. Gas Product Distribution for Birch Wood Flour at Various Temperatures 135
31. Mass Fraction of Carbon Monoxide and Carbon Dioxide in the Product Gas at Various Temperatures 136

LIST OF FIGURES (continued)

Page

32. Mass Fraction of Ethylene, Ethane and Acetylene in the Product Gas at Various Temperatures 140
33. Mass Fraction of Methane, Propylene and Hydrogen in the Product Gas at Various Temperatures..... 142
34. Molar Ratio of Carbon Monoxide to Carbon Dioxide in the Product Gas at Various Temperatures..... 146
35. Molar Ratio of Hydrogen to Carbon Monoxide in the Product Gas at Various Temperatures. 148
36. Molar Ratios of Ethylene and Acetylene to Ethane in the Product Gas at Various Temperatures..... 149
37. Molar Ratio of Propylene to Ethane in the Product Gas at Various Temperatures. 151
38. Molar Ratios of C_2's to Methane, and Ethylene to C_2's in the Product Gas at Various Temperatures. 153
39. Mass Fraction of Total Hydrocarbons and Unsaturates in the Product Gas at Various Temperatures. 155
40. Mass Fraction of Unsaturates in the Hydrocarbon Content of the Product Gas at Various Temperatures..... 158
41. Mass Fraction of Ethane in the Saturated Hydrocarbon Content of the Product Gas at Various Temperatures..... 159
42. Mass Fraction of Methane and C_2's in the Total Hydrocarbon Content of the Product Gas at Various Temperatures..... 161
43. Mass Fraction of Ethylene, Acetylene and Propylene in the Unsaturated Content of the Product Gas at Various Temperatures..... 162

LIST OF FIGURES (continued)

Page

44. Higher Heating Value of the Product Gas Over the Range of Reaction Temperatures..... 166

45. Molecular Weight of the Product Gas at Various Temperatures..... 168

1.0 INTRODUCTION

A considerable effort has been made over the past decade to research, develop and update (or modernize) traditional thermochemical conversion processes for biomass, in order to demonstrate technically viable technologies suitable for industrial applications. Some of these processes, which include air, steam and oxygen gasification along with pyrolysis and catalytic liquefaction, have been successfully implemented in industry.

Fundamental research, which had previously demonstrated the potential for such applications, was then initiated to investigate a new generation of thermochemical conversion pathways leading to products of a higher quality than the more traditional routes. Vacuum, flash, fast and plasma pyrolysis were among some of the bench-scale research studies with particularly promising yields of valuable chemical intermediates from biomass.

At the University of Western Ontario, a fast pyrolysis program (ULTRAPYROLYSIS) was conceptualized with the intention of engineering a continuous process which would exploit the favourable product yields reported in the bench-scale studies. This report summarizes the project objectives, theoretical base, process development, equipment design, and experimental work carried out during the development of the ULTRAPYROLYSIS process at the University of Western Ontario (in cooperation with the Forintek Canada Corp.) under the sponsorship of the Enfor program (Environment Canada/Energy Mines & Resources Canada).

2.0 PROJECT OBJECTIVES

The primary objective of the ULTRAPYROLYSIS project was to engineer a **continuous** process which would successfully demonstrate the chemistry of fast pyrolysis. In effect, a successful demonstration would require that valuable non-equilibrium thermochemical conversion products (olefins, BTX and reactive intermediates) and synthesis gas (carbon monoxide and hydrogen), be generated continuously in equipment that could be used as a conceptual basis for eventual commercial scale-up. The heart of this primary objective was the development of a new reactor design in order to exploit and optimize fast pyrolysis product yields.

Secondary objectives included the rough design of pilot and commercial plants based on the ULTRAPYROLYSIS approach. However, due to the priority of time and effort devoted to cold modelling, design of the new reactor and actual experimental work, the completion of these designs was delayed until the second phase of the work, which is currently underway (sponsored by NRC Energy Project Office under DSS contract 05SU.3115-2-2647: "An Investigation of the Fast Pyrolysis of Wood and its Components").

3.0 FAST PYROLYSIS THEORY

Any serious review of biomass and coal conversion literature indicates the ambiguity of the conversion terminology. The following discussion will define and briefly characterize the concept of fast pyrolysis and relate it to conventional and flash pryolysis. A review of the proposed pyrolytic mechanisms and chemical pathways will also be presented.

Pyrolysis, flash pyrolysis, pyrolytic gasification, and fast pyrolysis are terms which appear frequently in the biomass and coal thermochemical conversion literature. **Pyrolysis** may be defined in its broadest sense, as the thermal decomposition of organic matter occurring in the absence of air or oxygen. Some authors would consider oxygen-deficient (i.e. less air or oxygen than is required stoichiometrically for complete combustion) thermal decomposition to be a true pyrolysis process as long as the primary products are liquid or solid. When the primary products of the oxygen-deficient decomposition are non-condensible fuel gases, the process is known as **gasification.**

Conventional pyrolysis is typically characterized by a slow feedstock heating rate (less than 2°C/s), low temperatures (less than 500°C) and relatively long gas and solids residence times (greater than 5 s for the gas; solids residence times can be minutes, hours or days in duration).

Tar and char are the primary products due to slow devolatilization of the feedstock and the secondary coking and polymerization (recombination) reactions, which are allowed to occur in the reactor after primary pyrolysis has taken place.

Flash pyrolysis is a rapid heating rate process (greater than 2°C/s) occurring at moderate temperatures (typically 400 to 600°C) whose liquid tar/oil products are maximized at the expense of char and gas. Vapour residence times are normally less than 2 seconds. **Fast pyrolysis** is differentiated from flash pyrolysis primarily with respect to temperature, vapour residence times, and end-product. Extremely rapid heating rates (up to 10^5°C/s), high temperatures (greater than 600°C) and short vapour residence times (less than 0.5 s) are required to maximize the production of high quality gases (i.e. olefins, other hydrocarbons) at the expense of char and condensible liquids.

Pyrolytic gasification is a term applied to any anaerobic pyrolysis process, fast or slow, which gives a non-condensible synthesis gas or medium energy fuel gas (10 to 20 MJ/Nm^3) as the primary product. In pyrolytic gasification, tar and char are viewed as undesirable by-products.

It is important to note that the pyrolysis terms used in this report have been defined from a general consensus which was gleaned from an exhaustive literature survey. Terms such as **flash** and **fast** pyrolysis have been used interchangeably in some of the literature. The biomass

community should soon establish a standard nomenclature to avoid confusion and misunderstanding.

The recent interest in fast pyrolysis and its potential for producing high quality fuel and synthesis gas from biomass is due primarily to the fundamental research performed during the past decade by Soltes (1,2,3), Shafizadeh (4,5), Broido (6), Lewellen (7), Milne (8,9,10) and others (11). Their work has attempted to identify the major competitive and consecutive reactions which may occur during the thermal decomposition of biomass, and is summarized in an excellent review by the Solar Energy Research Institute (11). Fundamental research of this nature is extremely valuable and necessary for the engineering of a viable continuous fast pyrolysis process, and therefore a short discussion on pyrolysis mechanisms is given in the following paragraphs. Although much of the modelling is based on cellulose pyrolysis, these results appear to be consistent with those obtained in processes using wood and other biomass (3, 23).

The chemical mechanisms involved in pyrolysis (especially fast pyrolysis) are not well understood. However, an overall mechanism is presented in Figure 1. This figure is reproduced with permission from J. Diebold of the Solar Energy Research Institute, and was formulated from a general consensus of pyrolysis specialists at a workshop sponsored by SERI (11).

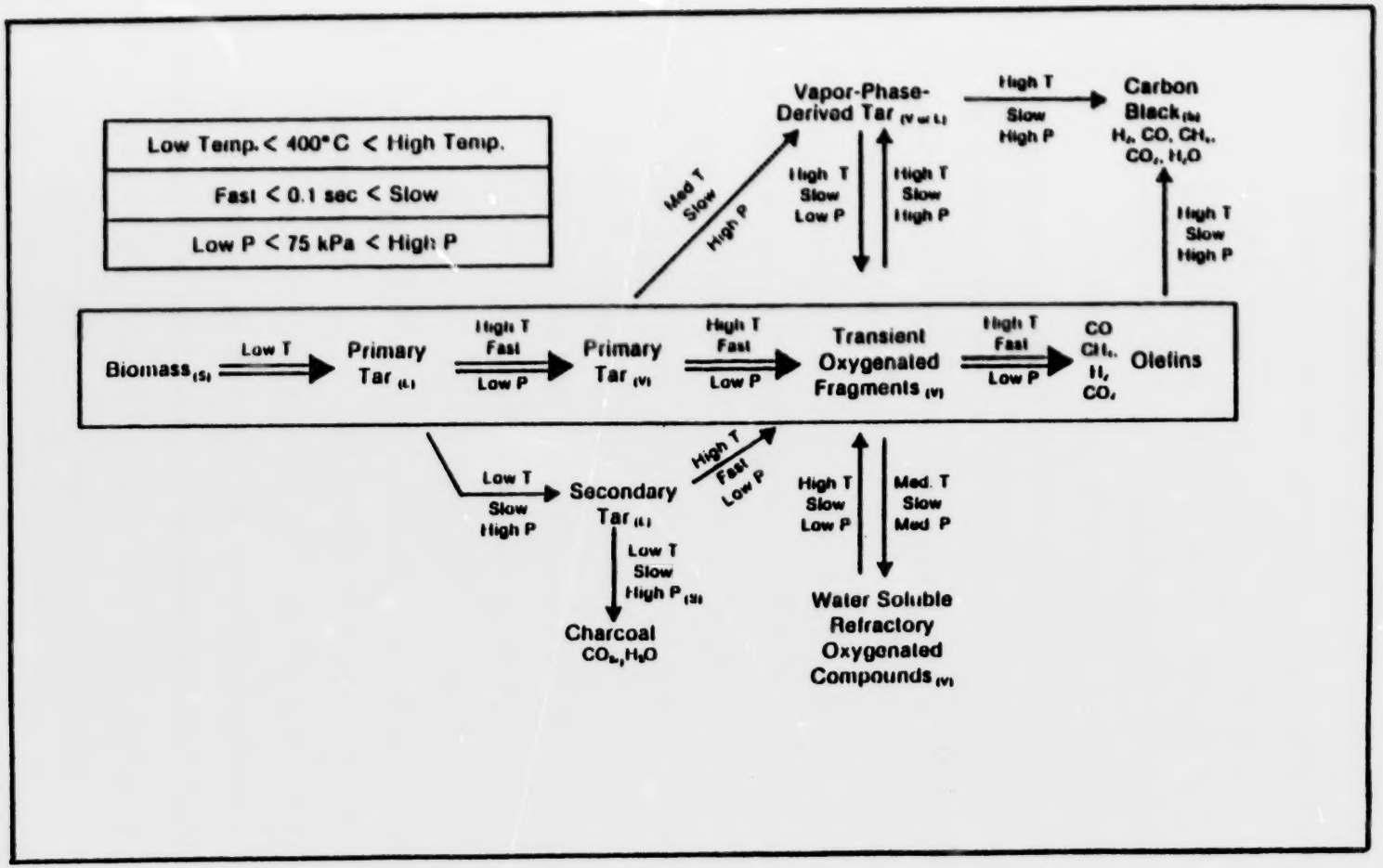
Low Temp. < 400°C < High Temp.
Fast < 0.1 sec < Slow
Low P < 75 kPa < High P
Biomass (s)
Low T
Primary Tar (L)
High T Fast Low P
Primary Tar (v)
High T Fast Low P
Transient Oxygenated Fragments (v)
High T Fast Low P
CO CH4, H2, CO2 Olefins
Med T Slow High P
Vapor-Phase-Derived Tar (v or L)
High T Slow Low P
High T Slow High P
High T Slow High P
Carbon Black (s) H2, CO, CH4, CO2, H2O
Low T Slow High P
Secondary Tar (L)
High T Fast Low P
Low T Slow High P (s)
Charcoal CO, H2O
High T Slow Low P
Med. T Slow Med P
Water Soluble Refractory Oxygenated Compounds (v)

Figure 1 - Reactions Competing with Fast Pyrolysis Reactions
(Reproduced with the permission of J. Diebold of the Solar Energy Research Institute).

The reactions of **primary** pyrolysis are those which directly affect the biomass feedstock, and can generally be classified either as fragmentation (fission) or dehydration reactions. Dehydration is dominant at lower temperatures (below 300°C), is typical of conventional pyrolysis, and involves a reduction in molecular weight, the evolution of H_2O, CO and CO_2, and the formation of char (5,23). Fragmentation predominates at higher temperatures (greater than 300°C) and involves the depolymerization of biomass to anhydroglucose units (i.e. levoglucosan) and other light combustible volatiles. These higher temperature reactions are of more interest with respect to the development of a flash or fast pyrolysis process.

The primary products of pyrolysis may repolymerize (re-combine), undergo further fragmentation (cracking) or react with free radicals depending on their temperature, residence time and pressure. These **secondary** reactions must be better characterized in order to engineer a system which can selectively maximize one or more of the many possible products or intermediates.

The recombination of primary products to form stable secondary tars is favoured by long vapour residence times, low to medium temperatures (200 to 600°C) and high partial pressures. These conditions allow the primary molecules to be in close proximity for significant periods of time in the condensed phase, and permit frequent collisions to occur in the vapour phase. Extended reaction times at lower temperatures result in the

formation of char, water and carbon oxide gases from secondary tars. Elevated temperatures favour the cracking of the secondary tar to hydrocarbons, H_2, CO, CO_2 and carbon black.

A pyrolytic pathway which clearly favours olefin production is illustrated in Figure 1. Once the liquid primary tar is formed on the biomass surface, high temperatures, rapid heating rates, and low vapour partial pressures will promote olefin formation by the following reaction sequence (12):

(i) Primary tars are vapourized from the liquid tar surface. This precludes the formation of stable secondary tars by recombination (re-polymerization).

(ii) The vapourized primary tars are thermally cracked to produce transient oxygenated fragments. These fragments can form pyroligneous acids (i.e. acetaldehyde, methanol, furan, acetic acid, acetone, etc.) and vapour-phase-derived tars (by recombination) under conditions which are not suitable for olefin production.

(iii) The transient oxygenated fragments are thermally cracked to yield olefins, other hydrocarbons, carbon oxides and hydrogen.

Extended reaction times will allow the olefins and related products to react and form carbon black, permanent equilibrium gases, and condensible aromatic vapours. Therefore, to preserve the olefins, the pyrolysis pathway must be interrupted by rapid quenching of the

intermediates before equilibrium can occur. Experimental work has demonstrated that little or no char was formed during the fast pyrolysis of biomass (7,11,12,13,18,23) and that olefin yields of 10 to 15 percent by mass of the biomass feedstock can be realized (11,12,23).

Recent research by Milne (9,10) in a molecular beam mass spectrometer apparatus has generally confirmed the fast pyrolysis mechanism outlined in Figure 1. Real time sampling, precise control of vapour residence times, and the development of an excellent technique to quickly (microseconds) "freeze" intermediate products has permitted the observation of the transient oxygenated fragments, and olefins as a function of time. Quantification of the results and continued systematic studies using biomass feedstocks will allow the determination of an "olefin window" (i.e. a time interval after primary pyrolysis occurs). This in turn will permit process engineers to exploit maximum olefin yields. Preliminary results indicate that the olefin window occurs between 30 and 150 milliseconds after the primary tars vapourize from the liquid surface of the pyrolyzing biomass.

Fast pyrolysis research sponsored by Crown Zellerbach (11) has shown that ethylene is favoured at vapour-phase temperatures of 700 to 900°C, while acetylene is favoured in the range of 1200 to 1500°C. Mixtures of various proportions occur between 900 and 1200°C. The majority of the experiments were conducted in an induction furnace at temperatures above 1000°C. Yields of acetylene approaching 15 percent of the dry wood

feedstock were achieved in the batch-mode bench-scale apparatus. Calculations predicted a 40 percent theoretical acetylene yield, and a 25 percent yield was assumed to be reasonable for a continuous commercial-scale process.

Other fast pyrolysis work, using a variety of reactor configurations and heat transfer techniques, is being conducted or has recently been completed in Canada (14,23,25), France (11,16), Sweden (11) and the United States (11,17). Although the majority of researchers have concluded that temperature, residence time, and heating rate are equally the most important reaction conditions in determining the pyrolysis pathway, some have assumed that the heating rate effects are explicable in terms of their influence on the other two principal reaction conditions (3,17).

The success of a fast pyrolysis system depends on the development of good engineering technique which would facilitate the following:

(i) Rapid heat transfer to the biomass on a scale of tens of thousands of degrees celsius per second.

(ii) High reactor temperatures exceeding 700°C.

(iii) Short residence times on a millisecond time scale.

(iv) Rapid quenching of reaction products on a millisecond time scale.

4.0 ULTRAPYROLYSIS APPROACH

4.1 Novel Reactor Concept

In the current highly competitive market place, only advanced products and processes will survive. Advanced reactors, and a concerted program to develop them, are required in order to generate such products and processes. The discussions in the following sections summarize the various considerations which have clearly illustrated the general need for novel reactor designs, and also indicate the factors which led specifically to the new reactor concept (i.e. the THERMOVORTACTOR) which was developed during the course of the ULTRAPYROLYSIS project. Cracking and pyrolysis processes are particularly suited for such reactors in order to enhance selectivity, conversion and economics in the production of valuable petrochemical intermediates.

4.1.1 Recent Trends In The Petroleum Cracking Industry

Pioneering moves towards fast reactors were undertaken in the petroleum refining field a few decades ago. Thus, catalytic cracking has been evolving progressively towards the use of heavier feedstocks and higher temperatures to crack these feedstocks. This is being done today in riser cracking reactors at contact times of a few seconds resulting in superior product yield and quality compared to dense phase fluidized bed reactor products. A short and uniform contact time reduces coke (char)

formation, promotes increased catalytic activity, and gives a better overall product distribution. Feedstocks can crack (thermally) in the presence of coke, and produce additional undesirable coke and byproduct gas. Therefore "coke makes more coke" in an autocatalytic manner. In addition, the short contact time prevents valuable distillates from being further cracked to less desirable products.

Although the development of riser crackers has greatly enhanced the flexibility and economics of the hydrocarbon cracking industry, experience has shown that additional improvements are possible. The mixing of the hot regenerated catalyst with the feedstock at the base of the riser is one operation which can be significantly improved. The mixing relaxation time is currently of the order one second, whereas high temperature cracking reactions occur on a millisecond time scale (the mixing relation time in slow fluidized beds is typically between 2 and 40 seconds). Separation of the product from the catalyst at the top of the riser should be accomplished more quickly, and the product should then be immediately sent to the distillation column to avoid any further thermal degradation.

The considerations in the previous discussions led to the concept of ultra-rapid fluidization (URF) and its subsequent application to fast pyrolysis (ULTRAPYROLYSIS). The potential advantages associated with the use of URF in a biomass fast pyrolysis process were recognized by the Enfor program officials, and funds were made available to develop this new technology.

4.1.2 Advantages Associated With Ultra-Rapid Fluidization (URF)

In conventional hydrocarbon cracking and pyrolysis processes, solid particulates are often utilized in one way or another. These particulates are generally processed in reactors which can be considered to be slow, fast or ultra-rapid fluidized beds, with contact time ranging from a few hundred milliseconds to several seconds. Ultra-rapid fluidization (URF) is a recent development which is well suited for application to biomass pyrolysis, and has thus led to the concept of extremely fast pyrolysis (ULTRAPYROLYSIS) requiring high process temperatures. URF is a means of reducing the size of the equipment due to faster reaction rates and to a higher conversion per pass. Compactness, per se, is immensely advantageous in biomass pyrolysis applications. Due to the cost and logistics of biomass feedstock transportation, small local plants are feasible and economically attractive. This is particularly true for remote regions (i.e. those regions which are far from industrial centers) where biomass is plentiful and where natural gas and oil cannot be economically supplied.

Ultra-rapid fluidized reactors, which are small and relatively inexpensive, can be implemented in a modular fashion. This reduces the scale-up problems associated with conventional fluidized bed reactors where scale-up is a major uncertainty, and requires expensive and time consuming pilot plant development. With the utilization of URF in

pyrolysis processes (i.e. ULTRAPYROLYSIS), technological risks and long lead times can thus be significantly reduced. The modular approach enhances the market potential for standard units and accordingly facilitates further development (and a corresponding increase in demand).

Because of their compact size, URF reactors can be simulated on a cold model basis at full-scale in the laboratory. This makes the study of their fluid mechanids and mixing patterns much easier. On the other hand, conventional slow fluidized bed reactors (which are typically 10 to 20 m in diameter in commercial applications) cannot be adequately simulated in the laboratory. One has to rely on doubtful or crude empirical scaling laws to progress from the simulator stage to the full-scale plant. In addition, **relatively** few slow fluidized bed commercial units are ever built, and therefore the significant improvements associated with operating experience occur over a protracted length of time.

The reduction in cost associated with small URF reactors would mean that investment capital would be more readily available. Conventional fluidized bed systems, particularly those being developed for biomass or coal pyrolysis/gasification, require sums in the billion dollar range and several years are essential for design and construction. During this lead time, significant capital interest charges are incurred while no marketable product is made available to defray the costs. Modular URF units can be brought on stream relatively fast, and are therefore operational and generating cash with a minimal lag time.

Compact URF systems can be shop fabricated and shipped, completely instrumented, to the field. Shop fabrication is particularly advantageous over field construction. The total investment cost is lower, startup expenditures are reduced and commissioning procedures are shortened. Equipment tests and trial runs are carried out before delivery. Quality control is enhanced since equipment, piping, and instrument installations are performed by specialists under ideal conditions in the shop setting. In addition, shop fabrication puts less strain on the local industrial infrastructure (i.e. transportation system, utilities, temporary accommodations, etc.) and fewer delays are incurred due to foul weather.

The integration of URF into the petrochemical cracking industry could lead to greater feedstock flexibility (i.e. non-traditional feedstock use may be possible) and higher yields of selected products. The direct, high-temperature cracking of whole crude oil, residual oils, tar sand bitumen, and whole tar sand by means of URF and ULTRAPYROLYSIS proceses, may provide a wide range of feedstock and product disbribution options. This, in turn, would buffer the effects of fluctuating market values for a particular raw material feedstock or prcduct. This represents a significant advantage over conventional refining where large volumes of crude must be processed, and adequate markets must be found for all of the product cuts before profits are realized.

Due to high service costs and a reduction in off-specification production, an operation which can rapidly switch from one feedstock to

another has an economic advantage. The high solids inventory and large physical size of dense-phase fluidized beds both contribute to the requirement for relatively long periods of time to reach operational set points or to shut down. URF reactors, on the other hand, can quickly start up and shut down due to their small size and low solids inventory. Therefore a switch from one feedstock to another or from one product distribution to another is fast and cost-effective. The present dilemma of the petroleum and petrochemical industries is that the scarcest feedstocks are used, and that the least flexible reactor designs are employed. URF technlogy has the promise of flexibility which is lacking in these industries. Specific advantages associated with the use of URF reactors in the fast pyrolysis of biomass (i.e. ULTRAPYROLYSIS) are presented in Sections 4.3 and 4.4.

4.1.3 The Application of Ultra-Rapid Fluidization (URF) to Fast Pyrolysis Processes

In the conventional pyrolysis or gasification of coal, a portion of the feedstock is rapidly volatilized. Primary volatilization reactions are extremely fast and are essentially limited by the rate of heat transfer. The reactivity of the residual coal char is relatively low and therefore long contact times are required for steam or carbon dioxide to reduce the solid carbon yields. This is the case in the WINKLER process where very large reactors are necessary. Thus it is imperative to volatilize as much of the carbon content of the feedstock as possible in the initial contacting step. This can be accomplished by rapid heat

transfer rates, high temperatures, and extremely short contact times which are not adequately accomplished in conventional fluidized beds.

The situation is similar for the pyrolysis or gasification of biomass, although it is much more reactive than coal. The portion of the biomass feedstock which is not quickly volatilized, remains as char which is difficult to gasify. However, as was clearly indicated in Chapter 3.0 (Fast Pyrolysis Theory), under suitable reactor conditions, practically all of the biomass can be volatilized without generating char (coke) or persistent tars. Accordingly, there would be no need for the relatively slow carbon gasification step.

The initial temperature shock which is required for maximum volatilization can be realized, among other means, by quickly and efficiently (i.e. thoroughly) contacting the fine carbonaceous feedstock particles with a hot particulate heat carrier (THERMOFOR) in a new generation of URF reactors. One such reactor developed during this project and described later in the report, is a hot vortical contactor or "THERMOVORACTOR". The relaxation time of the mixing between the feedstock and the heat carrier must be shorter than the time required for adequate heat transfer to occur. Other cyclonic and opposed jet URF reactors are being developed and, when commercially proven, should experience widespread utility in cracking and pyrolysis processes where short contact times and high temperatures are essential.

4.2 General ULTRAPYROLYSIS Concept

A continuous process designed to exploit the high temperatures, rapid heating rates, short vapour residence times, and rapid quenching rates required for fast pyrolysis was developed over a two year period at the University of Western Ontario, and has been termed ULTRAPYROLYSIS. The most recent design and general approach are briefly summarized in the following paragraphs. Earlier designs and a detailed description of the equipment appear in later sections.

Figure 2 illustrates the ULTRAPYROLYSIS process at the laboratory scale, which employs particulate solids to carry heat to and from the reactants and products respectively. Rapid mixing and heat transfer are carried out in two vortical contactors. The first has been termed a THERMOVORTACTOR and allows heat to be transferred from hot solids (THERMOFOR) to the biomass. The second is a CRYOVORTACTOR and allows fast quenching of the products by the transfer of heat to cold solids (CRYOFOR).

THERMOFOR, CRYOFOR and wood feeders are employed in the system. They are all fluidized bed, pneumatic transport feeders which essentially pump the fluidized solids through a transport line. The THERMOFOR feeder sends the particulate solids to a preheater coil, the CRYOFOR feeder sends the particulates to the CRYOVORTACTOR, and the wood feeder supplies wood, cellulose or lignin powders to the THERMOVORTACTOR. The solids loading

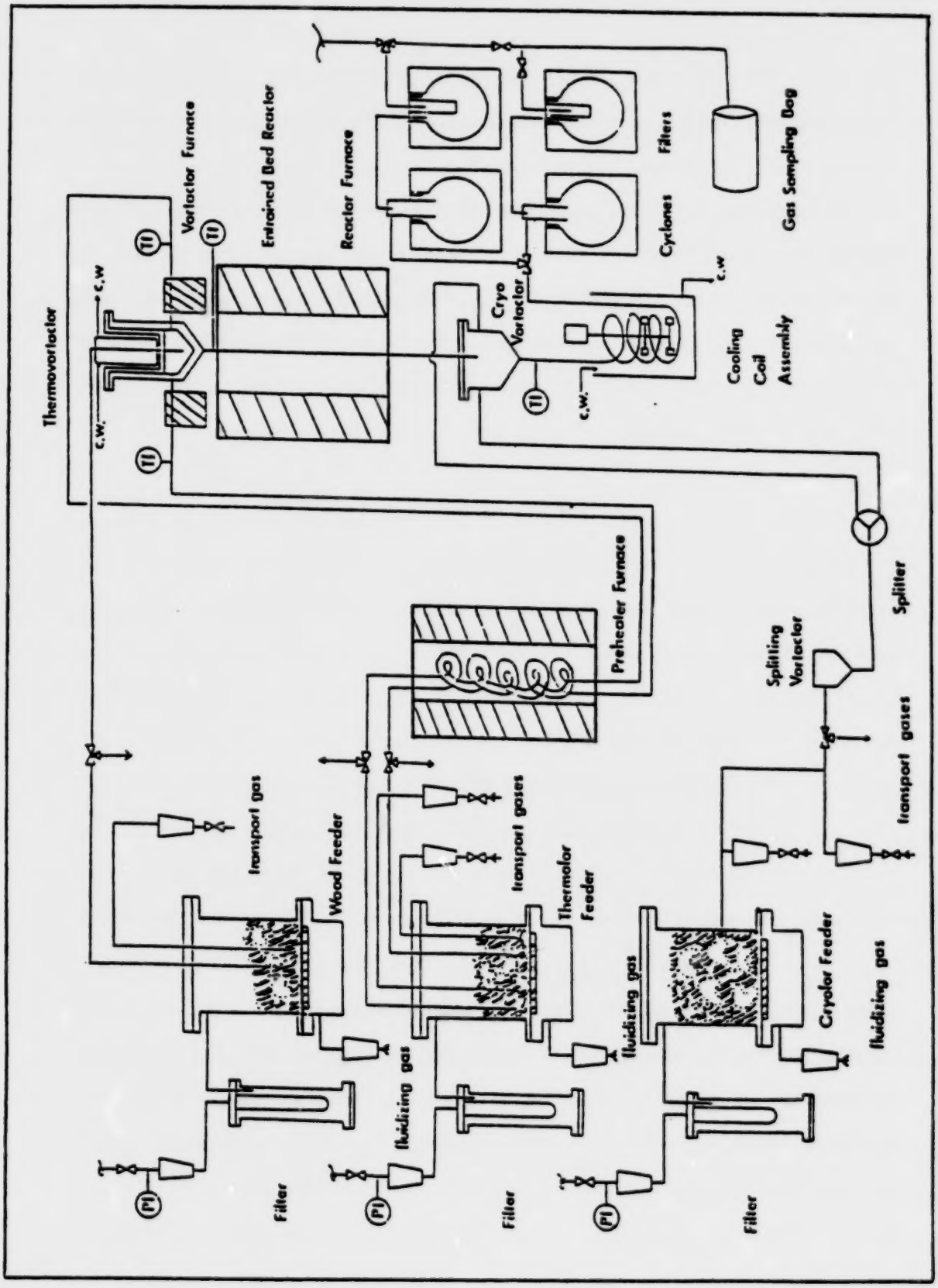

Figure 2 - ULTRAPYROLYSIS Flow Scheme

and mass flow rates are controlled by manipulating the pressure in the fluidized bed, and by varying the volumetric flow of the transport gas.

The preheater coil assembly consists of two separate coils which are housed in an electrical resistance oven, and allow the transfer of heat to the THERMOFOR (heat-carrying solid particulates). Each coil tube is 20 m in length and is made of 6.4 mm (outside diameter) Inconel 601 tubing. The coil loops are 100 mm in diameter and the overall length of the double coil unit is 1 m.

Rapid mixing and heat transfer between the THERMOFOR and the biomass feedstock occurs in the THERMOVORTACTOR. The THERMOVORTACTOR is a cyclonic vessel with two opposing tangential inlets for the THERMOFOR. One tangential stream effectively destroys the momentum of the other, causing severe turbulence. Biomass feedstocks are then injected from the top of the THERMOVORTACTOR through an air-cooled tube into the turbulent region. The design mixing time is 20 milliseconds.

The CRYOVORTACTOR is a cyclonic contactor which serves to quench the hot gaseous products by rapidly mixing them with cold solids (CRYOFOR). It is similar in design, but is larger than the THERMOVORTACTOR. Hot gases enter through a tube from the top of the vessel, and are injected into the turbulent zone which is caused by the destruction of momentum of two opposing cold solid tangential streams. The design quenching time is 20 milliseconds.

The fast pyrolysis of biomass commences in the THERMOVORTACTOR and continues in a plug-flow entrained bed reactor. The reactor is simply a tube or coil of varying length (to vary the residence time) which is housed in an electrical resistance oven. The mixture of hot solids and biomass passes from the THERMOVORTACTOR, through the entrained flow reactor, to the CRYOVORTACTOR. The total elapsed time from the heating of the biomass to the quenching of the product is between 320 and 520 ms.

The experimental parameters can be summarized as follows:

Reactor Temperature	700 to 1000°C
Solids/Biomass Mixing Time	50 ms
Reactor Residence Time	250 to 450 ms
Quenching Time	20 ms
Heating Rate	10^4 to 10^5°C/s
Maximum Feed Rate	1 Kg/h

4.3 Process Highlights

In addition to high heat transfer rates by conduction and convection, there are other advantages associated with the use of solids, rather than a gas, to carry heat in ULTRAPYROLYSIS. First, the heat capacity of solids is higher per unit volume resulting in the design of equipment which is more compact. Second, solids are more easily separated from the product gas allowing less dilution and a corresponding higher energy

density. The production of a relatively homogeneous and concentrated gas product further results in simpler (and thus more economical) upgrading and purification.

High yields of a non-condensible gaseous product and limited production of tarry liquids or solids are positive features of fast pyrolysis. Any tarry aerosols that are formed, due to lower reaction temperatures or extended reactor residence times, are condensed on the cooling solids thus reducing the expense associated with aerosol separation.

The primary product spectrum is flexible in fast pyrolysis. Olefins, synthesis gas (CO/H_2) or SNG can be individually optimized in response to the market demand. These primary products can also be processed to high quality secondary products such as petrochemicals (i.e., polyethylene) and synthetic gasoline (i.e. by polymerization, Mobil synthesis or Fischer-Tropsch synthesis pathways).

Operation at relatively low pressures (near ambient), the elimination of an oxygen plant required in some of the other thermochemical processes which produce a high quality gas, and the very fast reaction kinetics which permit the design of compact equipment, are additional features of fast pyrolysis which enhance process economics and tend to simplify the overall plant design.

4.4 Commercial Significance

The development of a successful fast pyrolysis technology for biomass will offer a product and process with the best features of conventional pyrolysis and air/oxygen gasification. Conventional biomass pyrolysis and flash pyrolysis research, which tend to maximize the production of a wide spectrum of condensibles, has definitely illustrated the need to characterize and upgrade the liquid products, and to identify viable industrial applications prior to successful commercial development.

On the other hand, the hardware and commercial viability of air/oxygen gasification has already been demonstrated, and the product end-use has been clearly identified in a variety of industrial sectors. A major consideration for air gasification product applications however, is their limitation to close-coupled combustion related processes (steam generation, space heating, drying and engine shaft power). Although these are valuable and important applications, storage and piping of the low energy gas (LEG) over any significant distance is not economically viable. LEG is not suitable as a synthesis gas for methanol or gasoline, nor is it suitable as a feedstock for the petrochemical industry.

Oxygen gasification gives a medium energy gas (MEG) which may be transported over moderate distances (50 to 80 km) and may be used for synthesis of methanol and ammonia (in addition to the LEG uses). However, the gas product can not be used directly as a petrochemical feedstock, nor as a syngas for commercial synthetic gasoline production. In order to

commercially generate gasoline as an end-product via the oxygen gasification route, biomass must be degraded to its simplest form (CO, H_2, C), then "reconstructed" to methanol, and finally converted from methanol to gasoline (i.e. Mobil synthesis). Available energy is lost in each step, and thermodynamically the biomass is converted from a very structured molecule to very simple molecules and then back several steps to a somewhat more structured gasoline precursor. Although oxygen plant cost has not rendered oxygen gasification economically unattractive, the removal of this step would allow even more favourable economics, and less dilution of the gas by combustion products.

In a more general sense, the new generation of unique pyrolytic processes outlined in this report would allow substitution of wood for oil and coal (where favourable) for the production of olefins, other reactive organic intermediates, and synthesis gas. Sectors of the petrochemical and petroleum industry could therefore utilize wood as their primary feedstock when necessary. Because of its high reactivity, wood might even be preferred to coal as a petrochemical feedstock. Ethylene from wood could be transformed directly into gasoline using a relatively new catalytic synthesis pathway developed by MOBIL OIL.

The intense mixers (VORTACTORS) developed for ULTRAPYROLYSIS could also lead to the development of very compact generators of enriched fuel gas suitable for power plants, industrial parks and even large mobile equipment.

4.5 General Accomplishments

Although the specific ULTRAPYROLYSIS project accomplishments which relate to the contractual specifications have been summarized in Chapter 11.0 (Conclusions) some general "byproduct" accomplishments are reported in the following paragraphs.

In addition to the successful demonstration of the chemistry of biomass fast pyrolysis in the current project, the critical research and development steps which must be taken along the path to commercial development have been identified. Several projects have been initiated to accomplish the goal of eventual commercialization and these are summarized in Section 4.6 (Future Imperatives for ULTRAPYROLYSIS Research). In the meantime, technology has already been transferred to Canadian and European development groups. Dr. L.A. Behie and Dr. W. Surcek, of the Chemical Engineering Department of the University of Calgary, are currently building an ULTRAPYROLYSIS pilot plant with a one barrel per day capacity, to crack heavy oils, tar sand bitumen and, eventually, whole tar sand to olefins and petrochemical intermediates. Other industrial research organizations in Europe and North America are also conducting work in this area based on the ULTRAPYROLYSIS experience. Confidentiality restrictions prevent the release of their names as they do not want to alert competition to what they are doing. Stelco, among other companies, is interested in an ULTRAPYROLYSIS-based scheme to increase the efficiency and profitability of their blast furnace operations. In this scheme, lignites would be pyrolyzed (via ULTRAPYROLYSIS) to make medium BTU gas for injection into blast furnaces. A significant reduction of coke (char)

make and an increase in furnace capacity would thus be accomplished with a relatively small capital investment.

Cost-effectiveness is another accomplishment associated with the ULTRAPYROLYSIS process (and other university-based process development work). In effect, a new reactor concept was developed without the costs associated with an industrial research team. The funds which were expended in this program and were sufficient in an academic setting, would have barely supported one man-year of an average process development engineer in industry (estimated to be $150,000 per year when operating and capital expenses are pro-rated). Even if a professional engineer had been employed, successful development of a new process would not have been guaranteed since background research experience is essential. This experience was transferred to the graduate engineering students from the pool of engineering specialists in the academic environment. As a result, the graduate students participated in novel process engineering research, which fostered creativity and provided excellent technical experience. These fresh skills can now be effectively used to supplement Canada's professional work force (rather than withdrawing qualified research people from the industrial research pool).

The ULYRAPYROLYSIS project was not state-of-the-art, step by step research, where successful progress is essentially guaranteed. Instead, it was of a pioneering nature where the risks of failure are high but where the rewards are also hgh. For Canada, indeed, not taking risks in the technlogical field, is the greatest risk of all.

4.6 Future Imperatives for ULTRAPYROLYSIS Research

Aside from the routine development steps required to bring any technology forward to commercial development, two major specific objectives must yet be accomplished in the ULTRAPYROLYSIS program. These include the characterization of the mixing in the THERMOVORTACTOR unit and the development of a separator for the reactor system to quickly remove hot solids from the product gas. Other significant objectives include the development of dependable consistent solids feeders and the generation of kinetic data for ULTRAPYROLYSIS reactions.

The mixing of the particulate heat carrier and the carbonaceous feedstock in the THERMOVORTACTOR is a function of the amount of shear between the two solids after injection. Cold modelling research is presently being conducted, under the sponsorship of NSERC, to investigate various designs which will maximize the extent and rapidity of mixing. The mixing time should be a small fraction of the total rector residence time (i.e. approximately 20 percent thereof) in order to preserve the yield and quality of desirable products.

In commercial operations, the THERMOFOR solids will have to be disengaged from the product gas at relatively high temperatures, before the product gas is quenched. This is essential for maximum **exergy** efficiency which requires the recovery of heat at the highest temperature level (the second law of thermodynamics). The disengagement of hot solids must be carried out within 20 or 30 milliseconds. Rapid THERMOFOR separation and fast quench of the product gas stream are essential in order to prevent

product degradation and to promote optimal product yields and selectivity. The amount of product gas which is lost to the THERMOFOR reheat step, should also be minimized.

A THERMOFOR stripper-separator concept is currently being researched. It will consist of an underflow cyclone with steam (or some other appropriate gas) being injected in the rotating boundary layer to effect the stripping. A separator will also be required in the THERMOFOR reheat loop in order to prevent inert combustion product gases from contaminating the ULTRAPYROLYSIS product gas stream. Such inert gases dilute the product gases and require costly separation steps prior to final product processing.

The mass flowrate of THERMOFOR and carbonaceous feedstock solids must be precisely controlled so that cracking severity does not vary significantly with time. Feeding devices which are used for slow fluidized beds and lower temperature reactions may not be adequate for the ULTRAPYROLYSIS and URF reactors. This area is also being investigated. In addition, the kinetics of ultra-rapid pyrolysis and reactor development are being studied in depth under a National Research Council project which was referenced in Chapter 2.0.

5.0 ULTRAPYROLYSIS DESIGN

5.1 Chronology of the General Design

The general design of the ULTRAPYROLYSIS equipment evolved significantly from the first concepts to the most recent design which is detailed in this report. In the early stages of the project it was quickly recognized that the design requirements for the major system components were beyond the state-of-the-art, and that the technology of the process would have to be developed during the course of the project. Therefore, a significant amount of time and effort was initially devoted to various process configurations and to cold model experiments. An overview of the major components, which includes the feeders, heat sources, and reactors (solid contactors), is presented in this section.

Two alternatives were initially considered for the feeding of the biomass and particulate thermofor solids. The first was simply a pressurized hopper where transport gas was introduced at the top, percolated down through the solids, and exited from the bottom while carrying suspended solids into the transport line. The second was a fluidized bed feeder where solids were pumped through a submerged transport line by manipulating the bed pressure and gas flow rates. The experience of Dr. de Lasa with the fluidized bed feeder and cold modelling experiments which demonstrated better control using this design, both contributed to the decision to reject the pressurized hopper approach.

Significant continuous design improvements were made, especially with respect to the mode of solids injection into the transport line. The wood and thermofor feeders were of a similar design in that the suspended solids were transported in an **upflow** mode out of the vessel.

It was initially proposed that the quenching solids (CRYOFOR) feeder would consist of a pressurized hopper similar to the one proposed for the other solids feeders. However, problems in maintaining constant flow during the cold tests, and also design changes in the cold solids contactor (CRYOVORTACTOR) led to the adoption of a fluidized bed feeder. To achieve the high loading required in the CRYOVORTACTOR, a **downflow** mode of solids flow from the fluidized bed was selected.

During the course of the project, three basic methods of heating the solid heat carriers (THERMOFOR) and maintaining the reactor temperature were considered. The first method, consisting of two variations, would utilize a hot fluidized bed of sand to supply the thermal requirements of the cyclonic reactor. Electrical heaters and the reactor would be submerged in the bed allowing very rapid heat transfer from the heat source to the heat carrier (THERMOFOR) and finally to the reactor walls. Precise temperature control was a significant advantage of this approach. The first variation allowed for a portion of the hot particulate bed material to be transported to the THERMOVORTACTOR by means of a transport line (and solids injecter) which would also be submerged in the bed. The second variation included a cold vessel which would serve as a distinct

feeder to supply suspended solids to an electrically heated coil. Solids would then exit the coil at reaction temperature and be led directly to the THERMOVORTACTOR in the hot fluidized bed. Both alternatives were conceived to employ a second vortactor (CRYOVORTACTOR) which was submerged in a cold fluidized bed to quench the reaction. A portion of the cold bed solids would be pneumatically transported to the CRYOVORTACTOR to mix with the hot products. The first general approach was rejected for the laboratory process development equipment due to its complexity, cost and potential danger should the hot solids accidently exit from the fluidized bed into the laboratory. The concept is yet thought to be viable for a pilot or commercial scale design.

The second general method considered for supplying heat to the solids and reactor, was an Inconel coil in which an electrical current was directly passed. Direct electrical resistance heat would therefore be transferred to the flowing solid suspension. Calculations indicated that very specific voltage and amperage tolerances were required necessitating a transformer on the line. Cost and safety considerations led to the rejection of this design.

The final proposed method for transferring heat to the solids and reactor consisted of enclosing the thermofor heater coil and THERMOVORTACTOR in separate electrical resistance ovens with independent temperature control. This approach was selected due to safety, cost and ease of implementation.

At the heart of the development of ULTRAPYROLYSIS was the design of a particulate solids contactor which would allow rapid, efficient mixing of hot solids with biomass. A simple vessel with two radially opposed THERMOFOR jets was considered but quickly rejected due to the problems associated with maintaining precise jet radial alignment in a hot erosive environment. Precise alignment would be necessary to guarantee thorough mixing. It was then decided to employ a cyclonic vessel to accomplish rapid mixing using tangential particulate streams. This general reactor design was termed a VORTACTOR (vortical solids contactor).

Several VORTACTOR designs were considered in the early stages of the project, and it was anticipated that a final selection could be made on the basis of a theoretical evaluation alone. However, as the literature was reviewed, the extreme complexity of rapid particulate solids mixers became apparent, and it was evident that the vortactor configuration would have to be selected on the basis of cold model experimentation. Although the results of the modelling are reviewed elsewhere in this report, the three initially proposed configurations are mentioned as follows:

(i) Tangentially opposed injection of the THERMOFOR and wood streams in the cylindrical barrel of the cyclonic vessel. Presumably, the two streams would impact and mix in the vessel cavity as their momentum was destroyed.

(ii) Tangential injection of the THERMOFOR stream in the cylindrical barrel, and axial injection of the wood into the throat section (i.e. at the apex of the cone). The anticipated turbulence of the throat section would allow for thorough mixing.

(iii) Tangentially opposed injection of two THERMOFOR strams and axial injection of wood. It was assumed that essentially complete destruction of momentum would be guaranteed by contacting two equal but opposed tangential streams. Thorough mixing of the wood would occur if injected in the midst of this turbulent environment.

5.2 Laboratory Flow Scheme

Although the ULTRAPYROLYSIS concept and system components have been identified and characterized in Chapter 4 (Section 4.1), the general laboratory flow scheme as depicted in Figure 2 is briefly reviewed here to provide a basis for the discussion of the ULTRAPYROLYSIS equipment design.

Two separate streams of heat carrying solids (THERMOFOR) were fed pneumatically from the THERMOFOR feeder and heated to 1100°C in two preheater coils which were placed inside a radiant furnace. The hot solid streams were then tangentially injected in opposite directions into the THERMOVORTACTOR. Momentum was thus destroyed creating severe turbulence and an ideal environment for efficient mixing and rapid heat transfer. Biomass particles were fed pneumatically from the biomass feeder into the

top of the THERMOVORTACTOR. The resulting biomass/inert solids mixture exited from the THERMOVORTACTOR and entered a downflow entrained bed tubular reactor. The THERMOVORTACTOR and entrained bed reactor were housed in separate furnaces thus allowing individual temperature control.

Reaction products entered the top of the CRYOVORTACTOR where they were quenched to below 300°C by two CRYOFOR (cold solids) streams which were injected in a manner similar to the THERMOFOR injection. A single CRYOFOR stream was fed pneumatically from the CRYOFOR feeder to a small splitting VORTACTOR where the solids become uniformly suspended before being split into two equal streams in a Y splitter (prior to CRYOVORTACTOR injection). The solid suspension segregated as it travelled in the single transport line from the CRYOFOR feeder. The splitting VORTACTOR was thus necessary to promote the production of a uniform suspension, which in turn facilitated an equal split into two CRYOFOR streams. The product mixture which exited from the CRYOVORTACTOR was further cooled to room temperature in a cooling coil assembly.

The flow direction of the final product suspension was regulated at the cooling coil exit by a remote control three-way valve. During startup and shutdown, the suspension was directed to a filter vessel where solids were collected and the gas was vented to the atmosphere. During steady state, the suspension was re-directed to a second filter vessel which removed the solids. The gases were then collected in gas sample bags for later analysis. Additional remote control three-way bypass and purge

valves were installed in the various feeder transport lines to facilitate smooth startup, shutdown, and operation.

5.3 Safety Design Features

Due to the flow of toxic gases and extremely hot solids (1100°C) through the system, it was necessary to incorporate several safety features into the equipment design. A separate reactor room was built inside the laboratory to house all of the hot units and the product gas handling components. The preheater coils, THERMOVORTACTOR, Reactor, CRYOVORTACTOR, cooling coil assembly, solids collection vessels, and gas sampling bags were installed in this room, which was also equipped with an exhaust fan for toxic gas removal and a carbon monoxide monitor for toxic gas detection.

The CRYOFOR and biomass feeders were operated at lower pressures than that of the THERMOFOR feeder. Therefore the possibility existed for hot solids to backflow into the CRYOFOR and biomass transport lines if a blockage occurred downstream from the CRYOVORTACTOR. To ensure safety in the event of such a blockage, short sections of plastic tubing were inserted in these transport lines prior to injection into the hot units. If contacted with hot solids, the tubing would melt, thus confining the hot solids to the reactor room and preventing their transport to the feeders. Remote control three-way valves were also installed in the transport lines to provide a secondary cut-off for solids backflow. All

feeders were equipped with pressure relief valves, and the biomass feeder was electrically grounded to reduce the generation of electrostatic charges and the possibility of a dust explosion.

5.4 Equipment Design

5.4.1 VORTACTORS

Two VORTACTORS (vortical contactors) were employed in the ULTRAPYROLYSIS mini pilot plant. Thorough mixing of the biomass with the THERMOFOR and the resulting rapid heat transfer took place in the THERMO-VORTACTOR, and rapid quenching of the hot product gas suspension with CRYOFOR occurred in the CRYOVORTACTOR. The design of both units is summarized in the following sections.

5.4.1.1 THERMOVORTACTOR

The THERMOVORTACTOR, illustrated in Figure 3, consisted of a stainless steel cylindrical heat exchanger assembly which was inserted into the annulus of an Inconel cylinder which in turn had an inner conical configuration at its base. The actual THERMOVORTACTOR cavity, with a cylindrical barrel and conical base, was thus formed when the two units were bolted through their respective stainless steel flanges (at the top of the units).

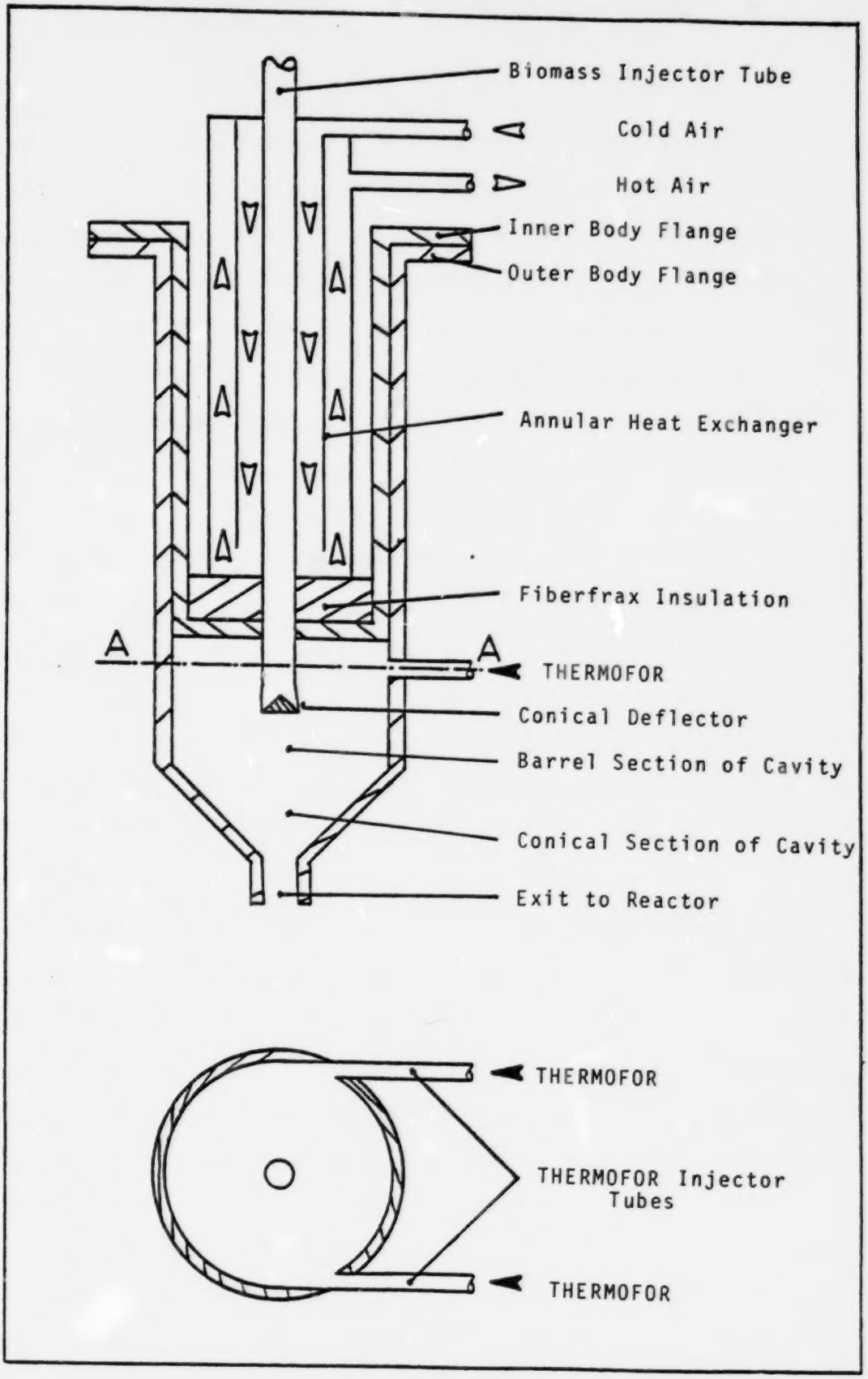

Figure 3 - THERMOVORTACTOR

The heat exchanger assembly housed a double concentric pipe cooler and a biomass injector tube at the central axis. Cool air (room temperature) passed through the inner annulus of the double pipe heat exchanger in contact with the biomass injection tube and travelled in the same direction as the biomass flow. The biomass was thereby prevented from pyrolyzing prematurely and plugging the tube prior to injection into the THERMOVORTACTOR cavity. After passing through the outer pipe annulus, the air was vented to atmosphere.

The biomass injector tube extended down through the base of the heat exchanger assembly (and also through a one inch disc of DURABOARD FIBERFRAX insulation inserted at the base of this assembly) into the upper portion of the THERMOVORTACTOR cavity. This injector was capped with a small conical deflector tube to deflect biomass particles towards the hot VORTACTOR wall. Biomass was thus prevented from exiting the cavity through the central axis.

The THERMOVORTACTOR cavity, whose volume was 38200 mm^3 had a cylindrical barrel length of 57.9 mm, a diameter of 27.9 mm, a wall thickness of 17.1 mm, and an included angle of the conical section of 90°. These dimensions were selected to optimize the heat transfer area between the solid particles and the hot wall. THERMOFOR from the preheater coils was injected into the upper portion of the cavity by two tangentially opposed

TABLE 1 THERMOVORTACTOR Design Parameters

THERMOVORTACTOR CAVITY	
THERMOFOR Injector Tube Inside Diameter	4.6 mm
Biomass Injector Tube Inside Diameter	4.6 mm
THERMOVORTACTOR Exit Tube Inside Diameter	10.0 mm
Cavity Volume	38,200 mm^3
Overall Cavity Length (Barrel and Cone)	67.6 mm
Barrel Section Length	57.9 mm
Conical Section Length	9.7 mm
Barrel Section Inside Diameter	27.9 mm
Barrel Section Wall Thickness	17.1 mm
Included Angle of Conical Section	90°
OVERALL THERMOVORTACTOR DIMENSIONS	
Length	760 mm
Cylinder Outside Diameter	57.2 mm
CONSTRUCTION MATERIALS	
THERMOVORTACTOR BODY	Inconel 601
Heat Exchanger	Copper, Brass SS 304
Flanges	SS 304

tube inlet ports with inside diameters of 4.6 mm and located 180 degrees apart. The relatively large cavity exit tube diameter of 10 mm was designed to prevent reverse flow.

The lower twenty percent of the entire THERMOVORTACTOR assembly was located inside the VORTACTOR furnace while the remaining upper portion was left exposed to ambient air. Exposure of this upper portion to ambient temperatures reduced the maintenance and material selection problems associated with high temperatures thus allowing reduction of flange costs (i.e. by using stainless steel instead of Inconel) and a wider selection of gasket materials. The relatively large mass of Inconel (i.e. thick walls) utilized in the THERMOVORTACTOR design provided an effective heat sink to dampen transient temperature fluctuations of the thermofor stream. A summary of the THERMOVORTACTOR design parameters is given in Table 1.

5.4.1.2 CRYOVORTACTOR

The design of the CRYOVORTACTOR, as illustrated in Figure 4, was much simpler than that of the THERMOVORTACTOR due to its exposure to less severe operating temperatures. Its cavity had a volume of 45,000 mm^3, thus allowing for a nominal design residence time of 30 milliseconds. The hot gas product and THERMOFOR mixture entered the cavity axially from the top of the CRYOVORTACTOR. They were then forced towards the wall and prevented from bypassing through the center axis of the CRYOVORTACTOR by a conical deflector which was installed in the inlet assembly. Two CRYOFOR

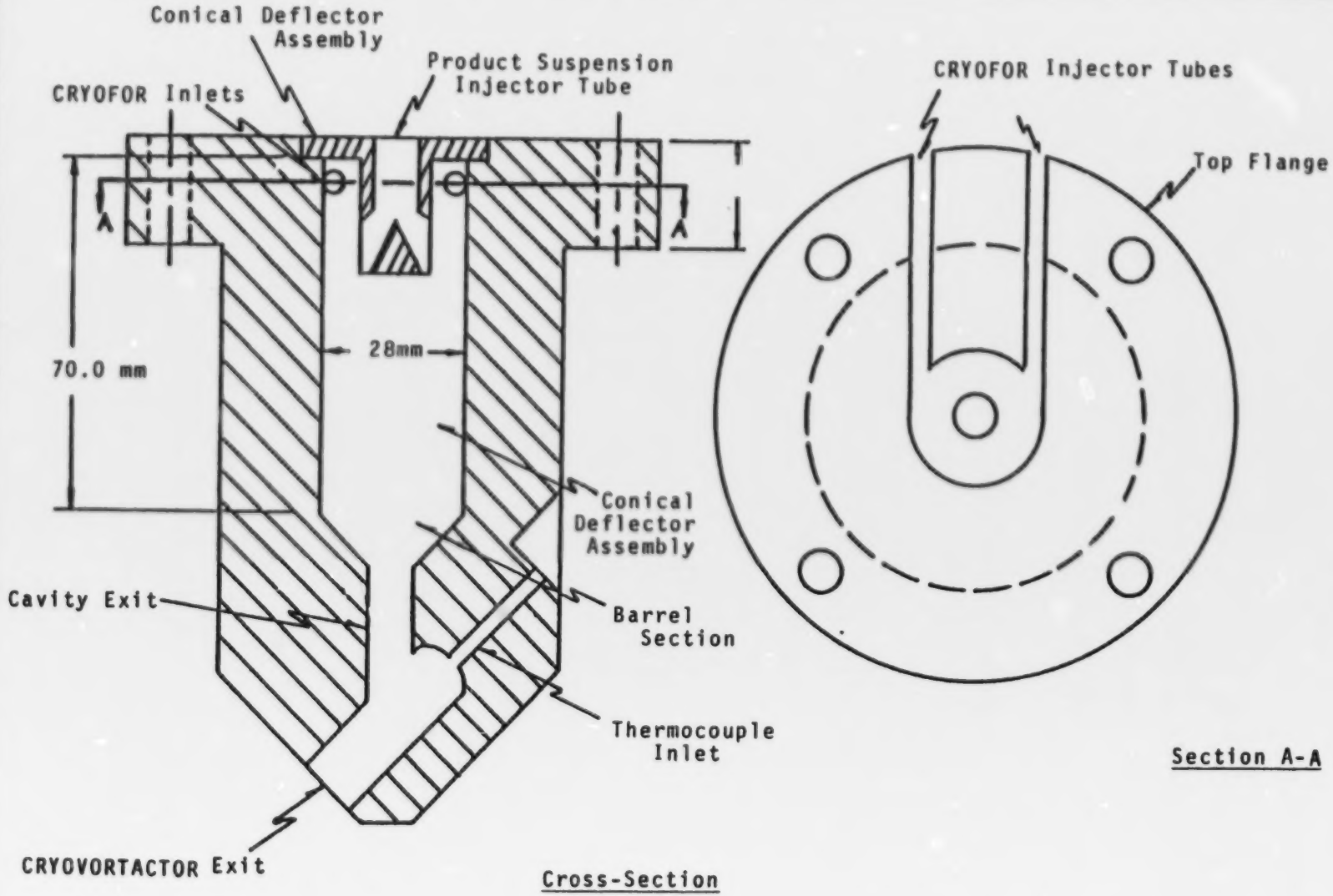

Figure 4 - CRYOVORTACTOR

TABLE 2 CRYOVORTACTOR Design Parameters

CRYOVORTACTOR CAVITY	
CRYOFOR Injector Tube Inside Diameter	4.4 mm
Product Suspension Injector Tube Inside Diameter	10.0 mm
Cavity Exit Tube Inside Diameter	8.7 mm
CRYOVORTACTOR Exit Tube Inside Diameter	12.3 mm
Cavity Volume	45,000 mm^3
Overall Cavity Length (Barrel and Cone)	79.7 mm
Barrel Section Length	70.0 mm
Conical Section Length	9.7 mm
Barrel Section Inside Diameter	28.0 mm
Barrel Section Wall Thickness	18.0 mm
Included Angle of Conical Section	90°
OVERALL THERMOVORTACTOR DIMENSIONS	
Length	125 mm
Cylinder Outside Diameter	64 mm
Construction Material	Stainless Steel
CONICAL DEFLECTOR ASSEMBLY	
Overall Length	24 mm
Flange Diameter	35 mm
Flange Thickness	4 mm
Cone Apex Angle	60°
Cone Base Diameter	13 mm
Construction Material	Stainless Steel

(cold particulate solids) streams were pneumatically fed in tangentially opposed directions causing the severe turbulence for thorough mixing and cooling of the hot suspension. A thermocouple was inserted at the outlet to measure the temperature of the quenched products.

Since the CRYOVORTACTOR was exposed to ambient room temperature and also due to the relatively low internal temperature (less than 300°C), 304 stainless steel was chosen as the material of construction. This reduced the material and fabrication costs which would have been substantially higher using Inconel. Design parameters are summarized in Table 2.

5.4.2 Feeders

Three fluidized bed feeders were employed to transport THERMOFOR, CRYOFOR and biomass to the ULTRAPYROLYSIS reacting and quenching systems. The THERMOFOR and biomass feeders employed **upflow** transport lines from their fluidized beds, while the CRYOFOR unit used a **downflow** transport line from its fluidized bed. Design details are reported in the following sections.

5.4.2.1 THERMOFOR Feeder

The fluidized bed THERMOFOR feeder, as illustrated in Figure 5, incorporated a pneumatic transport design similar to that used by de Lasa and Gau (21). It consisted of a cylindrical vessel, windbox, grid plate, pneumatic transport assembly, and an external filter assembly.

The cylindrical vessel, which held a nominal capacity of 70 kg of THERMOFOR, was constructed from a 860 mm length of 300 mm inside diameter carbon steel pipe. Several pressure taps were inserted along the length to measure the height of bed material.

To achieve good fluidization via an even distribution of fluidizing gas flow through the grid, a well designed grid and windbox are both essential. In commercial units where gas compression costs can be significant, the grid pressure drop is generally around 30 percent of the bed pressure drop. In the ULTRAPYROLYSIS unit where gas compression was an insignificant cost, a grid pressure drop equivalent to that of the bed pressure drop was selected. Good fluidization was thereby ensured. The grid plate had 109 holes of 1.2 mm diameter, and an open area of 0.17 percent. A **chinese hat** was located in the windbox to facilitate even distribution of the inlet gas as it approached the base of the grid.

An external filter vessel was used to replace both the transport disengaging section (which normally allows for significant deentrainment of suspended particulates) and internal cyclones due to a limitation of headroom. The filter separated entrained solids from the fluidizing gas before the gas was vented to atmosphere. Additional filter design parameters are reported in section 5.4.6.

The actual feeding assembly (Figure 5) consisted of a gas inlet line with a nozzle at its tip and a transport line which were submerged in the fluidized bed of THERMOFOR. Solids which were in the vicinity of the gap between the gas line nozzle and transport line inlet, were carried through

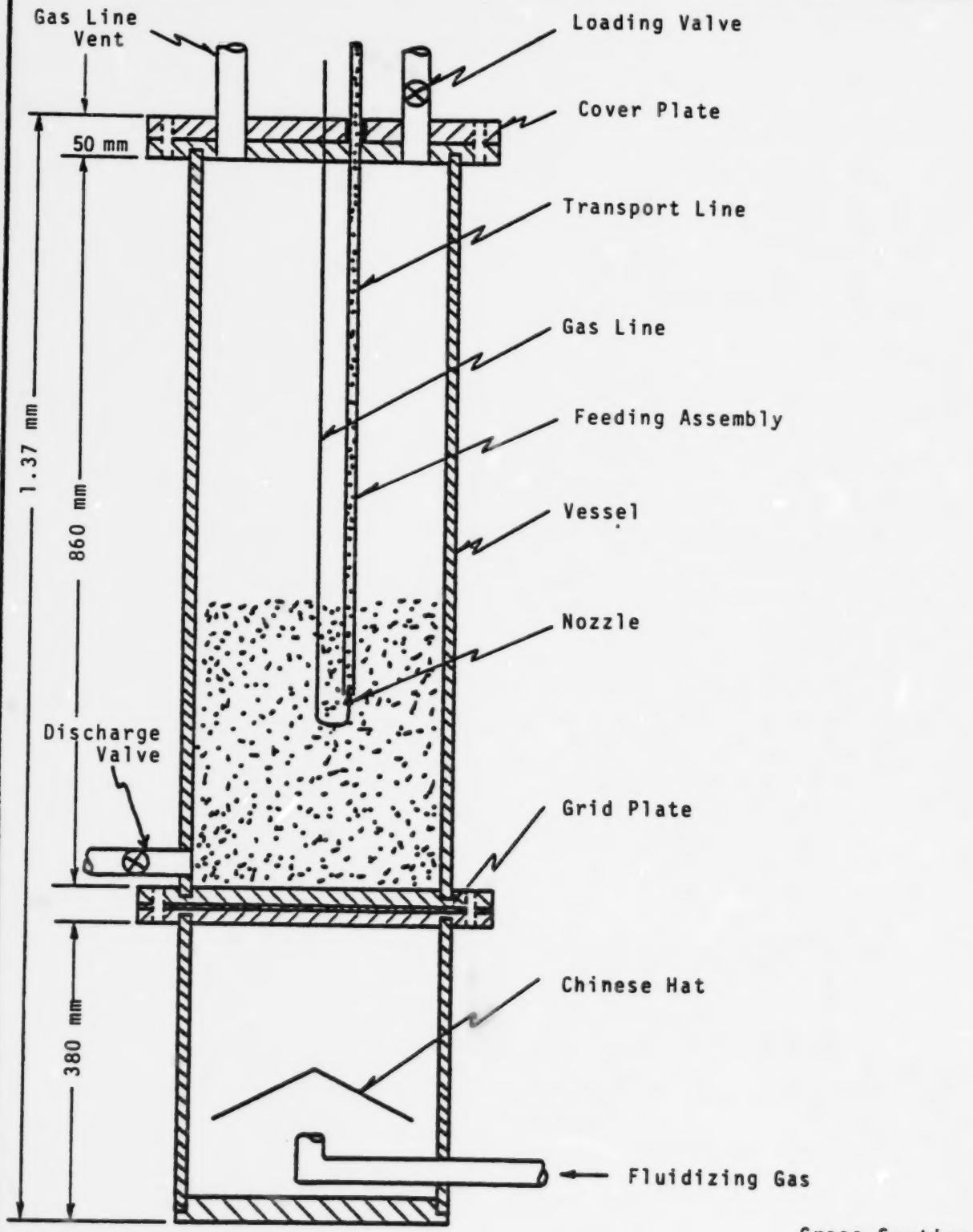

Figure 5 - THERMOFOR Feeder

TABLE 3 THERMOFOR Feeder Design Parameters

OPERATING CONDITIONS	
Pressure	780 kPa
Temperature	25° C
VESSEL SECTION	
Inside Diameter	300 mm
Outside Diameter	320 mm
Wall Thickness	10 mm
Length	860 mm
Flange Diameter*	420 mm
Flange Thickness*	26 mm
Cover Plate Thickness	24 mm
Construction Material	Carbon Steel
GRID PLATE	
Diameter	302 mm
Hole Diameter	1.2 mm
Number of Holes	109
Hole Pitch (Triangular Pattern)	26 mm
Plate Thickness	4.8 mm
Percent of Open Area	0.17%
Construction Material	Aluminum
WINDBOX	
Inside Diameter	300 mm
Outside Diameter	320 mm
Length	380 mm
Construction Material	Carbon Steel
FEEDING ASSEMBLY GAS LINE	
Inside Diameter	4.6 mm
Outside Diameter	6.4 mm
Nozzle Inside Diameter	2.5 mm
Nozzle Outside Diameter	3.5 mm
Nozzle Length	11 mm
Construction Material	Stainless Steel
FEEDING ASSEMBLY TRANSPORT LINE	
Inside Diameter	6.4 mm
Outside Diameter	9.5 mm
Construction Material	Acrylic

* Upper and Lower Vessel Flanges are identical

the transport line and out of the feeder. The 6.4 mm inside diameter transport line was constructed of transparent acrylic to allow for visual observation of solids flow. Since two THERMOFOR streams were required, a second identical feeding assembly was constructed and submerged in the bed.

A portion of the gas which entered the feeder either by the windbox (i.e. through the grid) or by the two gas lines, did not exit by the transport lines. This portion was vented to the atmosphere, after filtration, through a valve which controlled the feeder pressure. Therefore, the actual gas flow through two transport lines had to be determined by difference and was assumed to be equal in these two lines. Four rotameters were installed in the fluidizing gas, venting gas and two inlet gas lines, respectively. The actual gas flow in each of the transport lines was calculated by the following mass balance:

$$MT = \frac{(MFG + MTG1 + MTG2 - MVG)}{2}$$

where MT = mass flowrate of gas in each transport line

MFG = mass flowrate of fluidizing gas

MTG1 = mass flowrate of gas in transport line #1

MTG2 = mass flowrate of gas in transport line #2

MVG = mass flowrate of vented gas

The assumption that the gas flow rates in the two transport lines were equal, was valid so long as the downstream pressures for both lines were equal. Cold modelling experiments, summarized in Chapter 7 (Section 7.2), supported this assumption.

The solids loading (i.e. the mass ratio of solids to gas) was a function of feeder pressure, transport gas line velocity and downstream pressure. An increase either in the transport line velocity and downstream pressure, or a decrease in the feeder pressure, led to a drop in solids loading. Due to changes in downstream pressures during a run and between different experiments, it was difficult to maintain a constant solids loading. The THERMOFOR feeder design parameters are summarized in Table 3.

5.4.2.2 CRYOFOR Feeder

A **downflow** mode of solids transport from the fluidized bed of the CRYOFOR feeder was selected in order to accomodate the high solids loading (i.e. dense phase) required for product quenching. It was necessary for the CRYOFOR mass flowrate to be greater than that of the THERMOFOR by at least a factor of three, in order to ensure adequate quenching of the product mixture (gas and THERMOFOR) from a reaction temperature of 900°C to less than 250°C. Excessive dilution of the product gas by CRYOFOR transport gas (nitrogen) would occur if the CRYOFOR solids loading was too low (i.e. dilute phase feeding).

The CRYOFOR feeder, illustrated in Figure 6, was constructed from a 1.8 m length of 255 mm inside diameter carbon steel pipe (schedule 40) and

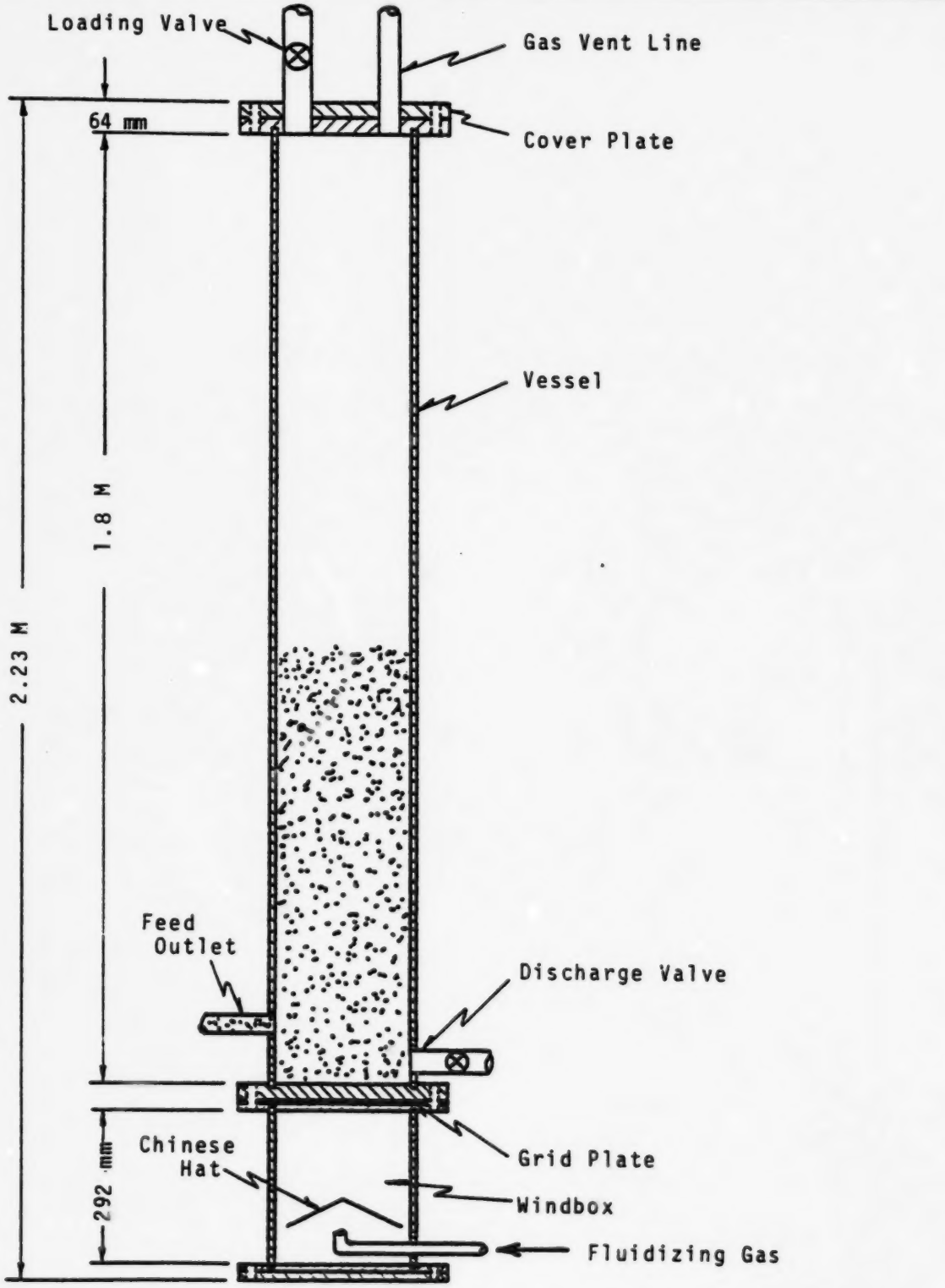

Figure 6 - CRYOFOR Feeder

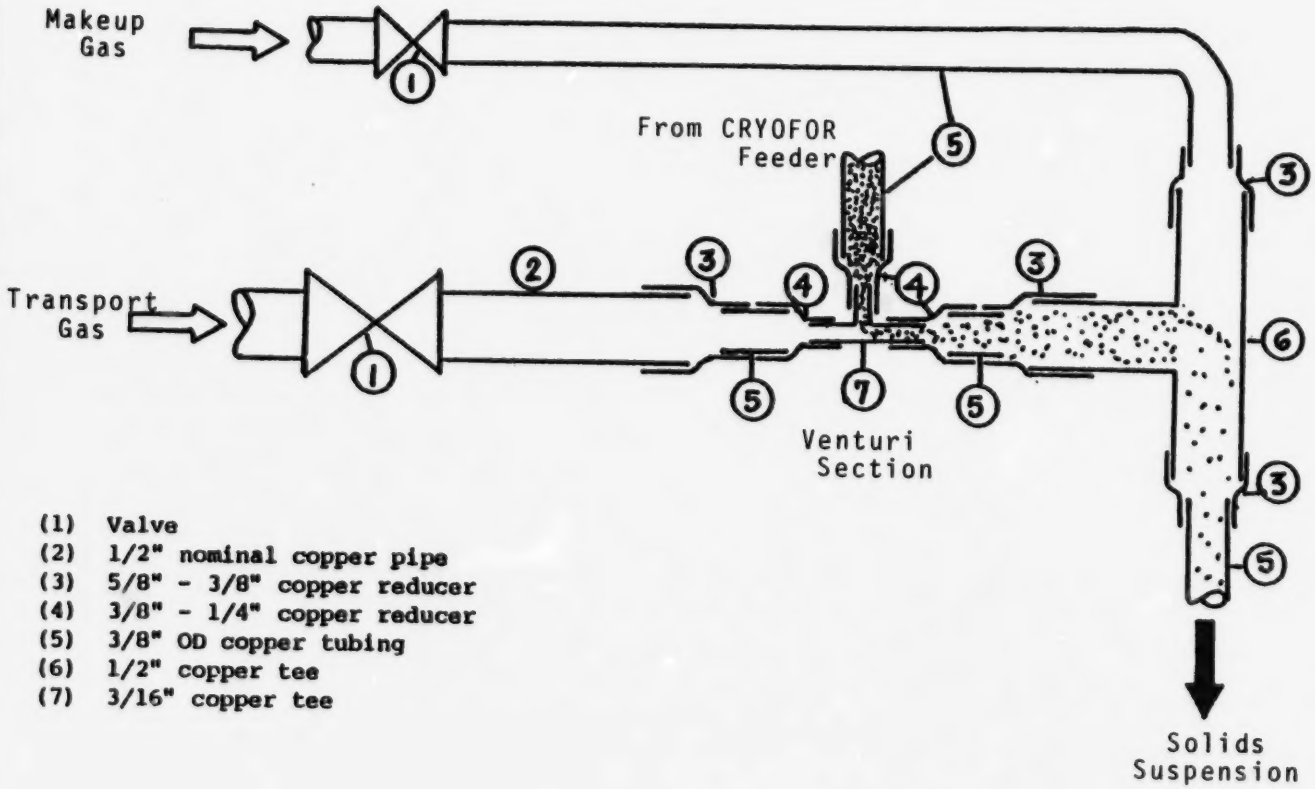

Figure 7 - CRYOFOR Feeder Assembly

TABLE 4 CRYOFOR Feeder Design Parameters

OPERATING CONDITIONS	
Pressure	780 kPa
Temperature	25 °C
VESSEL SECTION	
Inside Diameter	255 mm
Outside Diameter	273 mm
Wall Thickness	9 mm
Length	1.80 m
Flange Diameter*	384 mm
Flange Thickness*	32 mm
Cover Plate Thickness	32 mm
Construction Material	Carbon Steel
GRID PLATE	
Diameter	271 mm
Hole Diameter	2 mm
Number of Holes	91
Hole Pitch (Triangular Pattern)	21 mm
Plate Thickness	48 mm
Percent Open Area	0.56%
Construction Material	Aluminum
WINDBOX	
Inside Diameter	255 mm
Outside Diameter	273 mm
Length	292 mm
Construction Material	Carbon Steel

* Upper and Lower Vessel Flanges are identical.

had a capacity of approximately 90 kg of CRYOFOR. Its feeding assembly, shown in Figure 7, provided a mass flowrate of solids in excess of 6 kg/s from the vessel into the transport line with the aid of a Venturi injector. The Venturi was made from a copper tee and reducers. A summary of the design parameters is given in Table 4.

5.4.2.3 Biomass Feeder

An **upflow** pneumatic transport, fluidized bed feeder (Figure 8) similar to the THERMOFOR feeder design, was used to feed the various biomass feedstocks. The actual feeder vessel was capable of holding a 5 kg inventory of biomass and was constructed of a 910 mm length of 154 mm diameter carbon steel pipe (schedule 40). Three load cells were incorporated into the feeder support structure (Figure 9) to monitor the mass flowrate during the experiments. These load cells were a tension transducer type manufactured by Transducer, Inc. (Model Number T263-50-10 PI) of Cerritos CA, and had a load capacity of 23 kg each. One arm of each load cell was connected to the bottom flange of the feeder while the other was bolted to the support frame. The support frame, which was equipped with three leveling screws, was constructed of heavy carbon steel to minimize transducer errors due to vibrations and transient deflections. Output from the load cells was sent to a Doric digital meter (Model Number DS-300-T2A) which was supplied by Intertechnology of Toronto, and provided a system accuracy of 2 gram detection for a 70 kg load.

The biomass feeder assembly, which was similar in design to both of the THERMOFOR feeder assemblies (section 5.4.2.1) and was also submerged

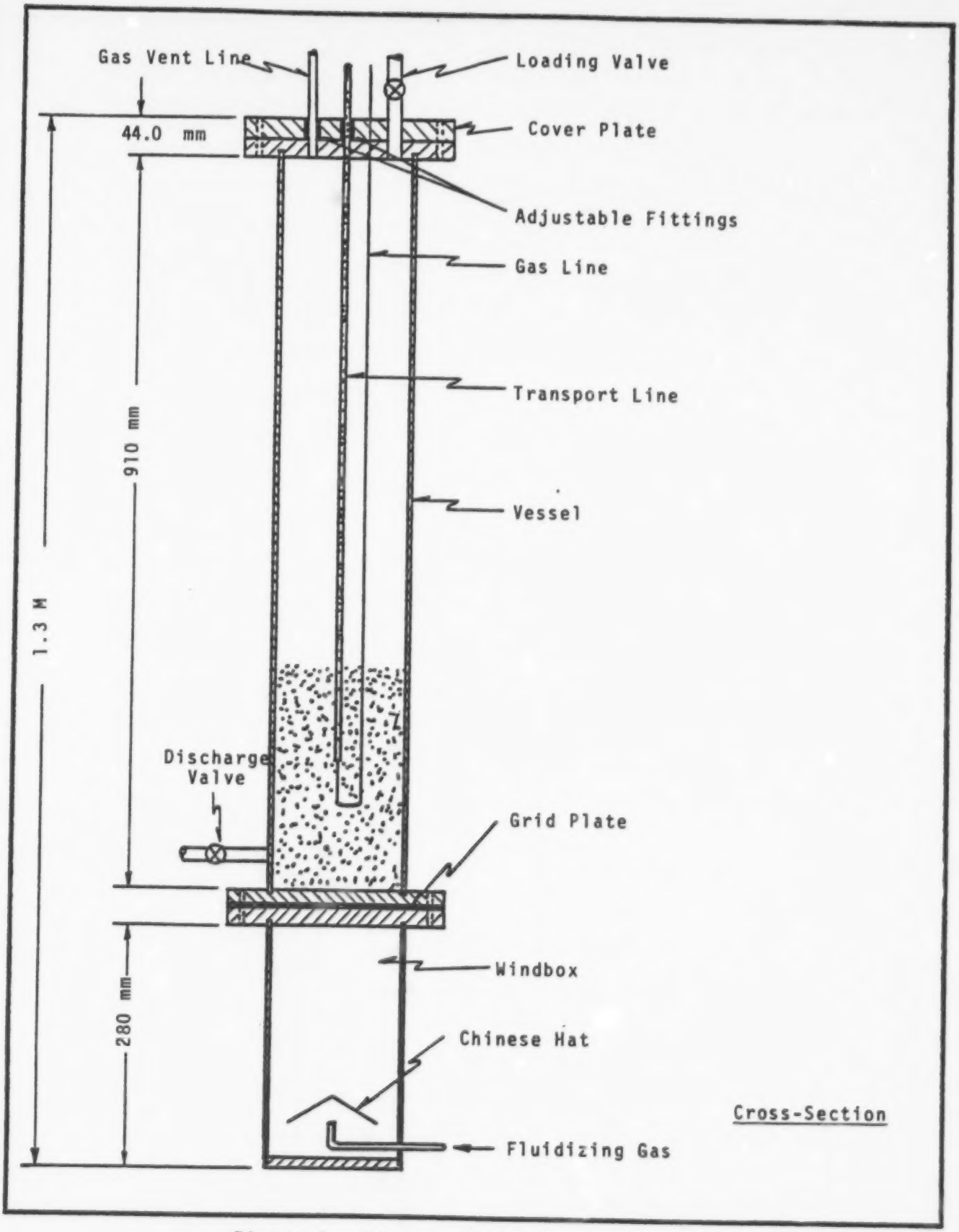

Figure 8 - Biomass Feeder

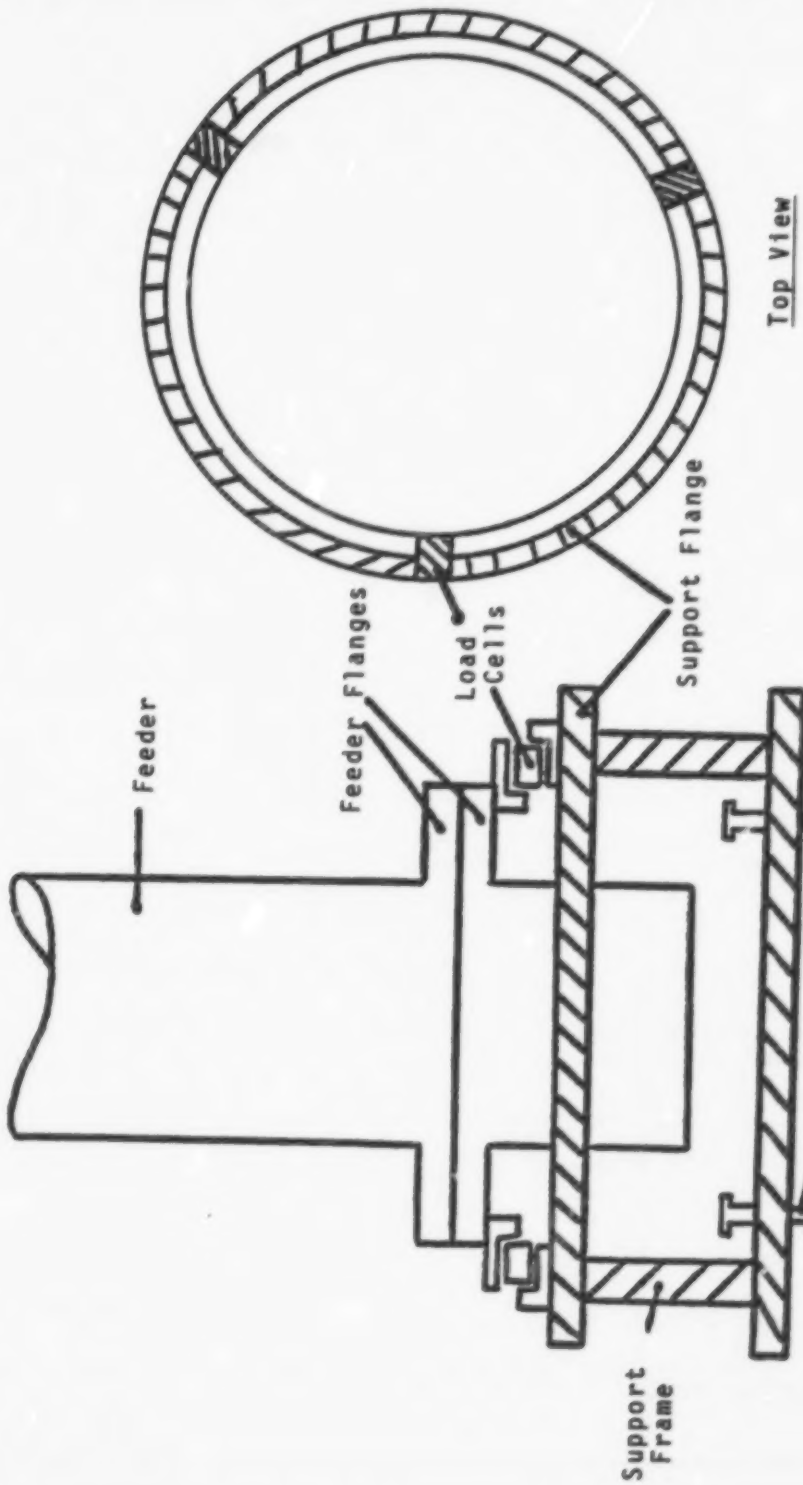

Figure 9 - Biomass Feeder Support Assembly

in the fluidized bed, consisted of a transport gas inlet line, an injector nozzle, and the actual pneumatic transport line. The inside diameter of the transport line was 3.2 mm and was selected to minimize the biomass feed rate without causing excessive plugging. An artifical pressure drop coil device had to be inserted in the transport line downstream from the feeder in order to obtain the correct loading for the desired biomass/ THERMOFOR mass ratio of 1 to 10. The coil diameter was 114 mm, and was formed from an 18 m length of 6.4 mm outside diameter plastic tubing. The transparency of the device permitted immediate detection of plugging or solids backflow.

The biomass feeder delivered an average of 6 to 8 grams of cellulose, lignin or birch flour per minute. Mechanical vibrations by tapping and rocking the feeder were required, however, to feed the birch flour smoothly and continuously due to its extremely fibrous nature. A mechanical feeder (i.e. double screw device) is recommended for future work to ensure constant, continuous flow of a variety of biomass materials into the transport line, and also to allow independent control of the solids loading. A summary of the feeder design parameters is given in Table 5.

5.4.3 Heat Transfer Coils

Two coil systems were employed in the ULTRAPYROLYSIS mini pilot plant. The preheater coil system consisted of two identical coils submerged in a tubular electrical furnace between the THERMOFOR feeder and

TABLE 5 Biomass Feeder Design Parameters

OPERATING CONDITIONS	
Pressure	780 kPa
Temperature	25 °C
VESSEL SECTION	
Inside Diameter	154 mm
Outside Diameter	168 mm
Wall Thickness	3.6 mm
Length	910 mm
Flange Diameter*	260 mm
Flange Thickness*	19 mm
Cover Plate Thickness	25 mm
Construction Material	Carbon Steel
GRID PLATE	
Diameter	150 mm
Hole Diameter	2 mm
Number of Holes	16
Hole Pitch (Triangular Pattern)	27 mm
Plate Thickness	32 mm
Percent Open Area	0.28%
Construction Material	Aluminum
WINDBOX	
Inside Diameter	154 mm
Outside Diameter	168 mm
Length	280 mm
Construction Material	Carbon Steel

* Upper and Lower Vessel Flanges are identical.

the THERMOVORTACTOR. This unit was used to heat the THERMOFOR solids from room temperature to 1100°C.

The cooling coil system was installed between the CRYOVORTACTOR and the collection filters, and was designed to cool the product suspension from 250°C to room temperature. It consisted of a coil submerged in a stirred water tank. The two coil systems are described in the following sections.

5.4.3.1 Preheater Coil

The THERMOFOR preheater unit consisted of two identical helical coils (Figure 10) installed in the central core of a tubular electrical resistance oven. Each coil was constructed from three 6 meter lengths of 6.4 mm outside diameter Inconel 601 tubing (0.89 mm wall thickness) which were welded in series. Each coil assembly was 100 mm in diameter, 965 mm in height, and had a pitch (spacing between each coil loop) of approximately 17 mm. Three Inconel strips were arranged longitudinally in an equilateral triangular pattern (i.e. at equal distances from each other around the coil perimeter) to provide structural support for the coils. Thermocouples were installed at the coil outlets to measure the suspension temperature. The preheater coil design parameters are summarized in Table 6.

5.4.3.2 Cooling Coil

The cooling coil assembly, installed between the CRYOVORTACTOR and filter vessels, was submerged in a stirred water tank to cool the product suspension from approximately 250°C to room temperature. The coil was constructed of a 7.6 meter length of 12.7 mm outside diameter stainless

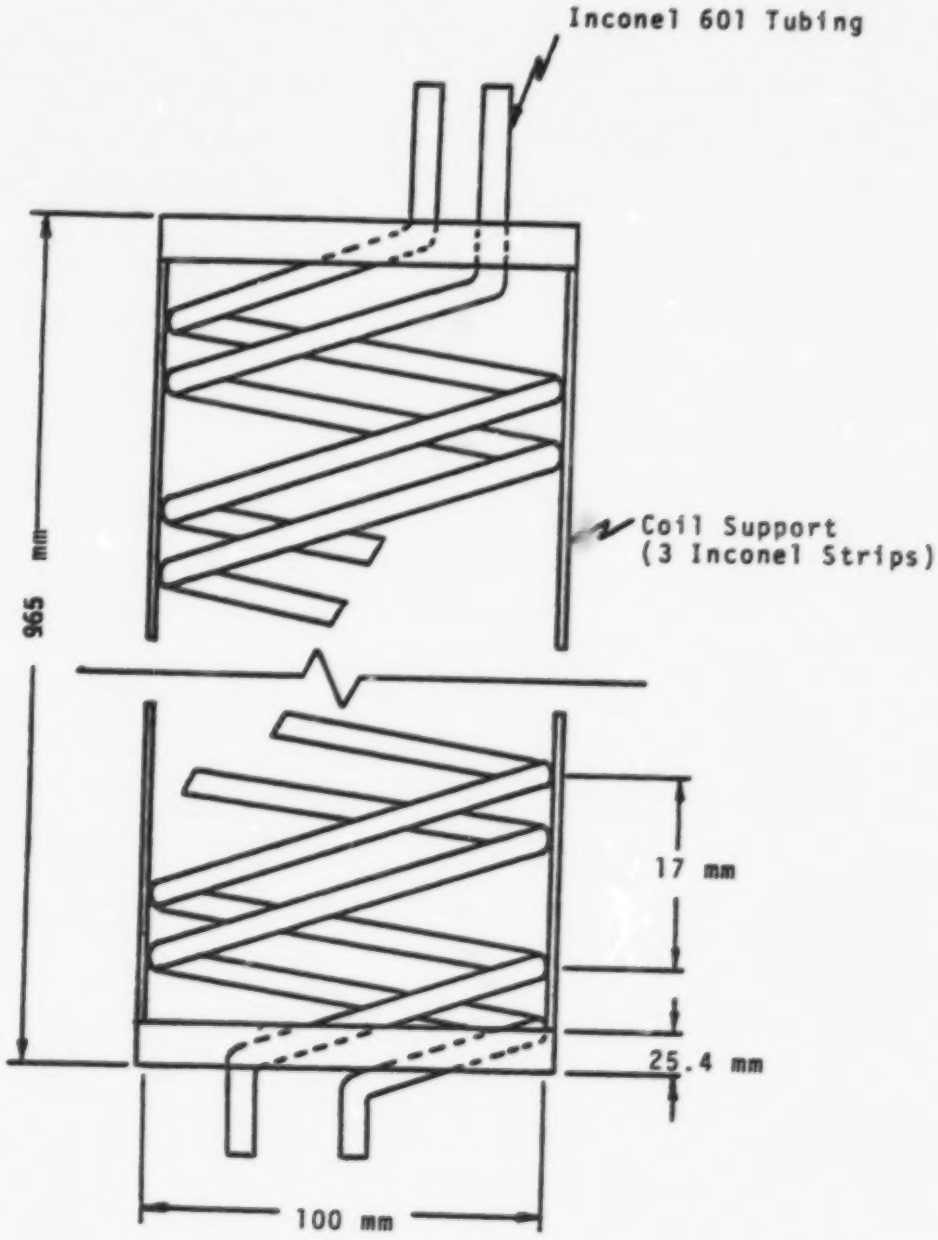

Figure 10 - THERMOFOR Preheater Coil Assembly

TABLE 6 Preheater Coil Design Parameters

Coil Diameter	100 mm
Coil Height	965 mm
Coil Pitch	17 mm
Tube Length (per coil)	18.3 m
Tube Outside Diameter	6.4 mm
Tube Inside Diameter	4.6 mm
Inlet Temperature (suspension)	≈20 °C
Outlet Temperature (suspension)	1100°C
Construction Material	Inconel 601

steel 304 tubing (0.89 mm wall thickness). The pitch of the coil, which had a diameter of 267 mm and a height of 203 mm, was 25 mm.

Water was supplied to the tank at a rate of 0.36 m^3/s (approx. 1.3 gpm) and was circulated by a turbine propeller. A summary of the cooling coil assembly is reported in Table 7.

5.4.4 Entrained Bed Reactor

The entrained bed reactor was simply a 1 meter length of 3/4" nominal Inconel 601 pipe with an outside diameter of 27 mm and an inside diameter of 21 mm. Pyrolysis of the biomass occurred primarily in this plug flow reactor, which was located in its own tubular furnace with its own temperature control.

5.4.5 Furnaces

Four electrical resistance tubular furnaces were used to raise or maintain the temperatures of the THERMOFOR and reacting suspensions. The preheater furnace heated the THERMOFOR which was transported through the two preheater coils, the injector furnace maintained the temperature of the THERMOFOR as it passed from the preheater coils to the THERMOVORTACTOR, the THERMOVORTACTOR oven housed the THERMOVORTACTOR assembly, and the reactor furnace maintained the reactor at the required temperature. These four furnaces are characterized in the following sections.

TABLE 7 Cooling Coil Design Parameters

COOLING COIL

Coil Diameter	267 mm
Coil Height	203 mm
Coil Pitch	25 mm
Tube Length	7.6 m
Tube Outside Diameter	12.7 mm
Tube Inside Diameter	11 mm
Inlet Temperature (suspension)	250 °C
Outlet Temperature	30 °C
Construction Material	SS 304

COOLING TANK

Inside Diameter	350 mm
Outside Diameter	356 mm
Wall Thickness	3.2 mm
Inside Height	480 mm
Impeller Type	4 blade turbine
Impeller Speed	150 rpm
Impeller Width	25 mm
Impeller Length	165 mm
Number of Baffles	4
Baffle Width	38 mm
Water Temperature	8 °C
Water Flowrate	0.36 m^3/s
Tank Construction Material	Carbon steel

5.4.5.1 Preheater Furnace

The preheater furnace, which was used to heat the THERMOFOR from room temperature to 1100°C, was a two zone electrical resistance tubular oven manufactured by Mellen Company (Model Number 6-520-2) of Penacook, New Hampshire. Each zone was individually controlled by two identical temperature controllers (Model Number PS-305-208-30-ZT), also supplied by the Mellen Company.

The oven core, which housed the preheater coils, had an inside diameter of 127 mm and an overall length of 914 mm. The actual heating length was 762 mm. Maximum power (per zone) and operating temperatures were 5.4 kw and 1300°C, respectively.

5.4.5.2 Injector Furnace

The injector furnace, used to maintain the high temperature of the two THERMOFOR transport line sections between the preheater coil exit and THERMOVORTACTOR injection ports, was a home-made oven constructed from two split type (clam shell) tubular heaters (Model Number 11-208) manufactured by the Mellen Company of Penacook, N.H. Each unit had a heating length of 102 mm, a diameter of 60 mm, a power rating of 0.36 kw, and was covered with a 13 mm rigid shell made from Supercastable 32 refractory (CE Refractories, Welland, Ontario). The overall length and total power rating were 128 mm and 0.72 kw, respectively.

5.4.5.3 THERMOVORTACTOR Furnace

The THERMOVORTACTOR furnace was an electrical resistance oven designed to supplement the THERMOVORTACTOR heat demand (since ULTRAPYROLYSIS reactions are endothermic) such that the desired reaction temperatures could be sustained in the entrained bed reactor. The oven consisted primarily of two Mellen clam shell tubular heaters (Model Number 11-600), a castable refractory, Carborundum silica/alumina FIBERFRAX and DURABORAD insulation, a sheet metal frame, and electrical accessories. Each clam shell heater had a power rating of 1.15 kw (230 volts), a maximum temperature of 1200°C, an inside diameter of 152 mm, and a length of 152 mm. Accordingly, the total power rating of the THERMOVORTACTOR oven was 2.3 kw (7850 BTU/h).

Oven dimensions, heat loss, and temperatures were calculated using Fourier's law of heat conduction applied to a composite cylinder, McAdams correlations for free convection heat transfer coefficients (using Nusselt, Prandtl and Grashof numbers for vertical plates), and the following design constraints:

(i) Maximum temperature of the heat source surface was 1200° C (i.e the tubular heater manufacturer specifications).

(ii) Air temperature was 21°C.

(iii) Maximum oven diameter allowed by the supporting structure was 508 mm.

(iv) Refractory thickness had to be minimized due to its relatively high thermal conductivity yet still be structurally sound to provide adequate support for the tubular heaters. The estimated minimum thickness was 6.4 mm. Thickness was also a function of available mold diameters.

(v) Heat losses from the oven had to be such that they could not reduce the net thermal output below the THERMOVORTACTOR heat demand

(vi) Oven skin temperatures were recommended to be less than 100°C for safety.

(vii) Oven height was fixed at approximately 254 mm due to heater length, Duraboard support thickness, and the THERMOVORTACTOR support structure.

(viii) The insulation and refractory materials could not be exposed to temperatures above their maximum rating. In this case, the maximum (1200°C/2190°F) was below the limits for the DURABOARD and FIBERFRAX fiber silica/alumina insulation.

It was necessary that the oven be designed to facilitate quick dismantling and to accommodate direct access to heaters, insulation, and electrical internals. Therefore, the oven structure was a self-supporting, interlocking design using no adhesives, bolts or welds, except in the external sheet metal shell. All internals could be accessed directly from the top of the oven by removing the interlocked Duraboard insulating layers. The design parameters are summarized in Figure 11 and Table 8.

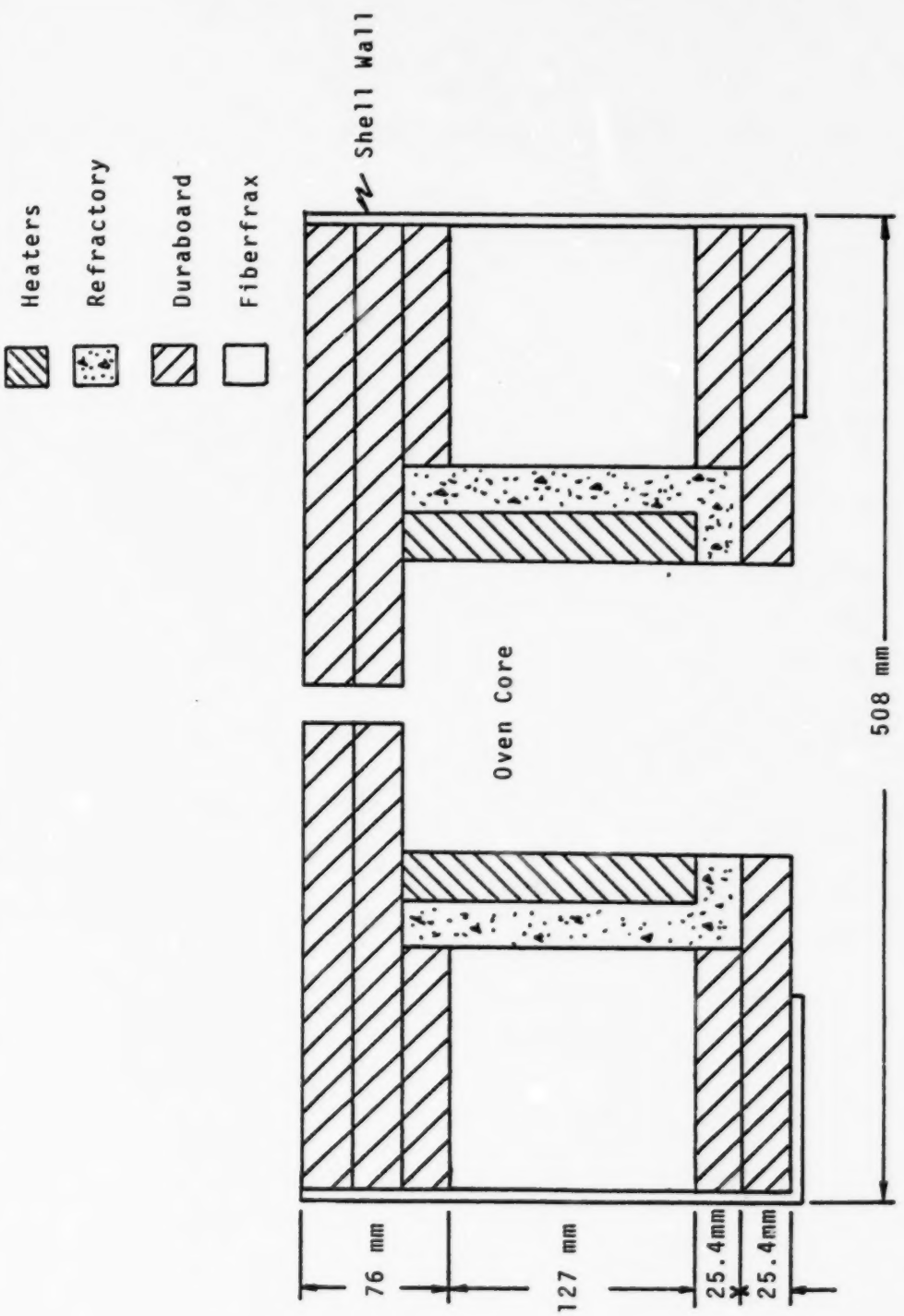

Figure 11 - THERMOVORTACTOR Furnace

TABLE 8 THERMOVORTACTOR Furnace Design Parameters

Inside Diameter (core)	152 mm
Outside Diameter	508 mm
Overall Length	254 mm
Heating Zone Length	152 mm
Refractory Thickness	16 mm
Operating Temperatures	0 to 1200 °C
Power Rating (maximum)	2.3 kw

5.4.5.4 Reactor Furnace

The reactor furnace was used to maintain the entrained bed reactor at the desired reaction temperature. It was a single zone, electrical resistance tubular oven (Model Number 5-165) manufactured by the Mellen Company (Penacook, N.H.). The furnace had an inside diameter of 152 mm, a heating zone length of 762 mm, an overall length of 914 mm, a maximum temperature of 1300°C, and a power rating of 7.2 kw. A model number PS-305-208-40 controller, also supplied by Mellen, was used to regulate the temperature.

5.4.6 Filters

Two filter systems were used in the product stream after quenching. The Bypass filter was used to separate and collect solids during startup and shutdown. These functions were performed by the **Mass Balance** filter during actual steady state experimental conditions. Both units are described in the following sections.

5.4.6.1 Mass Balance Filter

The mass balance filter effected the separation of solids from the product gas suspension during the steady state experimental conditions when mass balance closure was desired. It consisted of a 9.5 mm outside diameter central inlet tube, a cylindrical vessel and two stainless steel Mott filter cartridges with a 2 μm pore size (supplied by Scarborough and Grant of Downsview, Ontario). The entire filter assembly is illustrated in Figure 12.

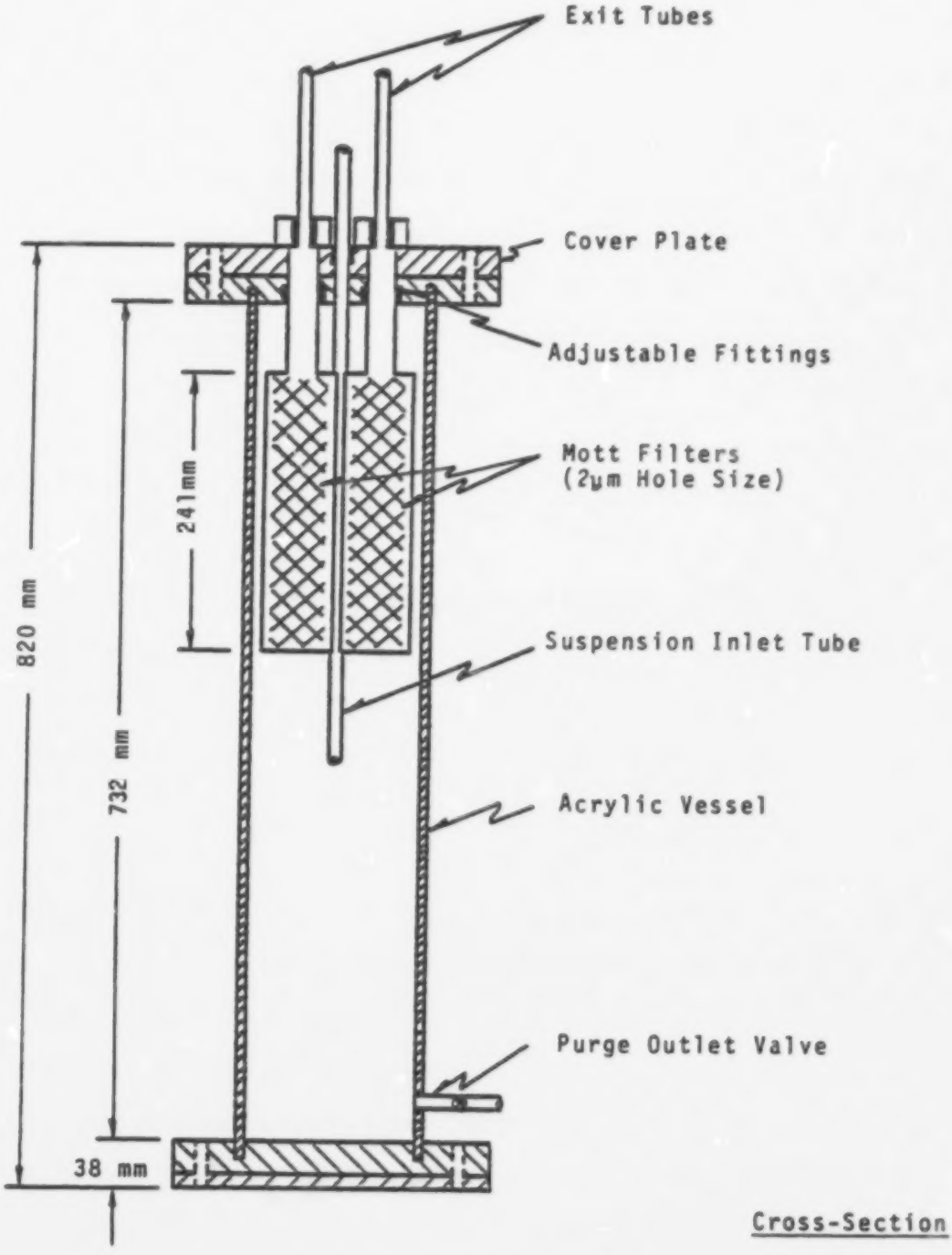

Figure 12 - Mass Balance Filter

TABLE 9 Mass Balance Filter Design Parameters

VESSEL

Inside Diameter	140 mm
Outside Diameter	153 mm
Wall Thickness	6.4 mm
Length	820 mm
Flange Diameter*	267 mm
Flange Thickness*	25 mm
Cover Plate Thickness	25 mm
Construction Material	Acrylic

FILTER (MOTT)

Outside Diameter	67 mm
Length	241 mm
Single Filter Surface Area	$\approx .06\ m^2$
Combined (double) Surface Area	$\approx .12\ m^2$
Pore Size	2 µm
Construction Material	SS 304

MOTT FILTER SUPPLIER

Scarborough and Grant
Downsview, Ontario

* Upper and Lower Vessel Flanges are identical.

The solid suspension entered the vessel through the central tube inlet which was extended below the filter cartridges. Clean gas left the vessel from the top through two exit tubes after passing through the two Mott filters. Solids were allowed to settle to the bottom of the unit and were collected for use in the mass balance closure. A purge valve was installed near the base of the vessel to replace air with nitrogen prior to the start of each experiment. Table 9 presents a summary of the mass balance filter design.

5.4.6.2 Bypass Filter

The bypass filter was used to separate solids from the transport gas during startup and shutdown, thus allowing the venting of a clean gas to atmosphere. The vessel which housed the filter was a 700 mm length of 292 mm inside diameter acrylic pipe. This relatively large diameter ensured that the superficial gas velocity was below the particle settling velocity to enhance solids separation from the gas. The actual filter unit was made from Nitex screening Fabric HD3-10 (Thompson and Company of Scarborough, Ontario) which was formed into a cylindrical shape around an internal support cage. The fabric had a pore size of 10 μm, a surface area of 0.17 m^2, and a superficial face velocity of less than 10 mm/s. Table 10 gives a summary of the bypass filter design.

5.4.7 Vortical Splitter

Since only one stream of CRYOFOR was fed from the CRYOFOR feeder and yet there were two CRYOVORTACTOR CRYOFOR inlets, the suspension had to be split into two nearly identical streams. Experimental tests using variety

TABLE 10 Bypass Filter Design Parameters

VESSEL

Inside Diameter	292 mm
Outside Diameter	318 mm
Wall Thickness	13 mm
Length	700 mm
Flange Diameter*	440 mm
Flange Thickness*	25 mm
Cover Plate Thickness	13 mm
Vessel Construction Material	Acrylic
Cover Plate Construction Material	Aluminum

FILTER

Diameter	89 mm
Length	610 mm
Surface Area	0.17 m^2
Pore Size	10 µm
Filter Fiber Material	NITEX Screen

FILTER FIBER SUPPLIER

Thompson and Co.
Scarborough, Ontario

*Upper and lower vessel flanges are identical.

of splitting units clearly indicated that this would not be an easy task. These cold model tests, utilizing various "Y" and "T" configurations for equal division of the initial single stream, are reviewed in Chapter 7 (Section 7.2).

The difficulty in achieving an equal split was probably due to the segregation of solids and their high momenta while travelling in the transport line. The solids tended to segregate and migrate to one side of the tube wall, especially after exiting a tube elbow or bend. Consequently, if a splitting unit was placed in the line after segregation had occurred, the split would not be equal. It was therefore decided, that a homogeneous suspension would have to be re-created to ensure adequate division of the stream. Another VORTACTOR unit, capable of providing the high turbulence required to homogenize the suspension, was designed and installed in the transport line immediately in front of the splitter. The split ratio into the two CRYOFOR streams was consistently 47 to 53 (expressed as mass percent in each line) or better (i.e. closer to 50:50). A sketch of the vortical splitter is given in Figure 13 and the design parameters are summarized in Table 11.

5.4.8 Gas Sampling Bags

Three gas sampling bags, purchased from Calibrated Instruments Inc. (Ardsley, N.Y.), were connected in parallel and used to collect the product gas. Each of the pillow-shaped bags had a capacity of 170 liters and measured 0.79 meters by 1.40 meters. Their leakproof walls were

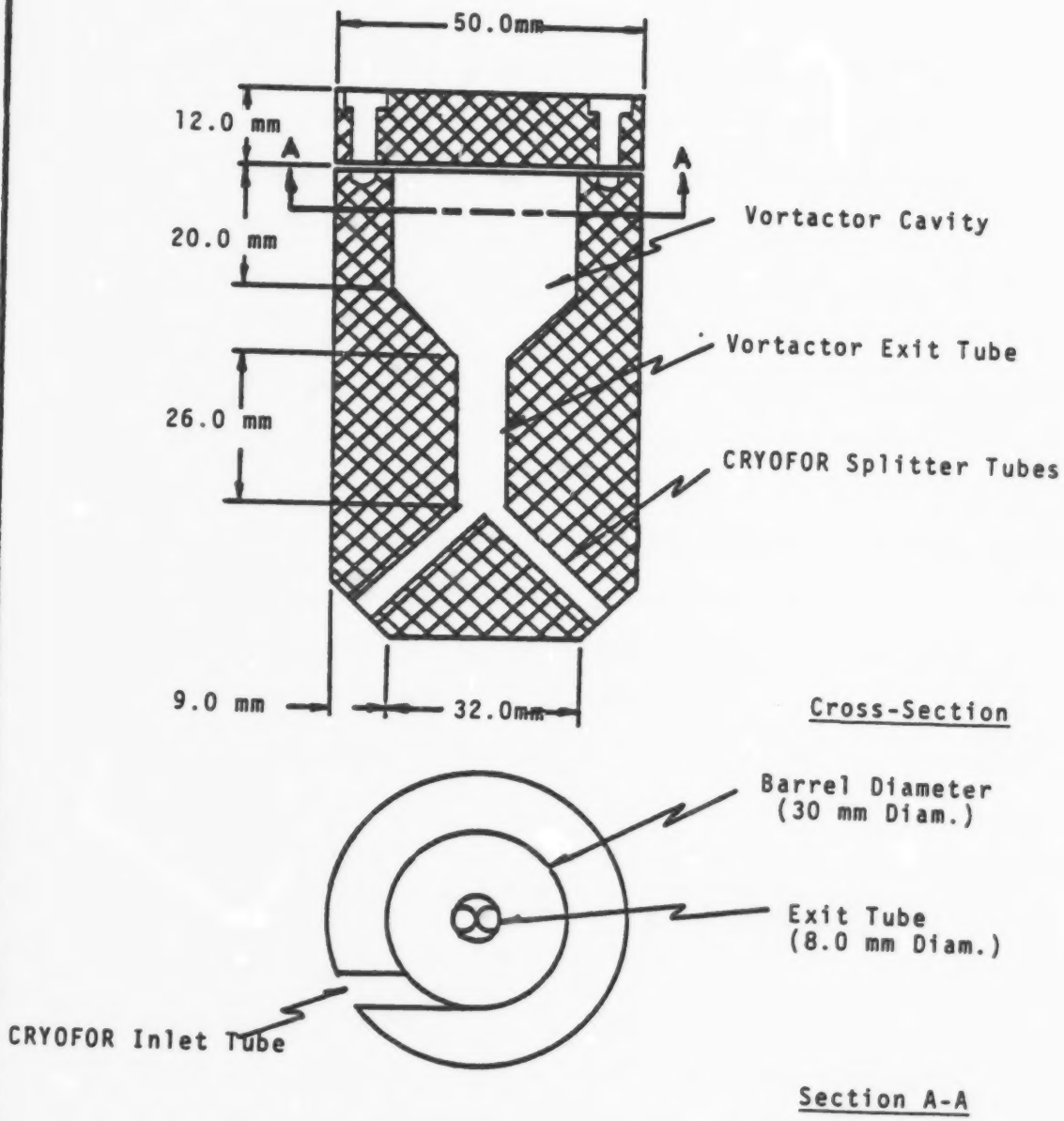

Figure 13 - Vortical Splitter

TABLE 11 Vortical Splitter Design Parameters

Outside Diameter	50 mm
Length	78 mm
Cavity Barrel Inside Diameter	30 mm
Include angle of conical section	90°
Vortactor Exit Tube Diameter	8 mm
Splitter Tube Diameter	4.5 mm
Construction Material	Brass

fabricated from five composite layers consisting of polyethylene, polyamide, aluminum, polyester and polyethylene (from the inner to outer surface). Maximum pressure and temperature ratings were 41 kPa gauge (6 psig) and 120°C, respectively.

The 19 mm inside diameter plastic nozzle on each sample bag was outfitted with a ball valve to control product gas flow from a manifold which was situated at the exit of the mass balance filter vessel. During experiments product gas flowed from the mass balance filter vessel, through the manifold and into the three sample bags through their respective ball valves and nozzles. A Minert valve and Luer lock syringe sampling device supplied by Chromatograhic Specialties Ltd. (Brockville, Ontario) was installed in each of the bag walls to permit sampling for gas chromatographic analysis. After gas analysis was completed, the sample bags were removed from their support structures (with their respective ball valves closed) and their contents were evacuated into the gas collection vessel which is described in the following section.

5.4.9 Gas Collection Vessel

In order to determine the total molar production of product gas after an experimental run, it was decided to either design and construct, or to procure a suitable gas collection vessel. This vessel would be evacuated prior to an experimental run and would then be allowed to draw in the product gas from the sample bags after the gas analysis was completed. Using the ideal gas law, the gas chromatographic analysis, and the differential pressure of the collection vessel (i.e. before and after the

introduction of the product gas), the total number of moles of the gas product (with nitrogen and nitrogen-free) could be calculated.

Since the shop fabrication cost estimates (which were high in order to meet the vacuum requirements) were prohibitive, local commercial gas suppliers were surveyed for cost estimates of standard gas tanks and cylinders. In due course, a Superior propane tank (model #123 USWG) was found to meet the required pressure and volume specifications, and was procured from their Courtland (Ontario) plant.

The tank was a dished cylinder with an outside diameter of 762 mm and an overall height of 1.12 m. Although the nominal tank volume was 0.466 m^3 (123 US gallons), the actual tank volume was experimentally determined to be 0.303 m^3.

6.0 BIOMASS FEEDSTOCKS AND SOLID HEAT CARRIERS

6.1 Biomass Feedstocks

Biomass materials consist primarily of varying proportions of three major constituents - cellulose, lignin and hemicellulose. In the ULTRAPYROLYSIS study, a representative woody bimass (birch wood flour) and two of the three major wood constituents (cellulose and lignin) were tested under similar pyrolytic conditions. These feedstock types were also used in some of the China Lake fast pyrolysis process studies (11).

6.1.1 Cellulose

AVICEL PH-102 crystalline cellulose, supplied by the FMC Corporation (Philadelphia, PA), was used as the representative cellulose feedstock in the ULTRAPYROLYSIS research. It was a free-flowing white powder with an average particle diameter of 100 μm, an as **received** moisture content of 4.0 percent by mass, and an empirical formula of $CH_{1.75}O_{0.89}$. Among the biomass feedstocks tested during the course of this project, cellulose had the highest hydrogen/carbon and oxygen/carbon ratios. Oxygen constituted approximately half of the macromolecule mass. The ultimate (elemental) macromolecule analysis of the AVICEL cellulose is reported in Table 12.

TABLE 12 Biomass Feedstock Analysis

MATERIAL	MASS % MOISTURE AS RECEIVED	C	H	O	S	N	ASH	EMPIRICAL FORMULA
		(WT.% DRY BASIS)						
CELLULOSE (AVICEL)	4.01	43.32	6.30	50.34	0.001	0.02	0.03	$CH_{1.75}O_{0.87}$
LIGNIN (INDULIN AT)	4.75	65.5	5.4	27.2	1.7	-	-	$CH_{0.99}O_{0.31}$
BIRCH WOOD (-100 mesh)	5.54	48.66	6.37	44.33	0.04	0.10	0.5	$CH_{1.57}O_{0.68}$

6.1.2 Lignin

Indulin AT lignin, utilized as the representative lignin in the ULTRAPYROLYSIS study, was extracted from pine through the Kraft process and was supplied by Westvaco of Charleston Heights (South Carolina). Although the actual lignin particle diameters were very small (several μm), they were formed into free flowing agglomerations whose average particle size was 100 μm. The chemical analysis, based on a thousand unit mass, indicated 4.8 methoxyl groups, 3.7 phenolic groups, 1.1 carbonyl groups, 2.1 aliphatic alcohols, 0.5 catechols and 5.8 benzene rings (19). The **as received** moisture content was 4.8 percent by mass.

Due to the aromatic nature of the lignin structure, the hydrogen/carbon ratio approached unity. Furthermore, the Indulin lignin, whose empirical formula was $CH_{0.99}\ O_{0.31}$, possessed the least amount of oxygen (by mass percent) of the feedstocks which were tested. The ultimate (elemental) analysis is given in Table 12. Sulphur, which was present in a thioether form, and a small amount of ammonia, were assumed to be introduced into the lignin during the Kraft process.

6.1.3 Wood

Birch wood flour, purchased from Composition Materials Co. (Stamford, CT), was a cohesive, fibrous biomass which tended to bridge in the feeder. This bridging tendency and poor fluidization qualities necessitated mechanical action to facilitate continuous feeding. The flour

had an average particle size of 85 μm, an empirical formula of $CH_{1.57}O_{0.68}$, and an **as received** moisture content of approximately 5.5 percent by mass. As indicated by the ultimate (elemental) analysis in Table 12, the sample was fairly oxygenated. Cellulose and lignin constituted 40 and 45 percent of the mass, with the remaining 15 percent being primarily hemicellulose (20).

6.2 Solid Heat Carriers

The THERMFOR and CRYOFOR solids were simply F-140 grade silica sand purchased from Wilkinson Foundry Supplies (Toronto, Ontario). Average particle size was 100 μm, the moisture content was less than 0.5 percent by mass, and other physical properties are reported in Table 13.

Cracking catalyst (porous silica/alumina) supplied by the Grace Davidson Co. (Valleyfield, Quebec) was used as the heat carrier for the initial hot experiments. However, its use was discontinued due to an operational problem which was associated with its high moisture content of approximately 20 percent by mass. During the heat up of the cracking catalyst THERMOFOR in the preheater coil assembly (from room temperature to 1100°C), moisture was driven out from the catalyst pores, became vapourized, and was subsequently condensed in the downstream cooling coil. This subsequent condensation caused the formation of a paste with the solids, and resulted in serious plugging of the system. The cooling of the gas was so fast that the condensed water did not have time to re-absorb fully into the catalyst, thus ending up as surface water and leading to cohesive conditions.

An attempt was made to collapse the catalyst pore structure, thereby reducing the ability to carry moisture, by heating at 900°C for four hours. The resultant moisture content, which remained relatively constant after prolonged exposure to ambient atmospheric conditions, was 3 percent by mass. However, a lack of facilities to treat bulk quantities of catalyst (i.e. 300 kg) rendered this procedure unsuitable.

TABLE 13 THERMOFOR (Silica Sand) Analysis

Physical Analysis

U.S. Sieve No.	Millimeter Designation	Mean % on Sieve	Std. Dev.	Mean % Cumulative	Mean % Passing
40	.420	-	-	-	100.0
50	.297	0.4	1.2	0.4	99.6
70	.210	2.0	1.2	2.4	97.6
100	.149	8.0	3.1	10.4	89.6
140	.105	35.5	5.3	45.9	54.1
200	.074	31.0	3.4	76.9	23.1
270	.053	12.4	2.5	88.3	11.7
PAN		10.5	1.9	98.8	0.0

	Mean
AFS Grain Fineness[1]	142.0
Actual Surface Area[2] (cm^2/gm)	317.4
Base Permeability[3]	18.1
Theoretical Surface Area[4] (cm^2/gm)	264.5
Coefficient of Area[5]	1.2
Density (Uncompacted)[6] (lb/ft^3)	86.8
Density (Compacted)[7] (lb/ft^3)	92.0

Chemical Analysis

SiO_2	99.188
Fe_2O_3	0.102
TiO_2	0.169
Al_2O_3	0.431
CaO	<.01
MgO	<.01
LOI[8]	0.10

Table 13 Thermofor (Silica Sand) Analysis (continued)

1. Standard used by the American Foundry Association to represent the average particle size of the sand grain. The grain number represents the mesh number of the sieve that will allow the average grain size in the sample to pass through.

2. The actual surface area of the sand grain measured by a surface area measuring instrument developed by the Detrich Company, Detroit, Michigan.

3. Porosity of the compacted sand.

4. Estimated surface area of the grain based on the sieve analysis results.

5. The ratio of the actual to the theoretical surface area.

6. Loose form bulk density.

7. Bulk density measured when the sand is compacted.

8. Loss on ignition.

7.0 COLD MODELLING STUDIES

7.1 VORTACTOR

The VORTACTOR design was constantly refined during the course of the ULTRAPYROLYSIS project with the use of cold model prototypes. Three prototypes, constructed from plexiglass or glass for visual assessment of performance, were tested and are summarized in the following sections.

7.1.1 VORTACTOR Mark I

The first cold model VORTACTOR (Mark I), which is illustrated in Figure 14, was designed to effect the solids mixing in the throat of the cyclonic cavity. A single THERMOFOR jet was injected tangentially into the vessel barrel and a negative pressure was assumed to exist in the throat region (i.e. at the cone apex) due to the formation of the vortex. The biomass suspension would then be injected into this reduced pressure region where efficient mixing was expected to occur.

The Mark I version consisted of two concentric cones and cylinders. The outer cone was made from a glass funnel which was fastened to a length of acrylic tubing thus forming the cylindrical barrel. The inner cone and barrel were machined from a plexiglass rod. The variable gap between the two bodies was assumed to enhance the regulation and control of the THERMOFOR flow pattern and vortex characteristics. This design also

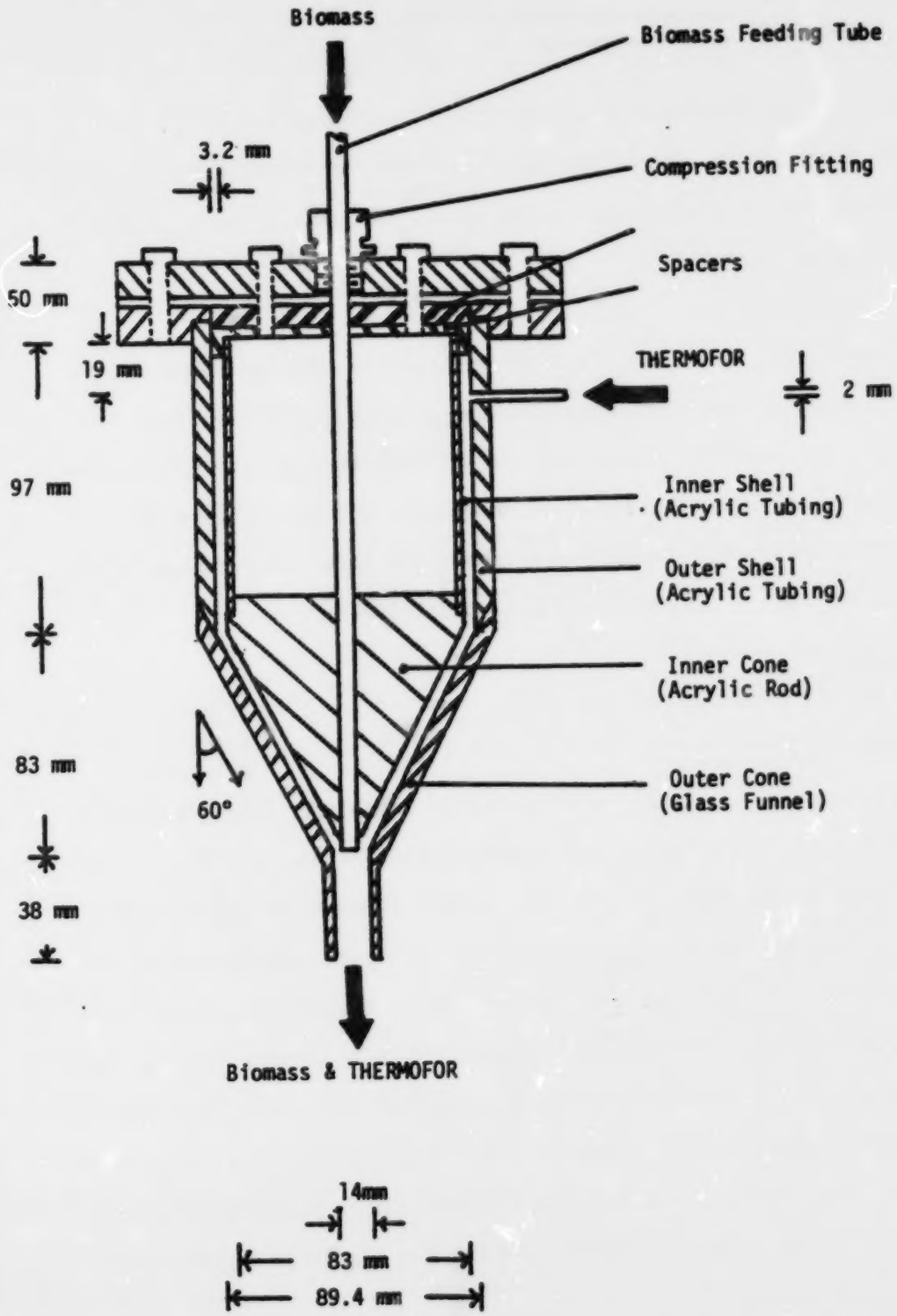

Figure 14 - VORTACTOR Mark I

provided for the installation of sufficient insulation around the biomass injector tube (at the axis of the inner cylinder) which would prevent premature pyrolysis of the biomass in the actual hot unit prior to injection into the throat region.

Although two gaps (1.5 and 3 mm) were tested, the weak flow pattern which resulted in each case prevented the observation of any significant effects. The THERMOFOR stream had not yet completed a full turn in the annulus before losing its tangential momentum and dropping straight down to the cone apex. The barrel diameter and gap width were thought to be too large for the jet to maintain its vortical flow pattern.

7.1.2 VORTACTOR Mark II

As a result of the tests with the Mark I prototype, a smaller design was selected and the idea of two concentric bodies was discarded. The acrylic Mark II version had a barrel inside diameter of 34 mm and an included angle for the conical section of 90° (corresponding values for the Mark I unit were 83 mm and 120°). These smaller dimensions were selected to increase the tangential momentum and thereby enhance the vortex strength. In addition, a second tangential inlet was incorporated for biomass injection in place of the axial inlet which was used initially. The THERMOFOR was injected tangentially in a clockwise direction while the biomass was introduced in a counter-clockwise directiion.

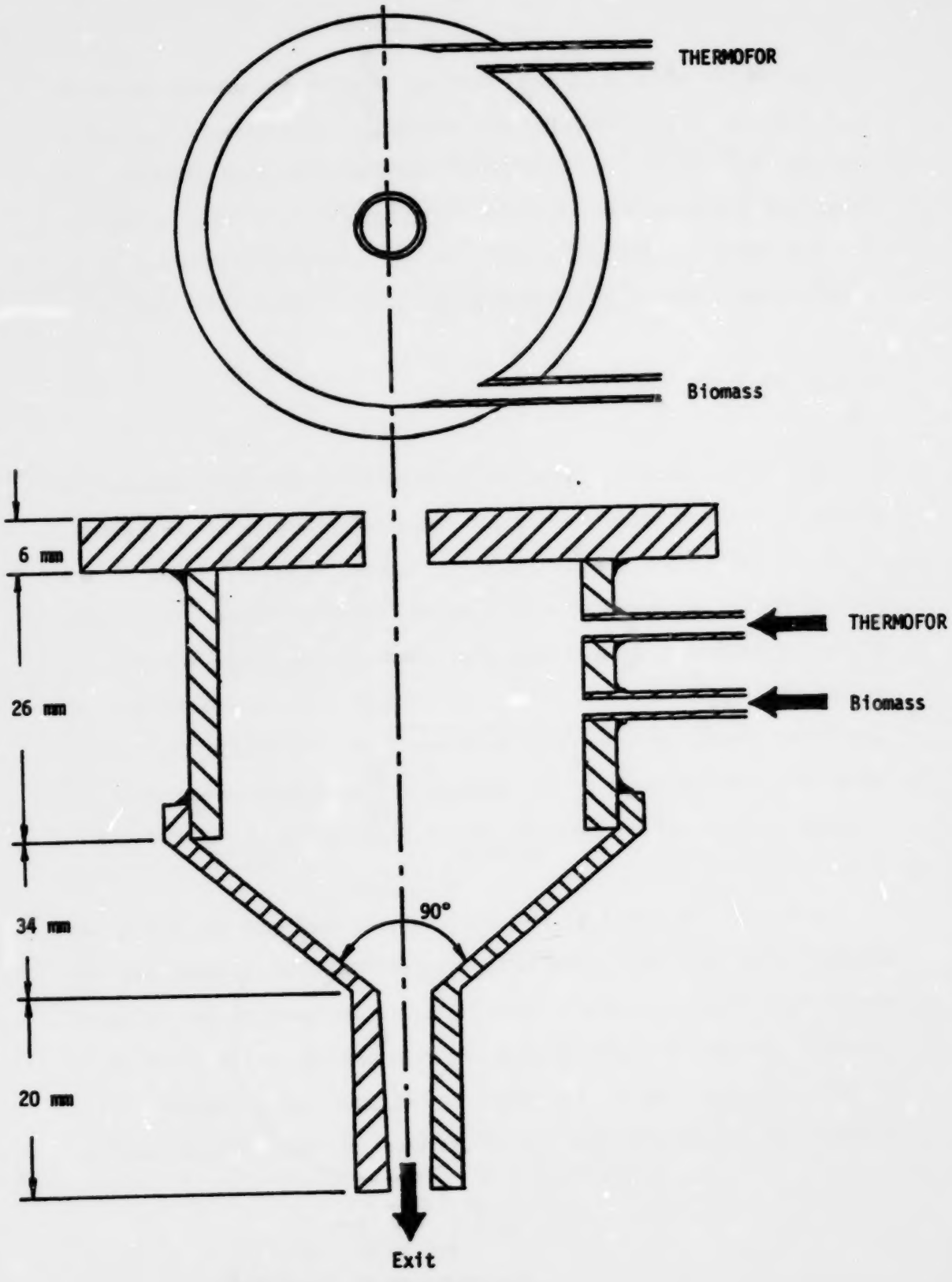

Figure 15 - VORTACTOR Mark II

During the actual cold model testing, in which the nominal gas residence time was 30 milliseconds, good mixing was qualitatively observed at the cone apex and the vortex strength appeared to be much improved. The tangentially opposed mode of solids injection was found to be a superior means of achieving thorough mixing, and was consequently retained in the later designs. Figure 15 illustrates the Mark II unit.

7.1.3 VORTACTOR Mark III

The third generation VORTACTOR retained the tangentially opposed jet mixing concept yet added a third jet for axial injection of the biomass. In this version, the counter-clockwise biomass injection (used in the Mark II design) was replaced with a second THERMOFOR stream. The momenta of the two tangential streams were thus similar in magnitude, and were expected to provide an ideal mixing environment (i.e. severe turbulence) when these momenta were mutually destroyed. It was assumed that mixing would be further enhanced by the momentum of the biomass stream which was injected axially into the turbulent region from the top of the VORTACTOR.

Tests with the VORTACTOR Mark III confirmed that superior mixing was achieved with the two tangentially opposed THERMOFOR streams and the single axial biomass stream. These tests are reviewed in the following section. The Mark III unit (Figure 16) retained the included cone angle of 90° which was used in the Mark II unit, but had a smaller inside diameter of 28 mm for the barrel section of the internal cavity.

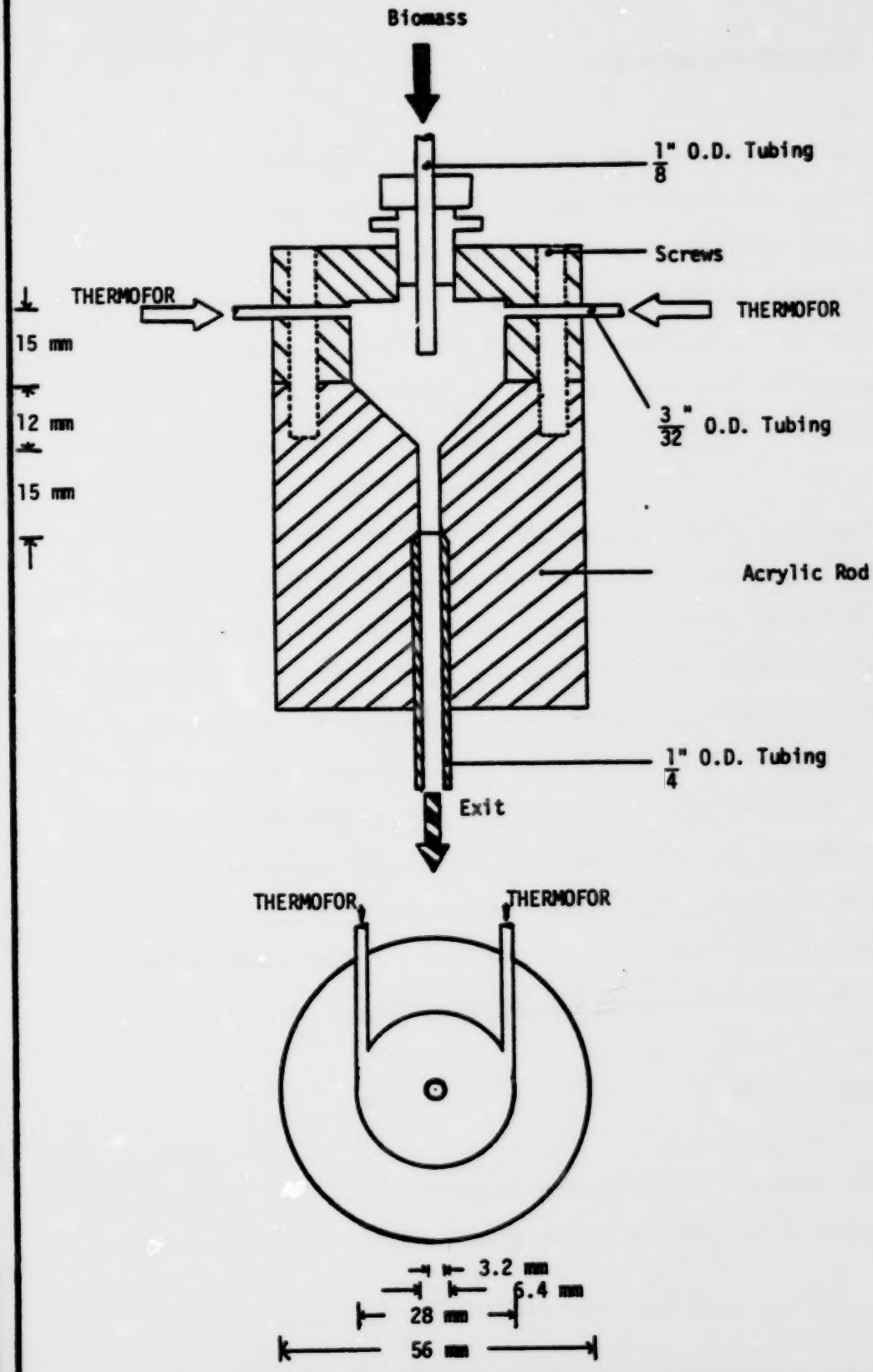

Figure 16 - VORTACTOR Mark III

7.1.4 VORTACTOR Mixing Studies

Visual observation of the performance of the VORTACTOR Mark III gave a preliminary indication that good solids mixing was possible with this design. Additional mixing studies were therefore initiated in an experimental apparatus which is illustrated in Figure 17. Stained cracking catalyst was used to simulate the biomass particles and was fed pneumatically into the VORTACTOR from the central axial inlet. Unstained catalyst, representing the THERMOFOR, was fed into the two opposed tangential inlets. During the startup and shutdown of the testing period, solids were shunted by a three way valve to a collection device. During the actual test period, which lasted for a fraction of a second, the three way valve directed the mixed solids to a large cylindrical vessel (0.23 m diameter). Due to the large diameter, the solid particles fell freely to the vessel base where a microscope slide, precoated with glue, was located. Observation of the very thin layer of solids which were deposited on the slide, indicated that excellent mixing had occurred for the double opposed THERMOFOR jet configuration. Although tests using a single THERMOFOR stream demonstrated adequate mixing, performance of the latter was inferior to that of the former. Consequently, the double THERMOFOR jet VORTACTOR design was selected for the hot unit.

7.2 CRYOFOR Splitter

Several types of splitters were investigated in order to achieve equal division of the CRYOFOR stream prior to its tangentially opposed

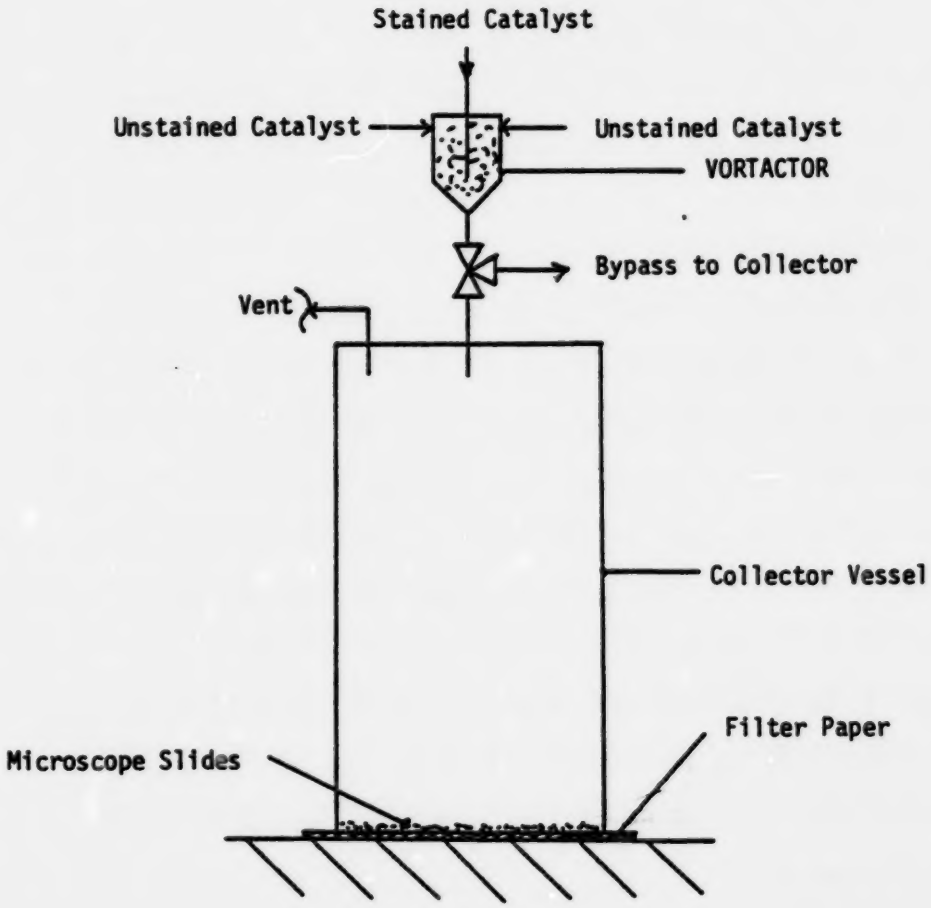

Figure 17 - Mixing Experiment Apparatus

double injection into the CRYOVORTACTOR. A simple Y shape, a T shape, a T shape with a trough, and flow straighteners at the splitter inlet were among the configurations and techniques used to effect an equal split.

A polypropylene Y shaped tubing connector was first tested in both a horizontal and a vertical position as reported in Tables 14 and 15, respectively. In the horizontal position, most of the splits were 55:45 (expressed as a percentage of the suspension mass in each of the two divided streams) or better (i.e. closer to 50:50). In all but two of the tests, the division was 60:40 or better. Although these results were relatively good compared to other configurations, they were not considered to be sufficiently reproducible to warrant the use of the horizontal Y splitter design in the actual hot unit (i.e. consider Runs S-28 to S-30 in Table 14 which were conducted under similar test conditions). Results with the Y tubing connector in the vertical position were poorer with respect to equal division of the stream and were less reproducible.

A second Y splitter, machined from plexiglass, was used in the next set of experiments. As is indicated in Table 16, the results were fairly reproducible but the split of approximately 70:30 was skewed in favour of the left arm of the Y .

A commercial T splitting device was procured for testing from the Ducon Company (Minneola NY). This device consisted of a jet tube along the T centerline which led to a trough (cavity) at the end of the

centerline. The trough was formed in the bar of the T and the bar led to the two exits of the splitting unit in opposite directions. It was expected that the jet of suspended solids would impact on the trough wall at the end of the T centerline. The resulting turbulence would then tend to homogenize the suspension and lead to an equal division of the suspension.

The results, as reported in Table 17, indicated an inadequate and nonreproducible split of the solids. It was apparent that the split ratio depended on the alignment of the central tube of the T , and it was assumed that the solids were already segregated prior to entering the splitter. This segregation, which would contribute to unequal division of the stream, was probably due to the large momentum of the solids and the migration towards the outside walls of bends in the transport line.

Flow straighteners, which were simply a series of smaller tubes bundled together, were used in an attempt to reduce segregation of the solids. However, due to the small diameter of these tubes (1.2 mm inside diameter), intermittent line blocking of some of the tubes was observed. This phenomenon indirectly confirmed that solids segregation ws in fact occurring even before entrance to the flow straightening section.

Table 18 summarizes the results of tests with the machined Y plexiglass device (mounted horizontally) which was modified with two screws installed in the splitter exits. The depth of screw penetration into the exits could be adjusted thus simulating the action

of miniature slide valves to control backpressure (and thus the flow through each of the two outlets). The results clearly indicated that the division of solids was not equal nor reproducible.

The final splitter design incorporated a small VORTACTOR unit which was intended to effect the re-entrainment of segregated solids into a homogeneous suspension. It was thought that subsequent splitting of the resulting pseudo single phase suspension in a Y splitter would be a relatively easy task. Consequently, a "vortical splitter" concept, which consisted of the Y plexiglass device positioned immediately after a small VORTACTOR, was tested. The reproducible test results, as reported in Table 19, clearly indicated that this approach would be suitable to achieve an equal division of the CRYOFOR stream in the actual ULTRAPYROLYSIS system. It is important to note that the VORTACTOR had to be placed in close proximity to the splitter to prevent re-segregation prior to division of the CRYOFOR solids stream.

TABLE 14 Results of Splitting Experiments Using a Horizontal Propylene Y Connector

Run No.	Solids Flow Rate(g/min)		Solids Loading (g solids/ g gas)	Gas Superficial Velocity (m/s)	Feeder Pressure (kPa gauge)	Solids Split (%)	
	Left Arm of Y	Right Arm of Y				Left Arm	Right Arm
S-1	70.14	88.21	38.7	4.19	94.2	44.3	55.7
S-2	61.65	88.03	45.4	3.40	92.2	41.2	58.8
S-3	81.98	75.92	39.2	4.13	94.2	51.9	48.1
S-4	77.70	77.80	38.9	4.09	93.2	50.0	50.0
S-5	72.33	80.59	46.2	3.42	93.2	47.3	52.7
S-6	74.82	74.07	45.9	3.35	94.2	50.3	49.7
S-7	41.82	58.34	7.8	12.71	92.2	41.8	58.2
S-8	42.66	55.10	7.6	12.78	91.2	43.6	56.4
S-9	43.27	97.27	25.2	5.64	91.2	30.8	69.2
S-10	73.60	67.24	25.8	5.52	92.2	52.3	47.7
S-24	12.78	24.79	13.9	2.69	44.6	34.0	66.0
S-25	6.95	6.86	1.5	8.86	28.4	50.3	49.7
S-26	6.86	7.17	1.6	8.82	27.4	48.9	51.1
S-27	6.82	7.24	1.6	8.86	27.4	48.5	51.5
S-28	15.07	18.55	6.8	4.88	26.3	44.8	55.2
S-29	16.79	16.06	6.7	4.84	26.3	51.1	48.9
S-30	16.01	17.21	6.9	4.76	26.3	48.2	51.8
S-31	2.74	3.54	0.7	8.44	22.3	43.6	56.4
S-32	2.81	3.94	0.8	7.86	22.3	41.6	58.4

TABLE 15 Results of Splitting Experiments Using a Vertical Propylene Y Connector

Run No.	Solids Flow Rate(g/min)		Solids Loading (g solids/ g gas)	Gas Superficial Velocity (m/s)	Feeder Pressure (kPa gauge)	Solids Split (%)	
	Left Arm of Y	Right Arm of Y				Left Arm	Right Ar
S-44	68.41	38.96	8.9	11.98	94.2	63.7	36.3
S-45	63.75	42.67	8.9	11.84	95.2	59.9	40.1
S-46	63.13	42.12	8.5	12.30	95.4	60.0	40.0
S-47	3.14	4.38	8.9	18.30	24.3	41.8	58.2
S-48	2.78	4.00	0.8	8.58	23.3	41.0	59.0
S-49	2.68	4.03	0.8	8.29	23.3	39.9	60.1
S-50	2.77	3.99	0.8	8.28	22.3	41.0	59.0
S-51	2.50	3.89	0.8	8.27	22.3	39.0	61.0

TABLE 16 Results of Splitting Experiments Using a Horizontal Machined Plexiglass Y Device

Run No.	Solids Flow Rate(g/min)		Solids Loading (g solids/ g gas)	Gas Superficial Velocity (m/s)	Feeder Pressure (kPa gauge)	Solids Split (%)	
	Left Arm of Y	Right Arm of Y				Left Arm	Right Arm
S-41	78.6	31.3	11.1	9.94	92.2	71.5	28.5
S-42	74.1	35.0	10.2	10.66	92.2	67.9	32.1
S-43	81.4	28.9	11.8	9.27	93.2	73.8	26.2

TABLE 17 Results of Splitting Experiments Using a Horizontal Commercial Ducon T Device

Run No.	Solids Flow Rate(g/min)		Solids Loading (g solids/ g gas)	Gas Superficial Velocity (m/s)	Feeder Pressure (kPa gauge)	Solids Split (%)	
	Left Arm of T	Right Arm T				Left Arm	Right Arm
S-37*	35.64	57.88	5.7	16.19	91.2	38.0	62.0
S-38*	50.00	43.82	7.1	13.08	91.2	53.3	46.7
S-39*	34.45	68.11	8.6	11.81	91.2	33.6	66.4
S-40*	59.55	39.90	8.6	11.40	91.2	60.0	40.0
S-33+	41.37	67.98	9.1	11.90	91.2	37.8	62.2
S-34+	52.47	83.89	21.8	6.31	91.2	38.5	61.5
S-35+	27.16	81.64	9.4	11.44	91.2	25.0	75.0
S-36+	49.92	63.97	9.7	11.21	92.2	40.2	59.8

NOTE:

* trough with 1/4" depth.

+ trough with 1/16" depth.

TABLE 18 Results of Splitting Experiments Using a Horizontal Machined Plexiglass Y Device with Adjusting Screws

Run No.	Solids Flow Rate(g/min)		Solids Loading (g solids/ g gas)	Gas Superficial Velocity (m/s)	Feeder Pressure (kPa gauge)	Solids Split (%)	
	Left Arm of Y	Right Arm of Y				Left Arm	Right Arm
S-12	55.85	30.79	23.6	3.66	50.7	64.5	35.5
S-13	48.36	33.84	20.4	4.04	47.6	58.8	41.2
S-14	56.09	27.37	23.0	3.66	49.6	67.2	32.8
S-15	44.28	21.76	5.4	12.16	66.9	67.0	33.0
S-16	32.89	16.32	4.6	10.66	66.9	66.8	33.2
S-17	38.14	20.97	6.4	9.20	67.9	64.5	35.5
S-18	38.77	21.78	6.5	9.27	67.9	64.0	36.0
S-19	55.91	22.22	11.8	6.60	67.9	71.6	28.4
S-20	30.74	34.90	12.0	5.46	67.9	46.8	53.2
S-21	38.77	39.26	18.2	4.30	69.9	49.7	50.3
S-22	41.95	42.39	19.2	4.40	70.9	49.7	50.3
S-23	38.99	31.80	14.8	4.79	70.9	55.1	44.9

TABLE 19 Results of Splitting Experiments Using the Vortactor and Vertical Machined Plexiglass Y Assembly

Run No.	Solids Flow Rate (g/min)		Solids Loading (g solids/ g gas)	Gas Superficial Velocity (m/s)	Solids Split (%)	
	Left Arm of Y	Right Arm of Y			Left Arm	Right Arm
S-52	49.6	51.4	20.0	4.2	49.1	50.9
S-53	51.1	51.2	19.3	4.4	50.0	50.0
S-54	51.1	49.7	22.2	3.8	50.7	49.3
S-55	49.9	49.8	20.6	4.0	50.0	50.0
S-56	53.1	47.2	20.6	4.1	53.0	47.0
S-57	47.0	51.2	20.5	4.0	47.9	52.1
S-58	43.0	46.0	18.8	4.0	48.3	51.7
S-59	49.0	51.7	21.6	3.9	48.7	51.3
S-60	51.8	48.4	22.5	3.7	51.7	48.3
S-61	48.5	50.4	21.9	3.8	49.0	51.0
S-62	32.7	30.4	23.9	2.2	51.9	48.1

7.3 General Feeder Studies

The solids mass flowrate of the fluidized bed feeders was controlled by manipulating the bed pressure and the volumetric flowrate of the transport gas. A portion of the gas, which entered the feeders either as the fluidizing or transport gas, was vented from the units through a valve/rotameter assembly. The feeder pressures were thus controlled with this assembly.

In order to better characterize the general behaviour of fluidized bed feeders, the THERMOFOR feeder was selected for cold model studies. The following experimental parameters were investigated:

(i) The solids loading (solids mass per unit transport gas mass) as a function of the coil gas superficial velocity (i.e. in the coiled transport line) at constant feeder pressure.

(ii) The solids loading as a function of feeder pressure at practically constant coil gas superficial velocity.

(iii) The solids mass flowrate as a function of the coil gas superficial velocity at constant feeder pressure

(iv) The solids mass flowrate as a function of the feeder pressure at practically constant coil gas superficial velocity.

During the tests, cracking catalyst was used as the bed material and the feeder pressure was kept between 50 and 100 kPa gauge (7.3 to 14.7 psig). The solids passed from the feeder through a coiled 15 meter length

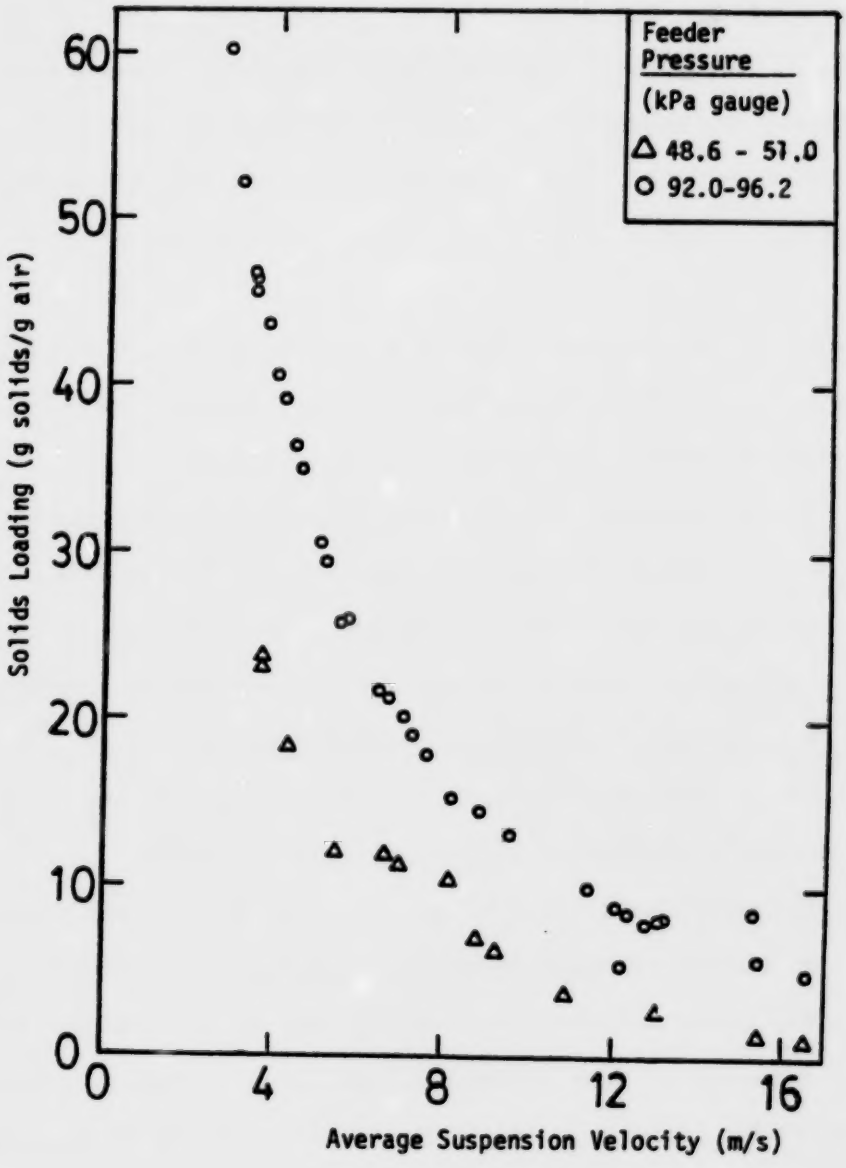

Figure 18 - THERMOFOR Feeder Test Results: Solids Loading vs Coil Gas Superficial Velocity at Constant Feeder Pressure.

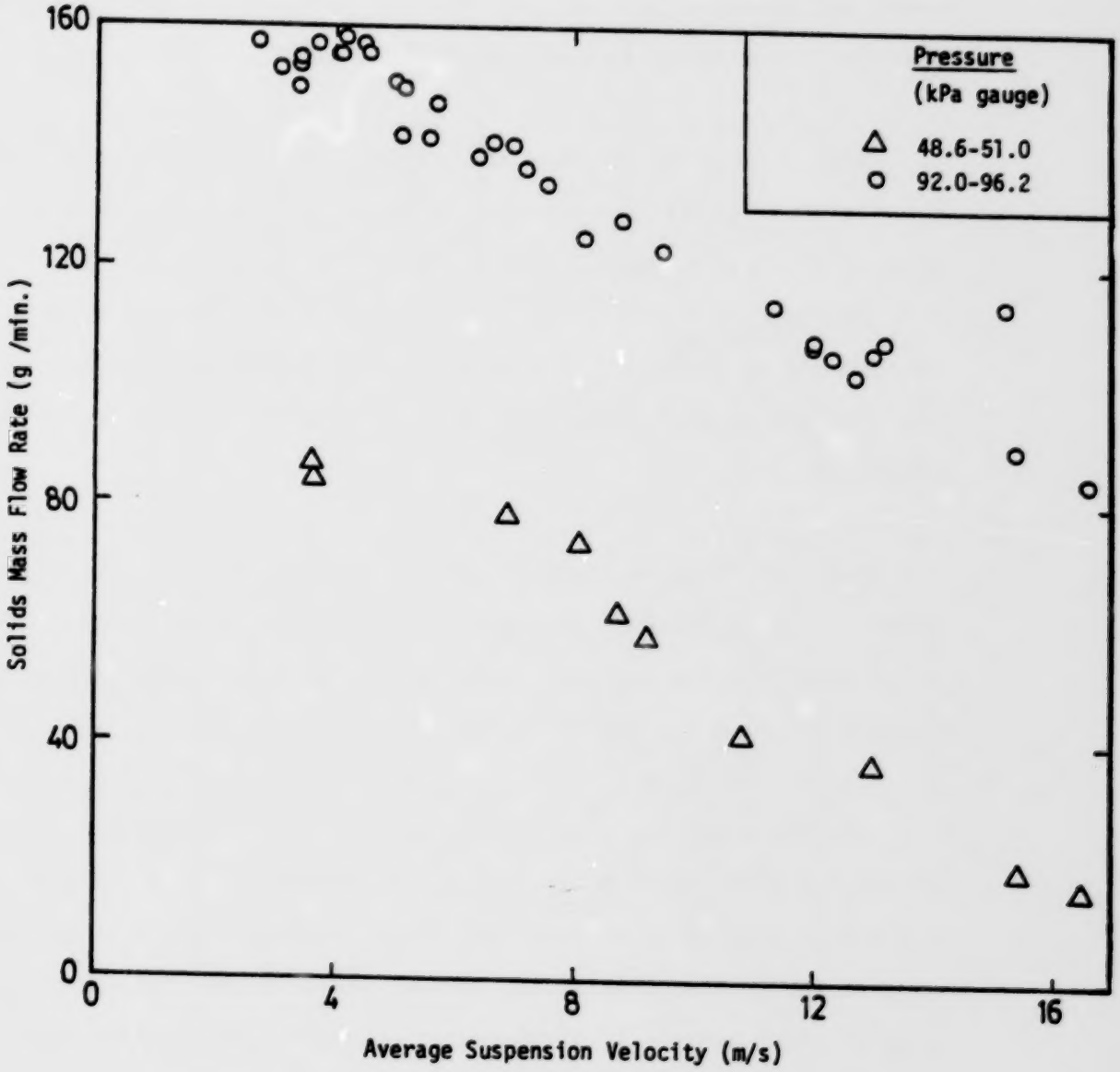

Figure 19 - THERMOFOR Feeder Test Results: Solids Mass Flowrate vs Coil Gas Superficial Velocity at Constant Feeder Pressure.

of 4.6 mm inside diameter polyethylene tubing (with a coil diameter of 100 mm), and was collected in a filter vessel. The vessel, whose weight was known, was connected to a wet test meter to determine the gas volumetric flowrate. Experimental data are reported in Figures 18 to 22.

Under conditions of constant feeder pressure, the lower gas superficial velocities in the coil resulted in higher solids loading (Figure 18). For a feeder pressure of 101 kPa gauge (14.7 psig) and a coil gas superficial velocity of approximately 3 m/s, the solids loading was 60 grams of solids per gram of gas. This loading corresponded to a mass flowrate of approximately 160 grams of cracking catalyst per minute (Figure 19).

Under conditions of constant gas superficial velocity, the higher feeder pressures resulted in higher solids loading (Figure 20). The solids mass flowrate was also increased, in a linear relationship, at elevated pressures as reported in Figure 21.

Additional testing with Avicel cellulose in the biomass feeder reflected similar behaviour to that of the THERMOFOR feeder. Figure 22 illustrates that a relatively low solids loading for cellulose was achieved due to the lower solids density and a smaller transport line diameter (i.e. compared to corresponding values for the THERMOFOR tests). At feeder gauge pressures between 42 and 47 kPa (6.1 to 6.8 psig), the loading was between 1 and 15 grams of cellulose per gram of gas.

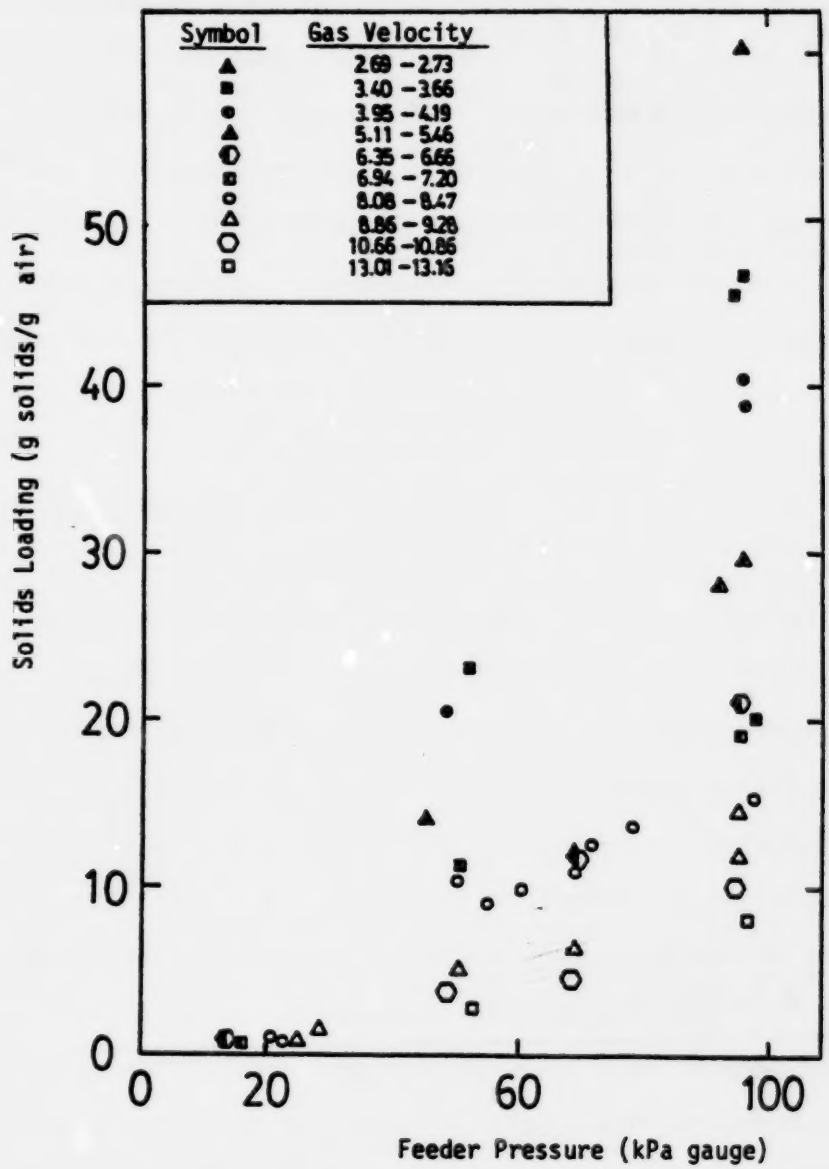

Figure 20 - THERMOFOR Feeder Test Results: Solids Loading vs Feeder Pressure at Constant Coil Gas Superficial Velocity.

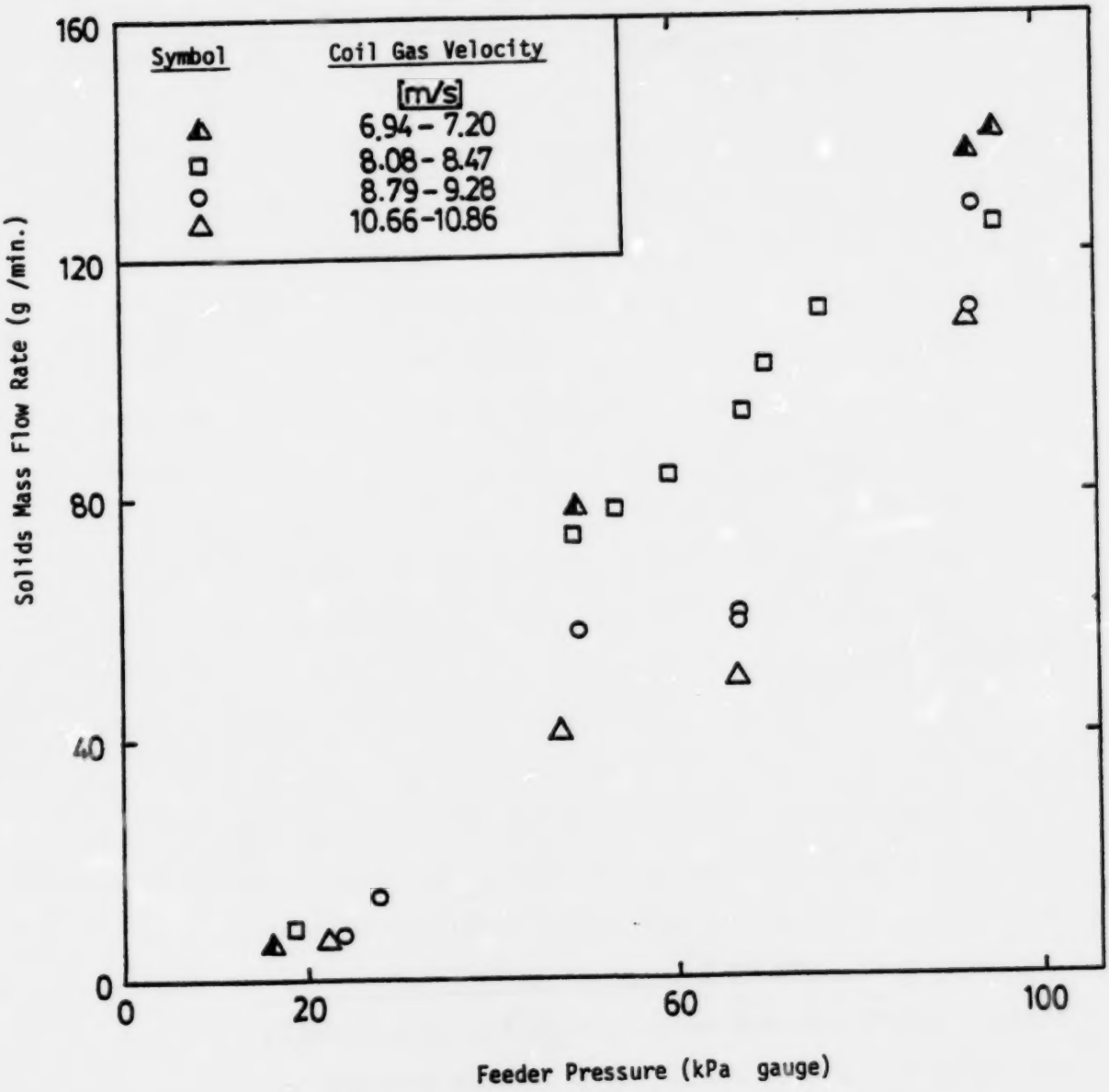

Figure 21 - THERMOFOR Feeder Test Results: Solids Mass Flowrate vs Feeder Pressure at Constant Coil Gas Superficial Velocity.

Some generalizations relating to the general behaviour of the fluidized bed feeders were made during the course of the cold model testing program. First, it was extremely difficult to independently adjust the solids mass flowrate, the solids loading, or the suspension velocity without directly affecting one or both of the other parameters. Second, the solids flow tended to pulsate at low transport line velocities and at high solids loadings. At higher velocities and lower loadings, the flowrate was smoother. The pulsation phenomenon was probably caused by bubbles which were generated in the fluidized bed and subsequently passed through the transport line injection region.

7.4 Wood Feeder Studies

Wood flour is extremely difficult to feed in a continuous steady manner due to its fibrous and cohesive nature. This nature lends itself to the formation of bridges and pockets in the feeding device. Dr. D.S. Scott and his co-workers at the University of Waterloo (Waterloo, Ontario) successfully developed a mechanical stirred feeder in their fluidized bed flash pyrolysis process. Although the feedrate was relatively constant, the small pulsations due to the stirring rotation and the paddle spacing were thought to be unacceptable in the ULTRAPYROLYSIS process where reactor residence times are measured in terms of milliseconds (therefore the process is very sensitive to even minor perturbations of flow). Consequently, a pneumatic stirring approach was considered to effect the continuous steady feeding of particulate biomass.

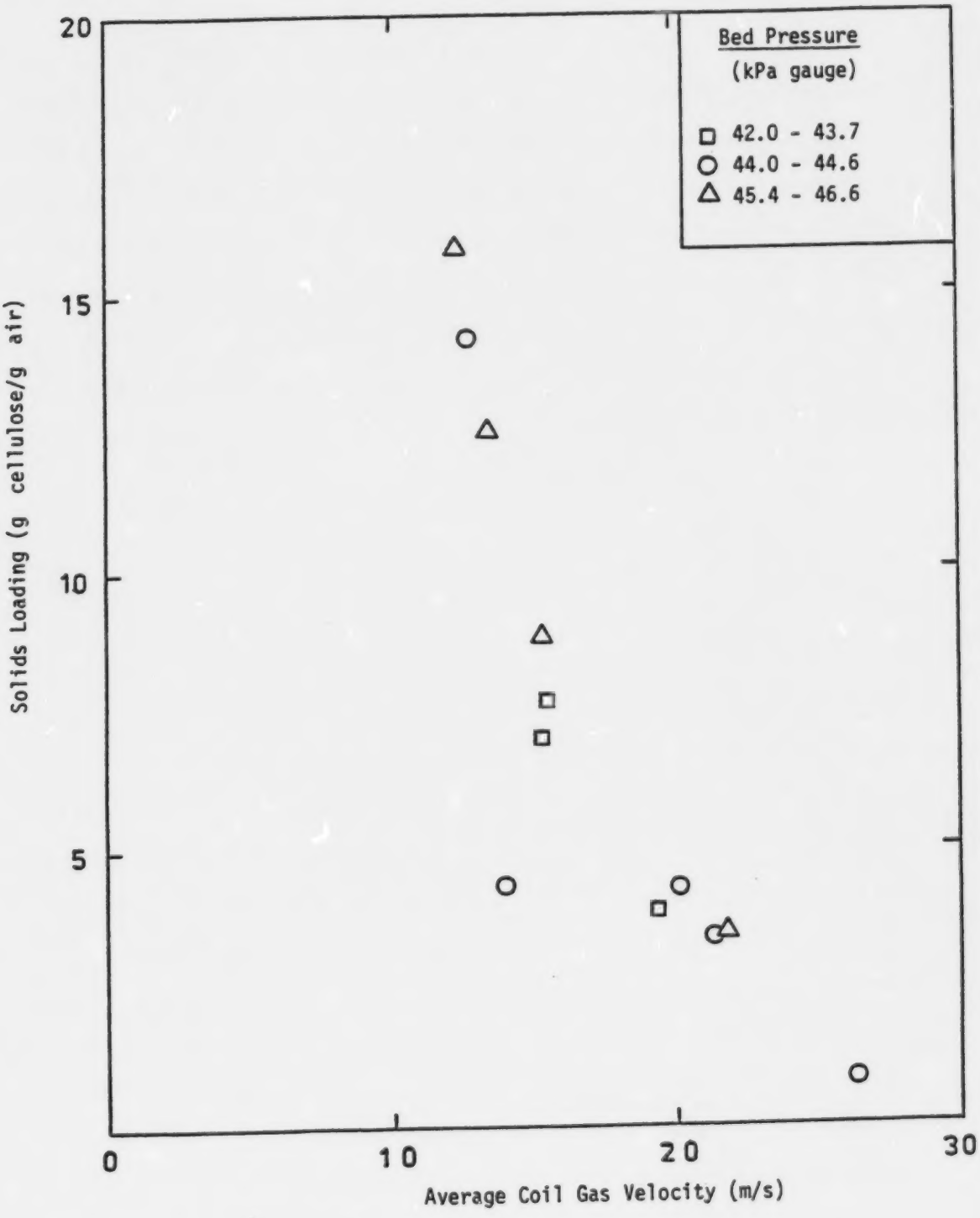

Figure 22 - Biomass Feeder Test Results: Solids Loading vs Coil Gas Superficial Velocity at Constant Feeder Pressure.

A total of three feeder concepts, all of which were designed to accomplish the movement of biomass particulate solids by pneumatic means, were built and tested. These included a spouted bed, a downflow feeder and a ring feeder.

In the spouted bed feeder, as illustrated in Figure 23, the transport line was placed directly above the gas line with a gap between the two lines. A spout at the top of the bed and an annulus of low solids density in the gap region, were formed when the transport gas was flowing. Part of the wood in the annulus was fed into the transport line and carried away (i.e. out of the feeder). The remainder of the wood in the annulus was ejected from the bed surface, thus forming the spout, and was recirculated within the feeder. Visually, the solids feed rate appeared to be steady and continuous. This steadiness of flow and also the reduction of transport gas consumption, were significant advantages over the fluidized bed transport line feeder. The absence of bubble interference (which occurred in the fluidized bed) was assumed to reduce the feedrate pulsations, while the requirements for local aeration only in the gap region minimized the flow of transport gas.

The downflow feeder (Figure 24) utilized a coil of copper tubing, with several 2.4 mm diameter holes drilled along the length, as the gas line. A transport line was installed from the base of the feeder at the central axis, and extended part of the way into the annulus of the coil. Transport gas entered from the top of the feeder and passed down through

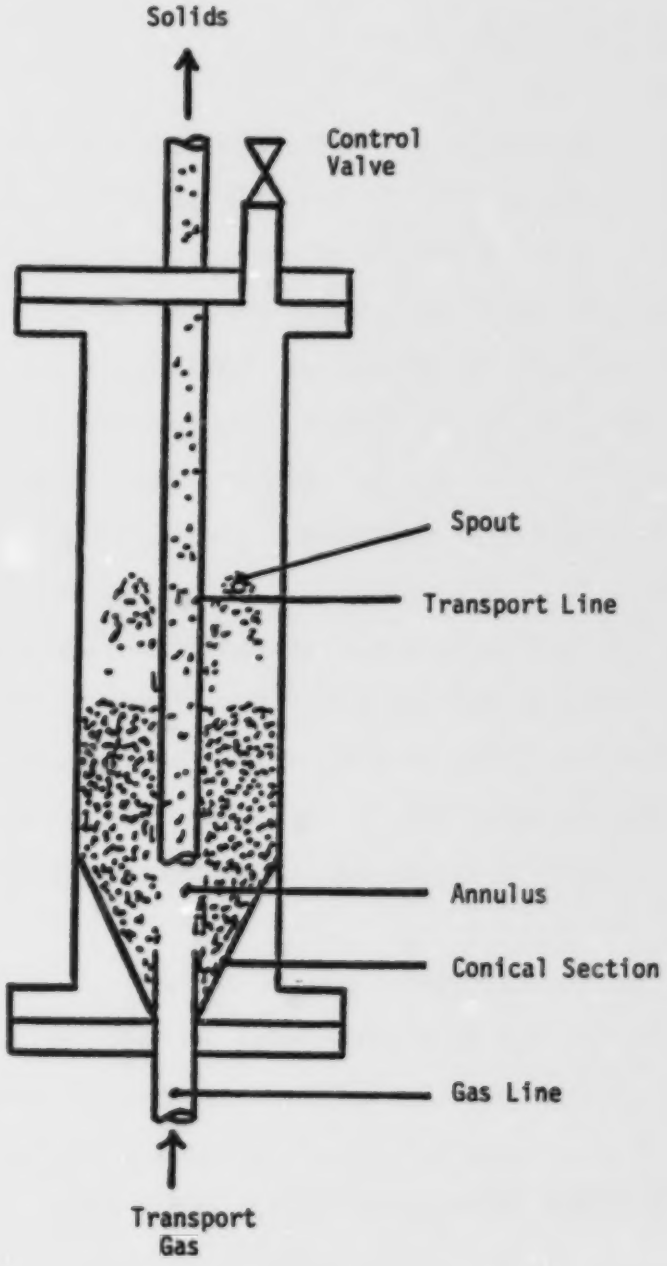

Figure 23 - Spouted Bed Wood Feeder

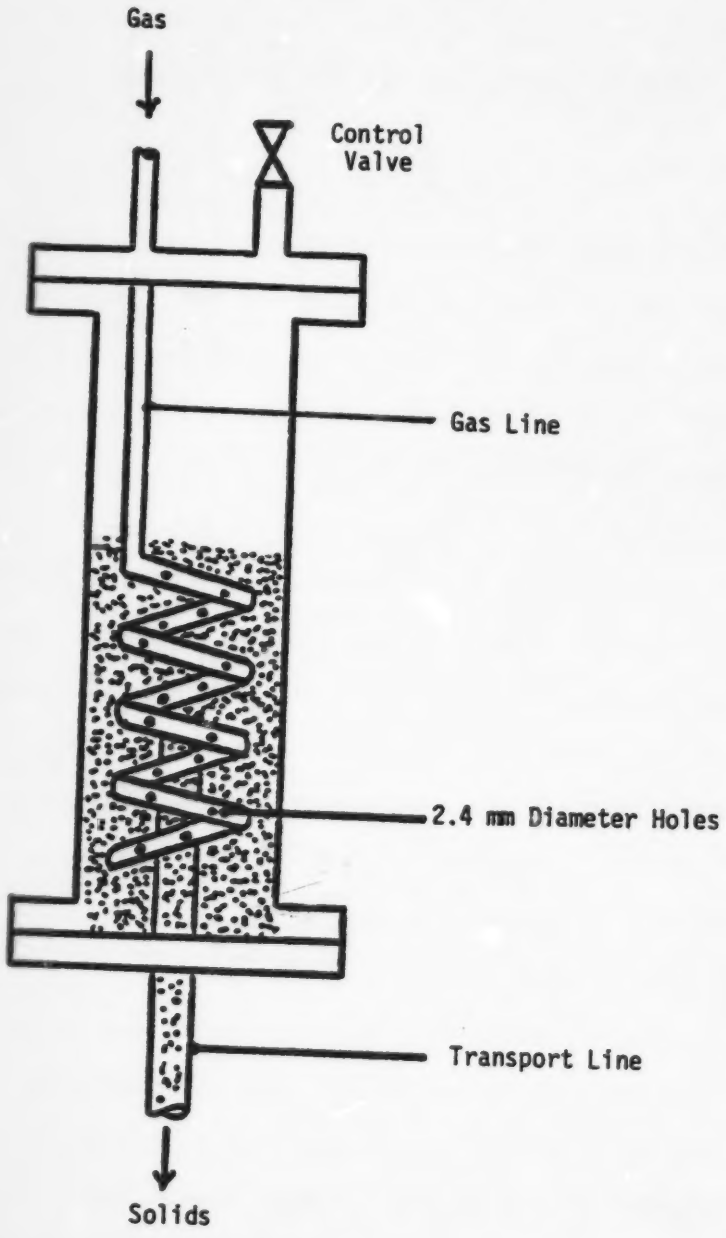

Figure 24 - Downflow Wood Feeder

the coil. Local aeration, which pneumatically stirred the solids, occurred when a portion of the transport gas exited from each of the holes. A stream of dense phase solids was observed to exit from the transport line through the base of the feeder.

In the ring feeder (Figure 25), transport gas was injected into the bed of wood flour through several 2.4 mm diameter holes which were drilled through the inner perimeter of the gas line ring. The solids suspension could exit from the feeder in a downflow or upflow mode depending on the positioning of the transport line. This feeder was able to feed dense phase streams in either mode.

All of the three feeders were capable of feeding the wood flour smoothly for short periods of time. However, sudden termination of the solids flow was inevitable, and was probably caused by the formation of pockets around the transport line inlet. These pockets were caused, in turn, by the fibrous and cohesive nature of the biomass. With the aid of mechanical vibration of the feeder, continuous flow of the suspended biomass solids could be maintained.

As a result of the cold model wood flour feeding tests, the advantages of the new designs were not considered sufficient (in terms of cost and time loss) to warrant their implementation. Consequently, the original fluidized bed biomass feeder design was retained. It is recommended that in future work where independent control of the solids

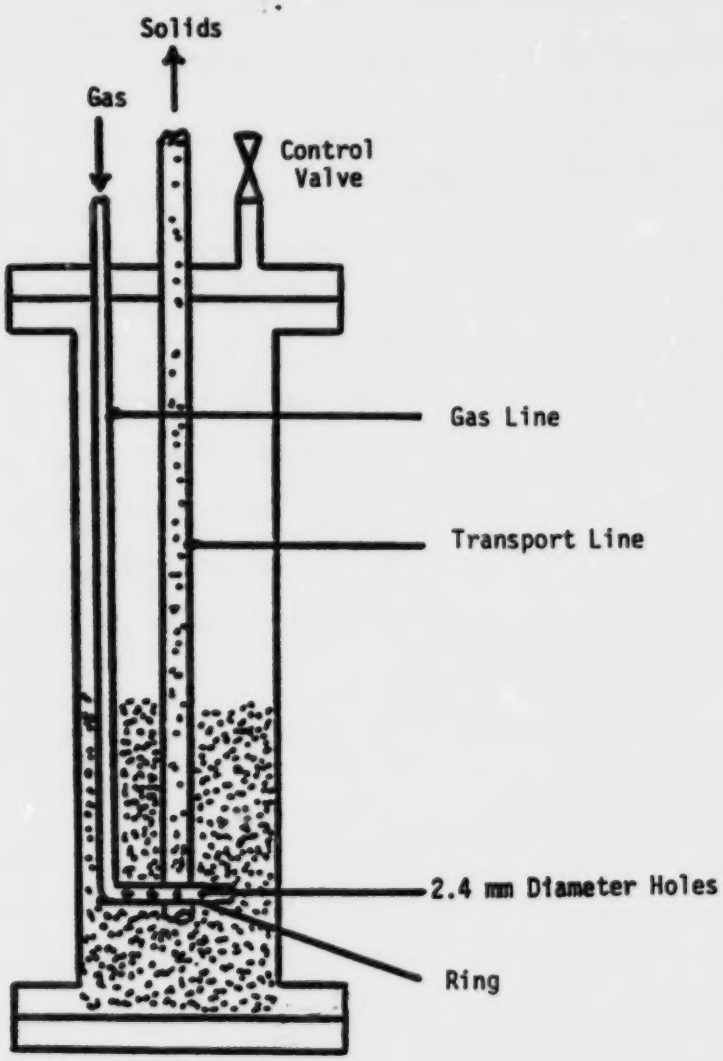

Figure 25 - Ring Wood Feeder

loading, mass flowrate and line velocities are required, a mechanical screw type feeder (feeding into a transport line) may be preferable.

7.5 Load Cell Testing

Several cold run experiments were carried out to test the load cell weighing accuracy. Avicel cellulose was fed from the biomass feeder, which was installed on the load cell structure, to a collector placed on a Sartorius balance. The balance had a 0.1 gram accuracy. The changes in weight, as indicated by the two devices, were recorded at 30 second intervals for 5 minutes. The weight loss recorded by load cells was then compared to the weight gain indicated on the balance.

The following feeder conditions were tested during the course of the experiments:

(i) The empty feeder with subsequent addition of dead weights.

(ii) The empty feeder with gas flowing through it at atmospheric pressure (to test potential flow interference).

(iii) The empty feeder with gas flowing through it at 138 kpa gauge pressure (20 psig).

(iv) The feeder actually feeding Avicel cellulose powder (i.e. with fluidizing and transport gas flow turned on).

The results indicated that the load cells could accurately detect 2 gram incremental changes with a total load of 70 kg (i.e. an accuracy of

0.003%). In the tests with gas flow alone, the load cells were capable of registering the weight of the gas.

Actual cellulose feeding tests, reported in Figure 26, were carried out at two distinct feeder gauge pressures of 13.8 and 68.8 kPa (2 and 10 psig). The ordinate in Figure 26 represents the load cell readings, while the abscissa represents the Sartorius balance readings. For both pressures the curves are identical and linear indicating satisfactory load cell performance.

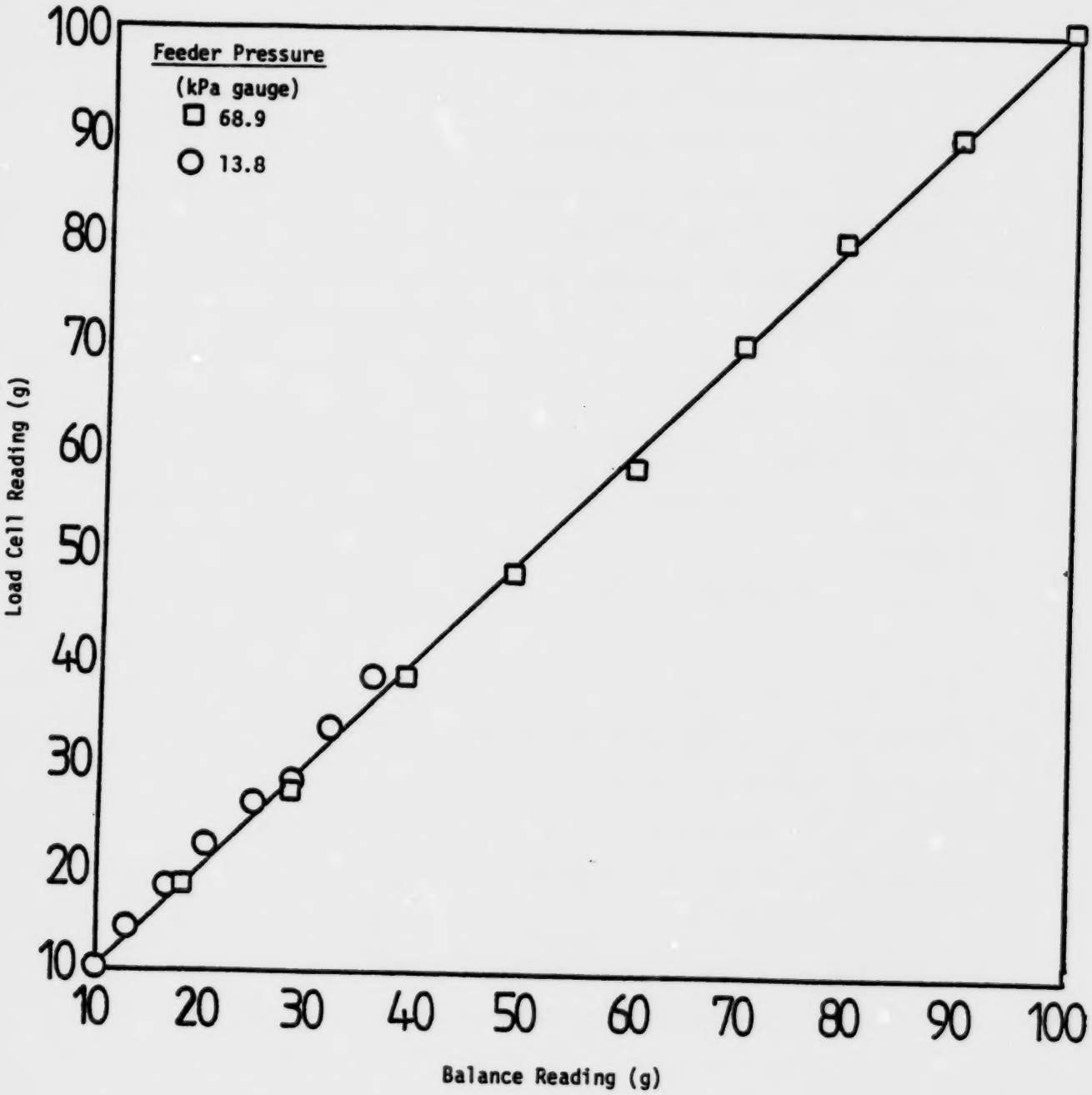

Figure 26 - Load Cell Test Results: Load Cell Reading vs Balance Reading

8.0 EXPERIMENTAL PROCEDURE

During an actual hot ULTRAPYROLYSIS experiment, the four furnaces in the preheating and reactor systems were set at their appropriate temperatures. The preheater and reactor furnaces, which took the longest period of time to heat up, were turned on first, and were followed by the subsequent activation of the THERMOVORTACTOR and injector ovens.

In a sequential manner, the CRYOFOR, THERMOFOR and biomass feeders were then put into operation, respectively. The actual start up procedure was identical for each of the feeders. The transport gas flow was first initiated, followed by that of the fluidizing gas. This sequence was essential to prevent plugging of the transport lines. In order to allow each feeder to reach its desired pressure, the valves on their gas vent lines were kept shut for an appropriate period of time. In addition, the solids flow in the transport line bypassed those system components (i.e. the preheater, THERMOVORTACTOR and reactor) which were in the process of heating up, and were led to plastic collection vessels via three-way valves.

When the oven temperatures and feeder pressures had reached their appropriate values (the feeder pressures were kept constant by opening the valves on the gas vent lines to appropriate settings), the three-way valve in the CRYOFOR transport line was switched from the bypass position to the

normal operating position allowing CRYOFOR solids to pass to the CRYOVORTACTOR. This was followed by the switching of the THERMOFOR solids from the bypass system to preheater coils and on to the THERMOVORTACTOR. During this time, all of the solids were passing through the ULTRAPYROLYSIS unit to a system bypass filter assembly at the tail-end (i.e. after quenching and cooling). Prior to the feeding of the biomass into the hot unit, the solids flow at the system tail-end was switched via a three-way valve from the bypass assembly to the mass balance filter and gas collection assembly. Therefore, as the biomass feeding was initiated in the THERMOVORTACTOR, the suspension passed through the reactor and was quenched in the CRYOVORTACTOR and cooling coil. Solids were then separated in the mass balance filter, and the gas was collected in the sampling bags.

When the volume of the collected gas approached the capacity of the sample bags, the biomass suspension was switched back to its bypass position and the THERMOVORTACTOR transport line was purged with nitrogen. This purging action ensured complete pyrolysis and recovery of all of the product gas. The solids flow in the system tail-end was then switched back from the mass balance mode to the original bypass mode. After this switching operation, the solids flow of the THERMOFOR and CRYOFOR suspensions was terminated. Transport lines were purged with nitrogen to prevent settling of solids and of plugging in the lines.

During the shutdown of the feeders, the operating pressures were reduced to atmospheric levels by fully opening the valves on the gas vent

lines and by stopping the flow of the fluidizing gas. In order to prevent plugging of the feeder transport lines, it was essential that the transport gas be left on until the feeder pressures had been fully released.

Due to limited electronic control and feedback in the ULTRAPYROLYSIS system, most control measures were conducted manually. This included the balancing of system pressures at several locations to prevent plugging and backflow in the transport lines. The electrically operated three-way valves and bypass systems played an important role in the control and smooth operation of the ULTRAPYROLYSIS system.

Dynamic gas samples were taken from the gas line during the experiments at 1 minute intervals (nominally) and analyzed immediately. Static samples were taken from the various gas collection bags and analyzed after completion of the run. Gas chromatographic analysis was accomplished using a Carle (Model 111-H/197A) refinery gas analyzer.

9.0 RESULTS

9.1 Overview

Although more than 50 hot runs were conducted during the program, only the latter runs are reported in this Chapter. Earlier runs are summarized in the Appendix. The experimental results of the ULTRAPYROYSIS of various biomass feedstocks between 750 and 900°C are given in Tables 20 to 23. Tables 20 and 21 present a summary of the product gas distribution in mole and mass percent, respectively, while Table 22 illustrates the yields of all product fractions and the corresponding mass balance closure. The elemental (i.e. C, H, and O) balance, higher heating value, and empirical formula of the product gas resulting from the pyrolysis of the various feedstocks are reported in Table 23.

No THERMOFOR solids were used in these experiments due to plugging problems which occurred in the preheater during earlier runs. The plugging was thought to be a consequence of oxidation of the Inconel coil material or of agglomeration and fusion of THERMOFOR sand impurities. These causes are both associated with high temperature operations. The THERMOFOR solids suspension was therefore replaced with hot nitrogen transport gas only (i.e a gaseous THERMOFOR). Experimental results of experiments with THERMOFOR solids, given in the Appendix, are similar to those with transport gas only. This was most likely due to the relatively small size of equipment which allowed a high surface area to volume ratio, resulting in turn, in significant wall effects and sufficiently rapid heat transfer to the biomass. Thus, the conditions required for fast pyrolysis were met even without THERMOFOR solids. In commercial operations, the use of a gaseous thermofor would not be desirable as it would unduly dilute

TABLE 20 ULTRAPYROLYSIS Product Gas Distribution (Mole Percent)

RUN NO.	TEMP. (0°C)	FEEDSTOCK TYPE	RESIDENCE TIMES (msec)		Mole Percent										
			Thermo-Vortact.	Reactor	H_2	CO_2	C_2H_4	C_2H_6	C_2H_2	CH_4	CO	C_3H_6	C_4H_8	C_xH_y	Unsat.
27	900	Cellulose	45	291	21.3	3.0	6.4	0.49	1.52	10.2	56.8	0.33	0	18.94	8.25
28	900	"	41	255	21.0	2.9	6.3	0.57	1.35	9.8	57.6	0.53	0	18.55	8.18
29	850	"	49	342	19.4	3.2	6.2	0.60	1.22	8.9	59.6	0.92	0	17.84	8.14
30	850	Cellulose	48	335	20.6	2.9	6.6	0.57	1.38	9.6	57.7	0.57	0	18.72	8.55
31	800	"	-	-	18.9	3.0	6.1	0.60	1.10	8.7	60.5	1.03	0	17.53	8.23
32	800	"	55	391	19.3	3.2	6.2	0.65	1.24	8.6	60.0	0.92	0	17.61	8.36
35	800	Cellulose	63	433	18.5	3.2	6.2	0.62	1.18	9.0	60.3	0.94	0	17.94	8.32
33	750	"	64	478	17.4	3.4	5.6	0.59	1.02	8.1	62.4	1.26	0.06	16.63	7.94
34	750	"	61	449	17.0	3.5	5.7	0.56	1.04	7.8	62.9	1.42	0.1	16.62	8.26
45	900	Lignin	53	460[a]	18.7	8.8	5.1	1.04	2.33	17.9	45.8	0.40	0	26.77	7.83
44	850	"	55	481[a]	18.7	10.1	4.8	1.62	1.38	28.4	44.5	0.57	0	26.77	6.75
41	800	"	57	504[a]	18.8	10.2	4.4	1.58	2.07	19.0	44.5	0.51	0	26.56	5.98
43	750	"	60	528[a]	9.3	11.7	4.7	1.93	0.76	21.7	49.3	0.50	0	29.59	5.96
50	900	Wood	64	557[a]	17.0	7.9	6.1	0.73	1.41	12.7	53.7	0.51	0	21.45	8.02
47	850	"	66	588[a]	16.4	8.3	6.0	0.76	1.20	13.0	53.9	0.58	0	21.54	7.78
48	800	"	69	609[a]	15.2	9.1	5.7	0.89	1.04	12.7	54.4	0.92	0	21.25	7.66
49	750	"	72	640[a]	12.0	10.6	5.0	0.98	0.74	12.7	53.7	0.51	0	19.93	6.25

a: Residence Times Based on the Carrier Gas Alone.

TABLE 21 ULTRAPYROLYSIS Product Gas Distribution (Mass Percent)

RUN NO.	TEMP. (0°C)	FEEDSTOCK TYPE	RESIDENCE TIMES (msec)		MASS Percent										
			Thermo-Vortact.	Reactor	H_2	CO_2	C_2H_4	C_2H_6	C_2H_2	CH_4	CO	C_3H_6	C_4H_8	C_xH_y	Unsat.
27	900	Cellulose	45	291	1.96	6.10	8.22	0.67	1.82	7.47	73.14	0.64	0	18.82	10.68
28	900	"	42	255	1.92	5.81	8.00	0.78	1.60	7.18	73.67	1.02	0	18.61	10.62
29	850	"	49	342	1.73	6.20	7.71	0.80	1.41	6.32	74.10	1.72	0	17.96	10.84
30	850	Cellulose	48	335	1.88	5.87	8.35	0.78	1.63	7.00	73.40	1.10	0	18.86	11.08
31	800	"	-	-	1.66	5.77	7.52	0.79	1.20	6.14	74.73	1.90	0.23	17.61	10.68
32	800	"	55	391	1.71	6.19	7.64	0.86	1.43	6.08	74.40	1.70	0	17.71	10.77
35	800	Cellulose	63	433	1.63	6.21	7.62	0.82	1.35	6.37	74.28	1.73	0	17.89	10.70
33	750	"	64	478	1.49	6.39	7.06	0.76	1.14	5.58	75.20	2.28	0.13	16.28	10.48
34	750	"	61	449	1.45	6.54	6.81	0.72	1.15	5.30	75.20	2.55	0.28	16.53	10.51
45	900	Lignin	53	460[a]	1.67	17.20	6.31	1.40	2.70	12.77	57.23	0.75	0	23.93	9.76
44	850	"	55	481[a]	1.65	19.64	5.90	2.14	1.58	12.97	55.08	1.05	0	23.64	8.53
41	800	"	57	504[a]	1.66	19.90	5.43	2.11	1.24	13.49	55.23	0.94	0	23.21	7.61
43	750	"	60	528[a]	0.75	20.71	5.25	2.33	0.80	13.94	55.40	0.83	0	23.15	6.88
50	900	Wood	64	557[a]	1.46	14.86	7.25	0.94	1.57	8.72	64.30	0.91	0	19.39	9.73
47	850	"	66	588[a]	1.40	15.41	7.08	0.97	1.33	8.79	64.00	1.04	0	19.21	9.45
48	800	"	69	609[a]	1.27	16.56	6.62	1.11	1.12	8.47	63.24	1.60	0	18.92	9.34
49	750	"	72	640[a]	0.95	18.43	5.56	1.16	0.76	8.02	62.82	1.97	0.25	17.82	8.54

a: Residence Times Based on the Carrier Gas Alone.

the pyrolysis products and make the product recovery expensive. Also the preheating of a gaseous thermofor would be awkward. Thus, if direct combustion took place in the gas, the product would be diluted with of CO_2 which would be expensive to scrub out from the product. If gas THERMOFOR were heated by indirect heat exchange, a lot of expensive heat transfer surface would be needed due to the low heat transfer coefficients of gases. THERMOFOR solids are, therefore, essential to the commercial success of a fast pyrolysis scheme.

9.2 Residence Time Determination

The THERMOVORTACTOR and reactor residence times, reported in Tables 20 to 23, were estimated using several important assumptions. It was assumed that both the THERMOFOR and biomass carrier gas reached the THERMOVORTACTOR temperature instantaneously, and that no biomass pyrolysis occurred in the THERMOVORTACTOR. Furthermore, the Avicel cellulose was assumed to react and form the final gas product distribution instantaneously at the reactor inlet. In the lignin and birch wood flour experiments, the mass balance was not determined, and the residence times were therefore calculated from the carrier gas flow alone.

Typical residence times in the THERMOVORTACTOR and reactor were estimated to be 40 to 72, and 250 to 650 milliseconds, respectively. In general, it can be assumed that actual residence times were somewhat shorter than the estimates. For the next phase of the research, reactor modifications will be made to accommodate direct control of the residence

TABLE 22 Cellulose ULTRAPYROLYSIS Product Yields and Mass Balance

RUN NO.	TEMP (°C)	RESIDENCE TIMES (msec)		YIELDS g/g cellulose				MASS BALANCE (%)
		THERMO VORTACT.	REACTOR	VOLATILES	HEAVY FRACTION[2]	C_5/C_6[3]	GAS[4]	
27	900	45	291	0.003	0.004	0.011	0.981	85
28	900	42	255	0.006	0.033	0.012	0.948	87.8
29	850	49	342	0.017	0.091	0.012	0.879	88.2
30	850	48	335	0.016	0.046	0.015	0.924	77.4
31	800	-	-	0.031	0.071	0.009	0.889	72.7
32	800	55	391	0.031	0.081	0.012	0.876	108.3
35	800	63	433	0.032	0.090	0.010	0.868	82.7
33	750	64	478	0.045	0.124	0.013	0.818	140.6
34	750	61	449	0.053	0.105	0.011	0.747	91.6

1. VOLATILES: water, organics with boiling points below 103°C.
2. HEAVY FRACTION: organic combustibles with boiling points above 103°C.
3. C_5/C_6: C_5 and C_6 hydrocarbons left uncondensed in the gas at room temperature (i.e. saturation concentration).
4. GAS: dry, nitrogen free

TABLE 23 Elemental Balance, Empirical Formula and Gas Higher Heating Value of Cellulose ULTRAPYROLYSIS Product Gas

RUN NO.	TEMP. (°C)	FEEDSTOCK	RESIDENCE TIME (msec) THERMO-VORTACT.	RESIDENCE TIME (msec) REACTOR	HHV[2,3] (MJ/Nm^3)	HHV[2,3] (Btu/scf)	GAS EMPIRICAL FORMULA	ELEMENTAL BALANCE C	H	O
27	900	Cellulose	45	291	15.9	403	$CH_{1.33}O_{0.72}$	93.1	76.5	71.0
28	900	"	42	255	15.9	404	$CH_{1.31}O_{0.72}$	93.0	76.6	69.8
29	850	"	49	342	15.9	404	$CH_{1.22}O_{0.73}$	86.4	72.2	60.6
30	850	"	48	335	15.9	403	$CH_{1.3}O_{0.71}$	80.1	65.6	59.6
31	800	"	-	-	15.9	404	$CH_{1.2}O_{0.73}$	72.0	60.2	49.6
32	800	"	55	391	15.9	403	$CH_{1.21}O_{0.73}$	105.5	88.6	73.0
35	800	"	63	433	15.9	405	$CH_{1.2}O_{0.73}$	79.9	66.9	55.0
33	750	"	64	478	15.9	404	$CH_{1.12}O_{0.74}$	127.3	108.8	81.9
34	750	"	61	449	16.0	406	$CH_{1.1}O_{0.75}$	82.6	70.8	52.0
45	900	Lignin	53	460[1]	18.1	459	$CH_{1.66}O_{0.62}$	-	-	-
44	850	"	59	481[1]	18.1	459	$CH_{1.69}O_{0.63}$	-	-	-
41	800	"	57	504[1]	18.0	458	$CH_{1.69}O_{0.66}$	-	-	-
43	750	"	60	528[1]	18.6	472	$CH_{1.48}O_{0.69}$	-	-	-
50	900	Wood	64	557[1]	16.2	411	$CH_{1.31}O_{0.74}$	-	-	-
47	850	"	66	588[1]	16.2	411	$CH_{1.30}O_{0.75}$	-	-	-
48	800	"	69	609[1]	16.3	414	$CH_{1.27}O_{0.76}$	-	-	-
49	750	"	72	640[1]	16.5	418	$CH_{1.15}O_{0.78}$	-	-	-

1. Residence times based on the Carrier Gases only.
2. HHV: Higher Heating Value
3. Nm^3: Normal cubic meter taken at 0°C and 1 Atm.

times rather than the passive manipulation (i.e. a function of other experimental variables) which occurred during this program.

9.3 Mass Balance

Mass balances (Tables 22 and 23) were determined only for the experiments with cellulose. As indicated in Table 22, the product spectrum was divided into four general categories - **volatiles**, **heavy fractions**, C_5/C_6, and **gas**. The **volatiles** were those liquid species (condensibles) with boiling points less than 100°C (i.e. water, benzene, acetone, methanol and other pyroligneous acid fractions). The **heavy fractions** included liquid species with boiling points greater than 100°C (i.e. toluene, xylene, tar, etc.) and also the solid char product. The C_5/C_6 category represented that fraction of five and six carbon products which is normally condensed in the liquid phase at room temperature, but was present in saturation concentration in the non-condensible product gas. This fraction was quantified by gas chromatograhic analysis. All other gaseous products, which were non-condensible at room temperature, were termed collectively as **gas**.

The mass balance closure was typically between 75 and 90 percent. Deficits in the balance were probably due to errors associated with the measurement of the feedstock mass flowrate and also with the inability to quantitatively account for pyrolytic water in the recovery of products.

10.0 DISCUSSION

The experimental results have been evaluated in the following sections so that individual gas component yields can be expressed as mass of product per unit mass of the **product gas** . Although this gives an adequate basis of comparison for the pyrolysis of the various biomass components, it must be noted that the mass balance calculation was done for cellulose trials only. Therefore, absolute yields (i.e. expressed as mass fraction of the biomass **feedstock**) were not determined. Accordingly, if the conversion of one particular biomass feedstock to a permanent gas product was relatively low compared to one of the other feedstocks, comparison of the results could lead to misleading assumptions with respect to absolute yields of a given component. Ratios of various individual gas product yields are presented in order to give an indication of the cracking severity and also to give an indication of the parent molecules of various lighter molecular fragments (i.e. carbon oxides, ethylene and ethane).

In general, the yields of various gaseous components from wood flour pyrolysis are intermediate with respect to those from cellulose and lignin pyrolysis. In other words, the curves of the gas component yields (expressed as mass fraction of the product gas) vs pyrolysis temperature for wood flour trials often lies between the two corresponding curves for trials with cellulose and lignin (the hydrogen and acetylene yield curves are exceptions to this generalization). This would seem to suggest that the birch wood pyrolysis is similar to the sum of the pyrolysis of its major components. The ULTRAPYROLYSIS birch wood sample was particularly suited for this comparison since lignin and cellulose were present in

roughly equal amounts and constituted 85 percent of the mass of the wood (Section 7.1.3).

It must be stressed that the results are preliminary. Due to the fixed reactor volume, it was extremely difficult to independently separate the effects of temperature and residence time. In the next phase of the work, reactor modifications will be made to allow control of the reactor residence times over the range of experimental temperatures.

10.1 Product Yields for Cellulose

The product yields for AVICEL cellulose ULTRAPYROLYSIS experiments at temperatures betwen 750 and 900°C are given in Figure 27. The ordinate represents the mass yield per unit mass of biomass (cellulose) feedstock while the abscissa indicates the values of the reaction temperatures. The yield of the non-condensible gas, which was the major pyrolysis product, increased with temperature and was approximately 0.96 gram per gram of cellulose at 900°C. This confirmed the proposition in the literature that cellulose can be completely, or almost completely, gasified at high temperatures and rapid heating rates.

The yield of the heavy fraction (i.e. the char, and liquids with boiling points above 100°C), which was 0.05 gram per gram of cellulose at 900°C, decreased as the temperature increased. At elevated temperatures approaching 900°C, the following general observations relating to the heavy fraction were made:

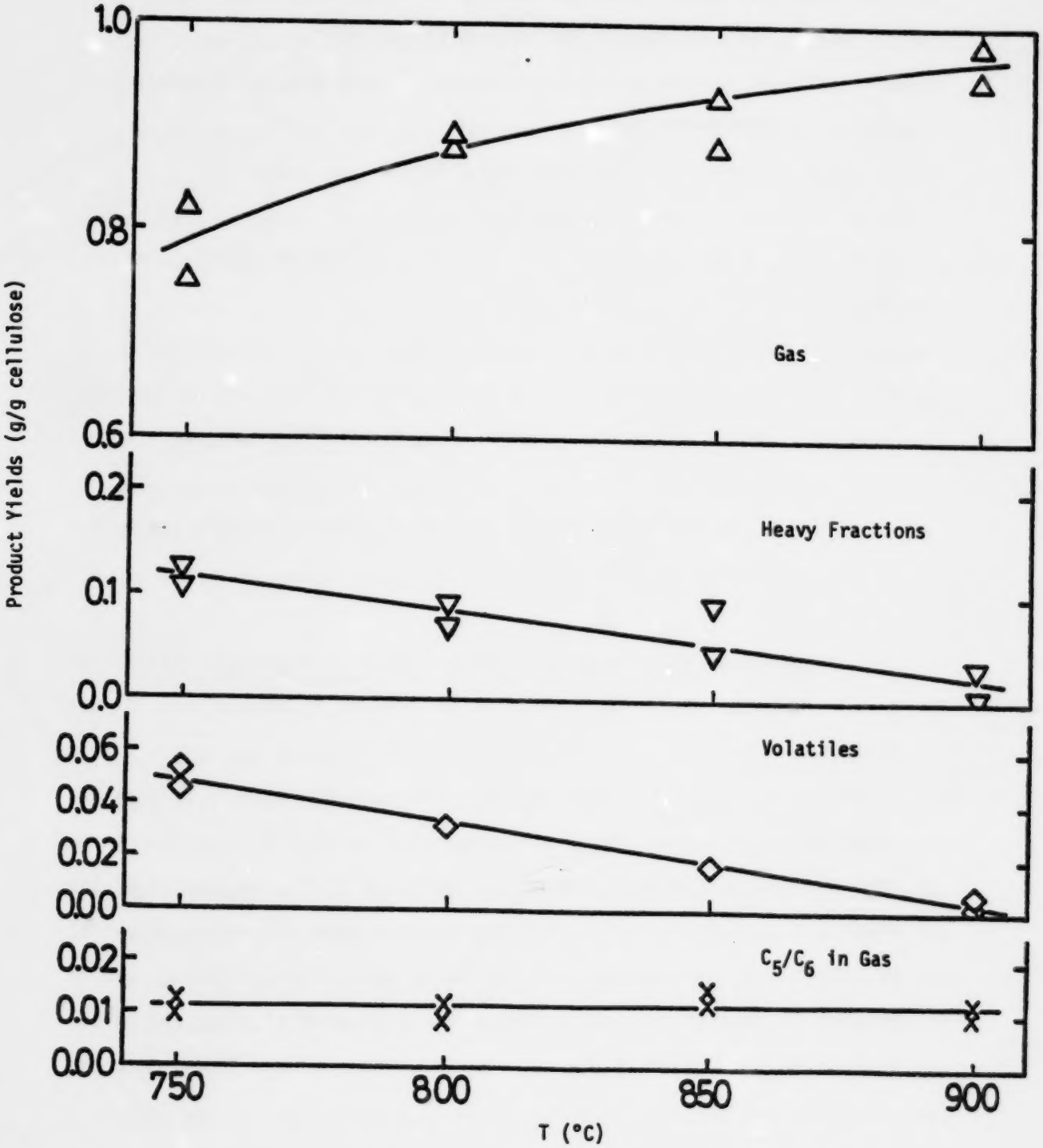

Figure 27 - Cellulose PYROLYSIS Product Yields At Various Temperatures

(i) Little (i.e. trace) or no char was detected.

(ii) The sand/product mixture was free flowing.

(iii) No agglomerations occurred in the sand even after remaining at room temperature.

(iv) A sweet olefinic odour was evident.

At lower temperatures of approximately 700°C, other observations were noted:

(i) Char and tar discolouration of the sand was noticeable.

(ii) The sand/product mixture was less free flowing due to agglomerations which were evident at room temperature within a couple of days.

(iii) A pungent acrid odour, typical of low temperature pyrolytic tar, was evident.

The yield of volatiles, (i.e. those liquids with boiling points less than or equal to 100°C) decreased with an increase in temperature. It was assumed that a large portion of the volatile fraction was water. This assumption was generally confirmed when the elemental (C,H,O) balance was observed to be better at temperatures approaching 900°C. At these temperatures, the forward step of the water-gas shift reaction (i.e. the production of hydrogen and carbon dioxide from steam and carbon monoxide) is faster than the reverse step (in terms of reaction kinetics) yet an approach to equilibrium clearly favors the production of steam and carbon monoxide at the expense of the hydrogen and carbon dioxide (23). Although

a quantitative assessment of kinetic and equilibrium considerations for the water-gas shift reaction (at the corresponding ULTRAPYROLYSIS pressures, temperatures and gaseous partial pressures), was not done,it can be speculated that the forward step was occurring by favourable kinetics. Therefore, little water would have condensed into the final volatile fraction, and the hydrogen and oxygen molecules would have been accounted for in the gas fraction (i.e. as hydrogen and carbon dioxide) by gas chromatographic analysis. The C_5/C_6 products were those species which were apparently present in saturation concentrations in the gas product, and included pentane, pentene, benzene, toluene and xylene (i.e. five and six carbon hydrocarbons which normally condense at room temperature). Changes in pyrolysis temperatures seemed to have no effect on these yields, thus confirming that they were present in saturated quantities. The yield was consistently around 0.012 gram of cellulose feedstock.

10.2 Comparison of Product Gas Yields for Various Feedstocks

The gas product distribution expressed as molar concentration for pyrolysis experiments with cellulose, lignin and wood (birch flour), is illustrated in Table 20 and Figures 28 to 30. Except for carbon monoxide, the ordinate on the left hand side of the figures represents the molar fraction of the individual gas species in the dry nitrogen-free gas. The molar fraction of carbon monoxide is represented by the ordinate on the right hand side of the figures. All biomass feedstocks produced different proportions of similar gaseous components, which primarily included hydrogen, carbon monoxide, carbon dioxide, methane, ethylene, ethane, acetylene and propylene. Butene and propane, which were found in trace

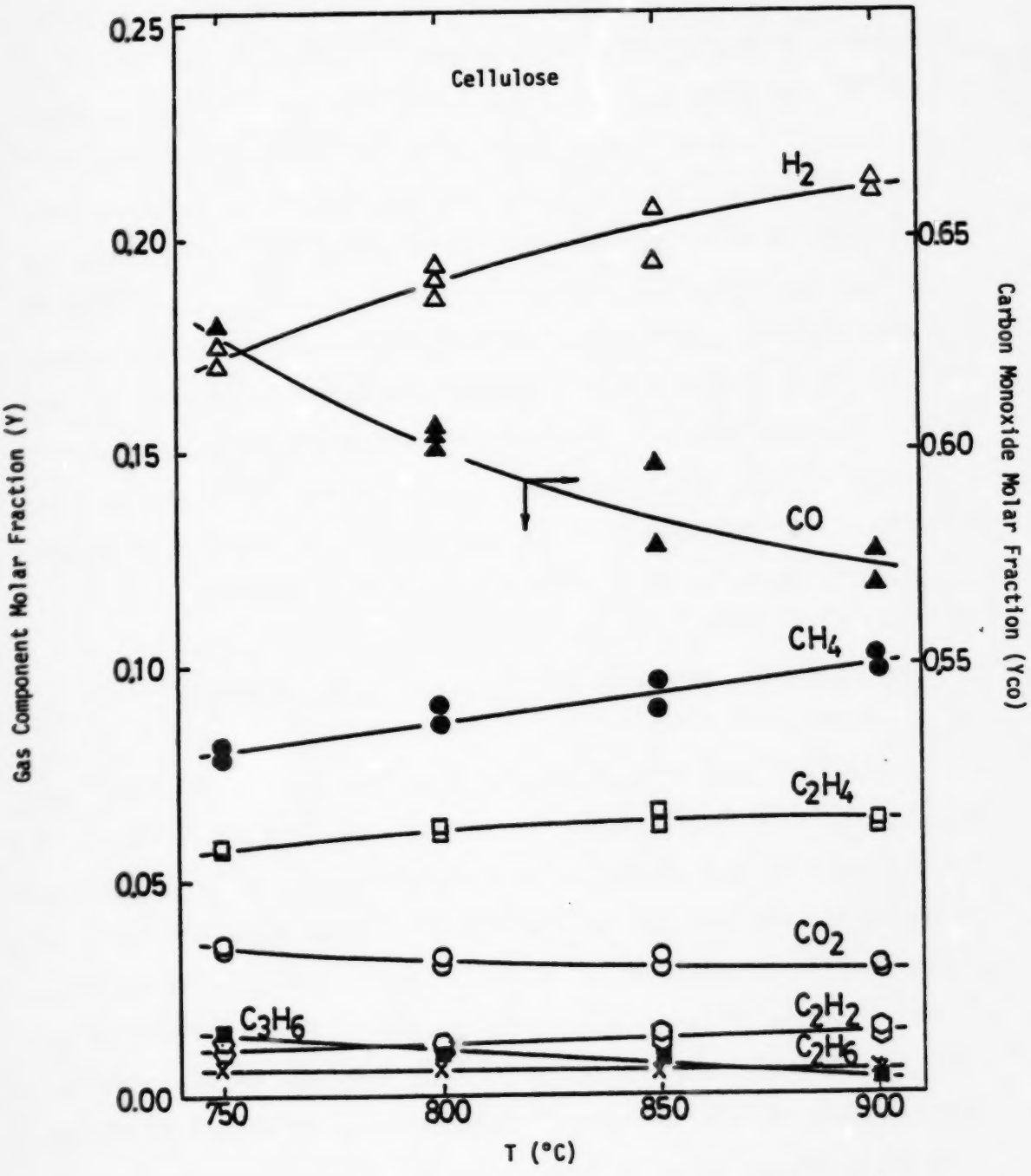

Figure 28 - Gas Product Distribution For Cellulose At Various Temperatures.

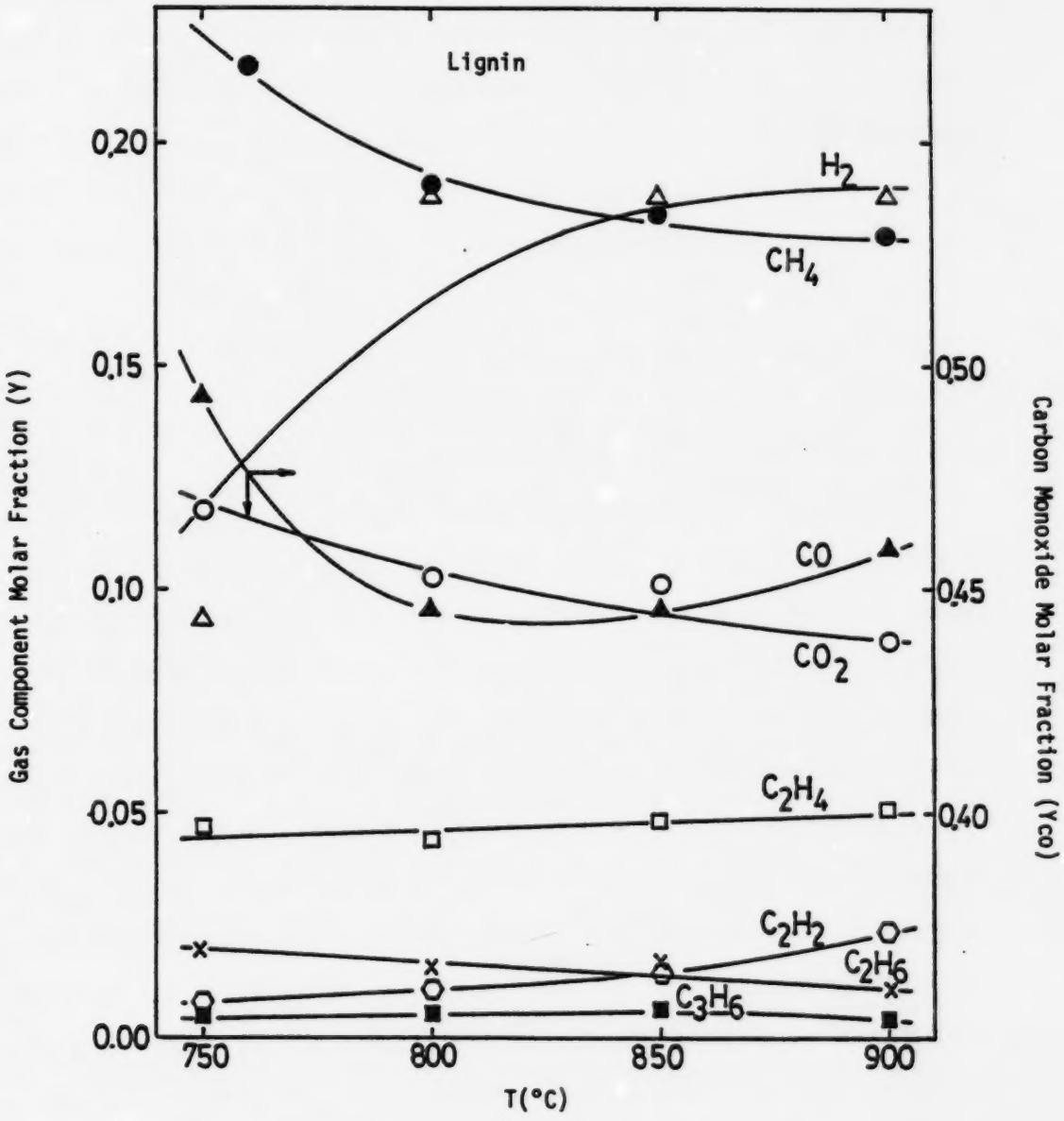

Figure 29 - Gas Product Distribution For Lignin At Various Temperature.

amounts in the gas produced at lower pyrolysis temperatures, were probably cracked during the higher temperature experiments. It is therefore expected that a reduction in residence time would result in the preservation of these heavier gaseous hydrocarbon components. The dominance of the yield of carbon oxide gases was associated with the high oxygen content of the biomass feedstocks. Individual gas component yields are detailed in the following sections.

10.2.1 Carbon Monoxide

Carbon monoxide is the major gaseous product for all biomass feedstocks. The pyrolysis of cellulose, lignin and birch flour gave a carbon monoxide yield of 75, 55 and 63 mass percent of the product gas, respectively (Figure 31). The yield of this component remained relatively constant over the experimental temperature range, showing a very slight decrease with increasing temperature for cellulose trials, and a very slight increase with increasing temperature for wood flour trials. The complex mechanism of primary carbon monoxide formation and the competitive secondary reactions both contribute to the difficulty in giving a clear theoretical discussion of the results of the yield of this component. Antal (24) speculates that a fixed fraction of carbon atoms are dedicated to CO formation from the cracking of the biomass-derived volatiles during fast pyrolysis at temperatures exceeding 600°C. As was reported in Section 10.1, the forward step of the water-gas shift reaction (i.e. the production of hydrogen and carbon dioxide from steam and carbon monoxide) is faster than the reverse step at temperatures exceeding 810°C. However,

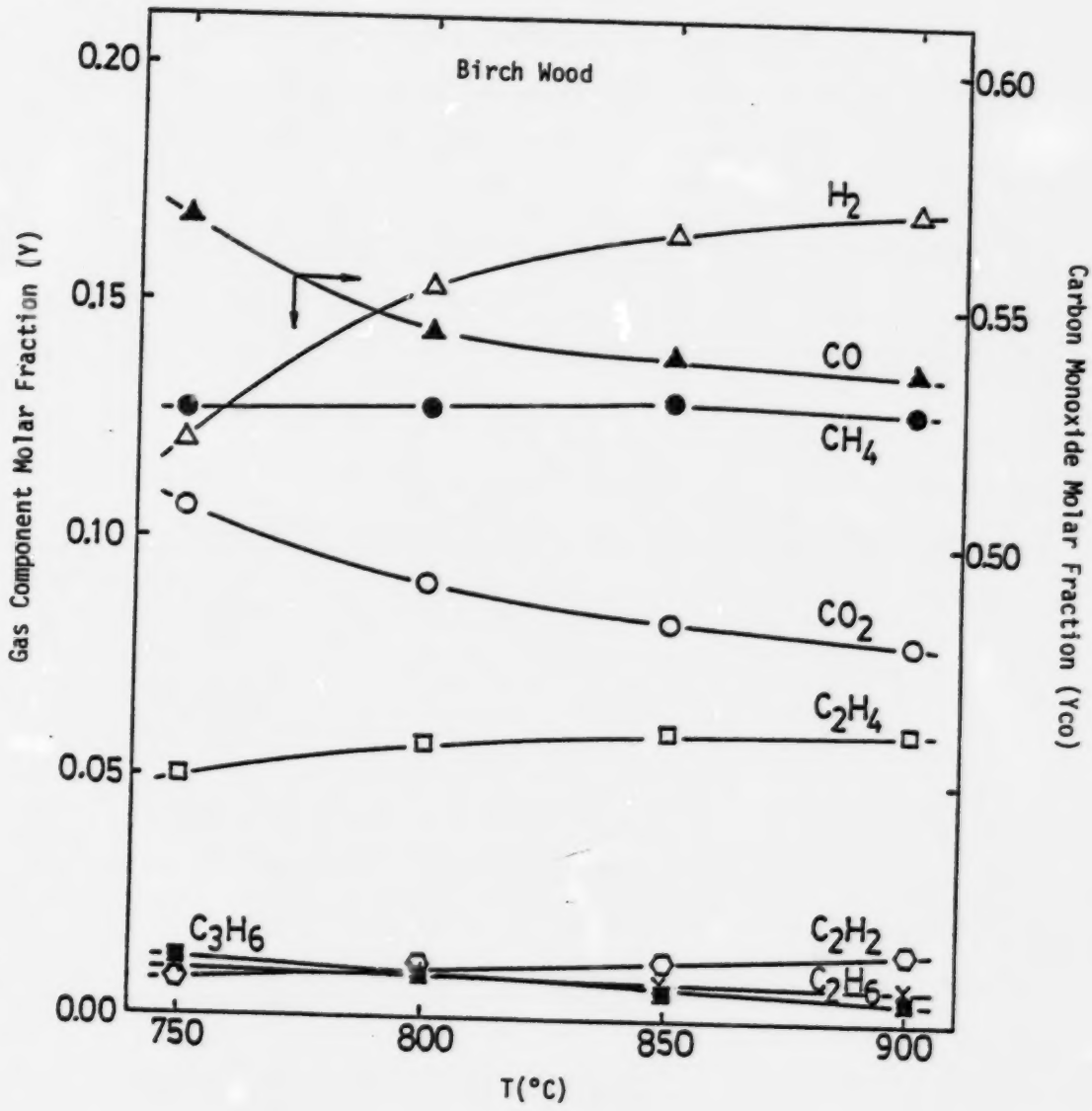

Figure 30 - Gas Product Distribution for Birch Wood Flour At Various Temperatures.

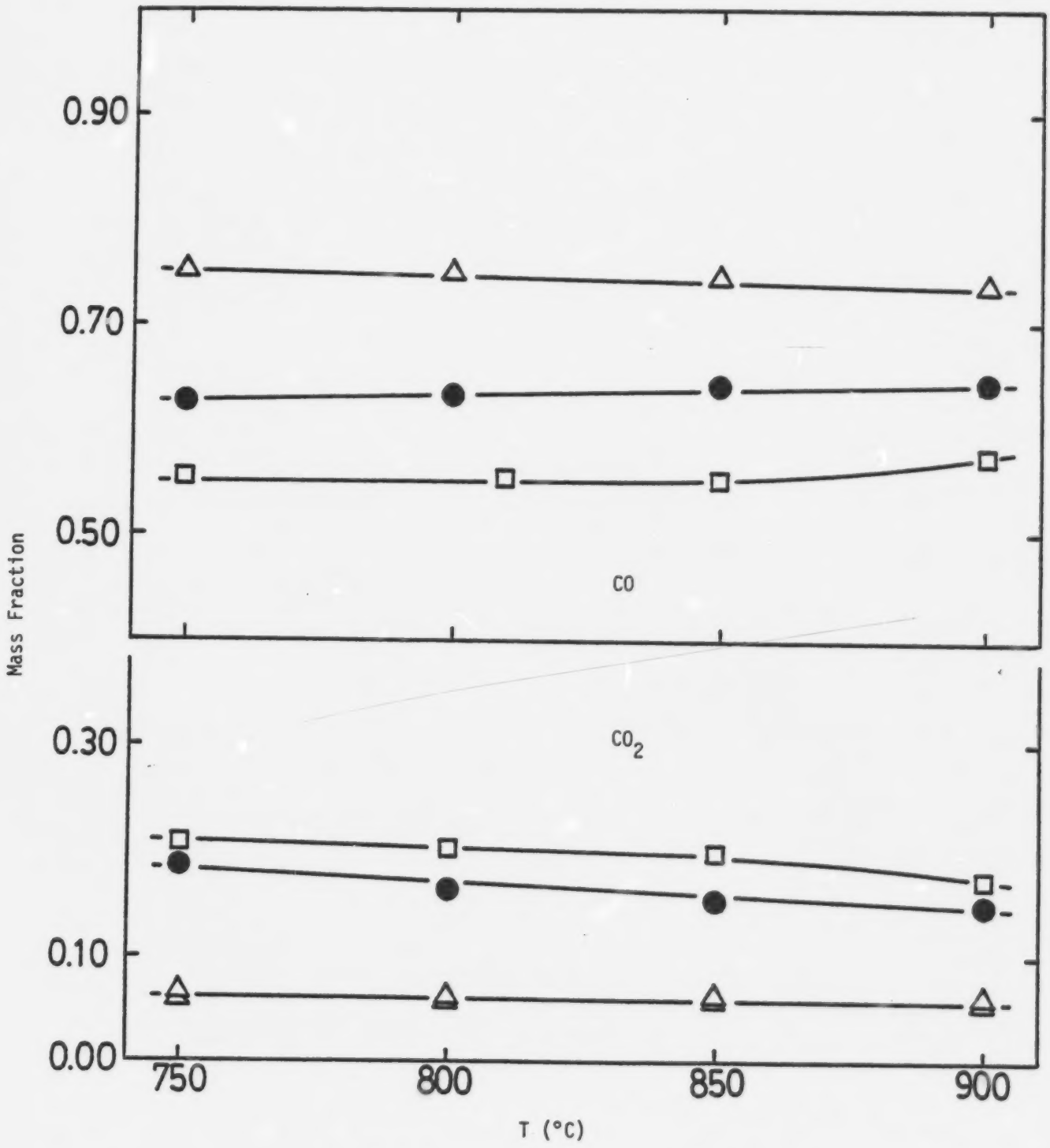

Figure 31 - Mass Fraction of Carbon Monoxide and Carbon Dioxide In The Product Gas At Various Temperatures.

△ Cellulose ● Birch Wood □ Lignin

even if reaction conditions were such that the forward step was allowed to occur, this would be significantly limited by the availability of water in the vapour phase (i.e. the biomass feedstocks were extremely dry and the carrier gas was inert during all of the ULTRAPYROLYSIS experiments). Equilibrium, on the other hand, favours the production of steam and carbon monoxide at the expense of hydrogen and carbon dioxide over the entire range of experimental temperatures (23).

The above speculation of Antal, the limited availability of vapour-phase water, and kinetic considerations provide an adequate explanation of the constant carbon monoxide yields. The carbon monoxide which was formed from the "dedicated" fraction of carbon atoms during the cracking of the biomass derived volatiles at ULTRAPYROLYSIS temperatures, simply had no opportunity to further react (in the secondary reactions), and therefore persisted in constant amounts in the final gas product.

10.2.1 Carbon Dioxide

The carbon dioxide yields, expressed as a fraction of the product gas mass, were highest for the lignin experiments and relatively low for those utilizing cellulose (Figure 31). At 750°C, lignin produced more than 20 percent of carbon dioxide by mass, wood flour produced a similar fraction, and cellulose gave a carbon dioxide yield of approximately 6 percent by mass. The yield of carbon dioxide expressed as a fraction of the product gas mass, remained relatively constant over the experimental temperature range with very slight decreases for lignin and wood trials as the temperature was increased.

Carbon dioxide is thought to be a primary pyrolysis product which is produced during the initial depolymerization of the biomass polymer (23). The final yield would accordingly be fixed by the chemical nature of the feedstock, and by the extent to which the subsequent secondary water gas shift reaction is allowed to occur. As was discussed in Sections 10.1 and 10.2.1, the kinetic and equilibrium effects are diametrically opposed with respect to their influence on the direction of the water-gas shift reaction at temperatures exceeding 810°C (both effects are similar with respect to the direction of the reaction at temperatures between 500 and 810°C). The secondary cracking reactions favour carbon monoxide formation over carbon dioxide formation at high temperatures (as equilibrium is approached), and therefore it is very evident that several competitive reactions which affect the final carbon oxide distribution are taking place.

A final comment on the apparent trends of carbon oxide yields, as well as the other gas species, relates to the extent of conversion of the solid feedstock to a non-condensible gaseous product. Since the mass balance was determined for cellulose runs only, there was no way of quantitatively knowing the fraction of the lignin or wood feedstock mass which was converted to a permanent gas product, and the absolute yield of a given component at a given reaction temperature could not be determined. Therefore it is quite possible that the yield of an individual gas species could be dropping with a temperature increase (or vice versa) relative to other components in the gas (i.e. expressed as a mass fraction of the whole gas product), and yet the absolute yield (i.e. expressed as a mass fraction of the feedstock) could be increasing as the total conversion of the biomass feedstock increases.

10.2.3 Ethylene

Ethylene yields are particularly interesting due to the utility of this gas as a petrochemical feedstock and synthetic gasoline precursor. At 900°C, cellulose pyrolysis produced an 8.1 percent yield of ethylene (relative to the mass of the product gas) while the corresponding values for lignin and birch wood were 6.3 and 7.3 percent, respectively (Figure 32). As predicted in the literature (23), the ethylene yield increased with a rise in temperature from 750 to 900°C, thus reflecting the increasing severity of the cracking reactions. Had temperatures been allowed to exceed 1000°C, the literature indicates that acetylene would be favoured over ethylene.

10.2.4 Ethane

During the ULTRAPYROLYSIS program, lignin consistently gave higher yields of ethane than the other biomass feedstocks. At 750°C, the mass fraction of ethane in the product gas was 2.4, 1.1 and 0.8 percent for lignin, wood and cellulose trials, respectively (Figure 32). In addition, the ethane yield for lignin was more sensitive to temperature, and dropped linearly with an increase in temperature. The yield was relatively constant over the temperature range for the other feedstocks.

As was noted in section 10.2.2, it is difficult to determine whether there is an absolute drop in the ethane yield for lignin trials since the mass balance was not determined. Lignin is the most thermally resistant of the biomass feedstocks (23), and would likely show a dramatic

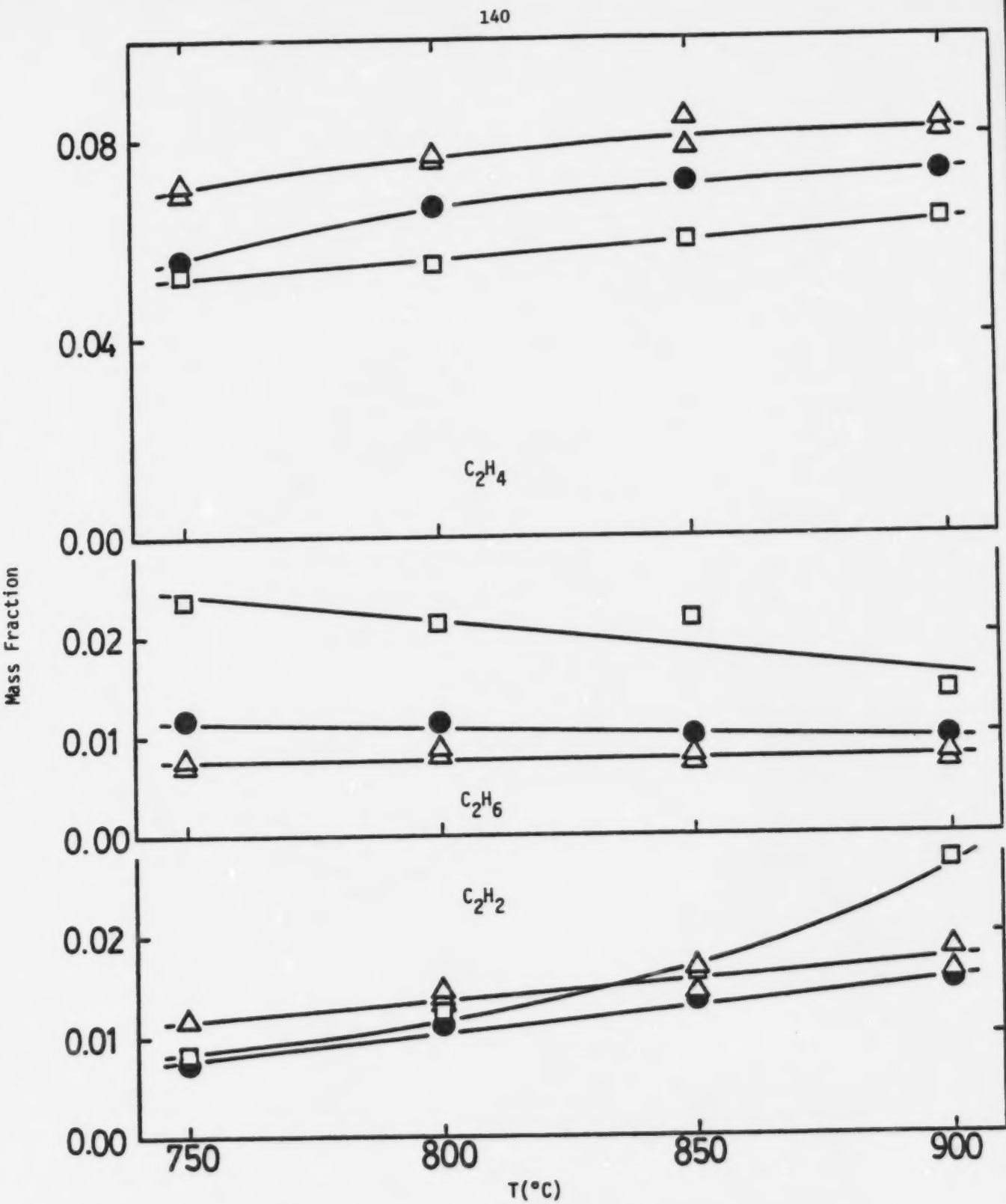

Figure 32 - Mass Fraction of Ethylene, Ethane and Acetylene In The Product Gas At Various Temperatures.

△ Cellulose ● Birch Wood □ Lignin

increase in conversion of the feedstock to a permanent gas at elevated temperatures, as the ring structure is cracked. Therefore, the ethane (and other aliphatics) which were probably formed at more moderate temperatures from the cracking of the propane chain, are simply being diluted at higher temperatures (i.e. the absolute yield is not decreasing).

10.2.5 Acetylene

The absolute yield of acetylene is expected to steadily increase with increasing temperature according to the literature (23), and this trend was apparently confirmed in the ULTRAPYROLYSIS trials (Figure 32).

The mass fraction of acetylene in the product gas rose in a linear relationship with increasing temperature for the experiments with wood and cellulose, and rose exponentially for lignin trials. The dramatic increase in acetylene from lignin at elevated temperatures, was probably due to the cracking of the ring structure which is thermally resistant at moderate temperatures.

10.2.6 Methane

As illustrated in Figure 33, lignin pyrolysis gave the highest mass fraction of methane in the product gas while cellulose pyrolysis gave the least. AT 750°C, the percentages (by mass) of methane in the product gas for lignin, birch and cellulose trials were 14.0, 8.0 and 5.5,respectively. Over the temperature range (750 to 900°C), this methane yield decreased with increasing temperature for lignin experiments and increased with increasing temperatures for those with cellulose. It remained

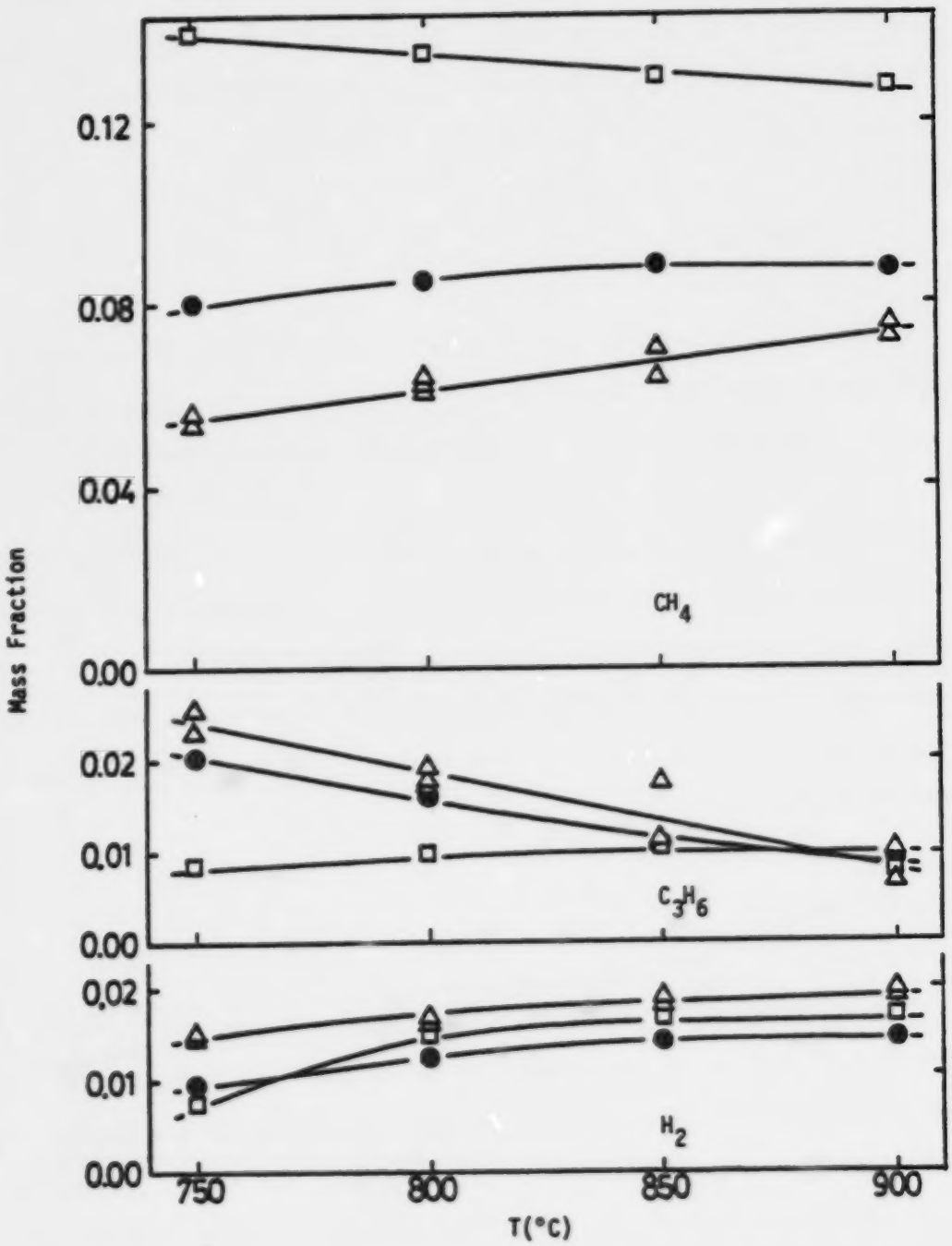

Figure 33 - Mass Fraction of Methane, Propylene, and Hydrogan In The Product Gas At Various Temperatures.

△ Cellulose ● Birch Wood □ Lignin

constant for wood trials indicating the relative contribution of the lignin and cellulose components. The relatively high concentration of methane which was observed in the pyrolysis of lignin, was probably due to the cracking of the methoxy group from the phenyl-propane lignin monomers, and the increase of methane with temperature for this component was most likely due to the corresponding increase in the cracking severity. Goheen (22) clearly demonstrated that there is no substantial cracking of methane in inert gas at temperatures up to 1200°C. Therefore, once formed by cracking of heavier molecules, methane will persist and appear in the final product gas.

The relatively low concentration of methane observed during cellulose pyrolysis, was assumed to be reflective of the heavily oxygenated nature of cellulose which increased the number of carbon atoms dedicated to the formation of carbon oxide gases. This, in turn, reduced the number of carbon atoms available for methane formation (23).

10.2.7 Propylene

Figure 33 indicates that at lower temperatures (750°C), the mass fraction of propylene in the product gas was 2.4, 2.0 and 0.8 percent for cellulose, wood and lignin experiments, respectively. At 900°C, the corresponding values were approximately 0.8 percent for all feedstocks. The decrease over the temperature range for cellulose and wood runs was linear, and attributed to an increase in cracking severity (propylene is not thermally stable at high temperatures).

Propylene yields for lignin were relatively constant over the temperature range with a slight increase at intermediate temperatures. As was indicated in previous sections, the benzene ring associated with the phenyl-propane lignin structure is more thermally stable than the aliphatic side chains. At lower temperatures the propylene was presumably formed from the cracking of the side chains. At higher temperatures, these aliphatic-derived molecules were rapidly cracked, but this effect could have been eclipsed by the production of propylene from the cracking of the relatively stable benzene ring. Propylene, thus formed, was not exposed to the reaction temperatures for the same period of time that the aliphatic-drived propylene was exposed to. Therefore, cracking of the former was presumably not completed and propylene appeared in the final gas product in spite of the high reaction temperatures.

10.2.8 Hydrogen

Over the entire experimental temperature range, cellulose gave the highest mass fraction of hydrogen in the product gas. The corresponding yield for lignin was the lowest of the biomass feedstocks at 750°C but rapidly overtook that of wood flour at 770°C and remained intermediate (i.e. between the yields for cellulose and wood flour experiments) up to 900°C.

The relatively low hydrogen yield for wood flour pyrolysis apparently suggests that some synergistic effect may be occurring such that the hydrogen production is not simply the sum of the pyrolysis of lignin and cellulose components. More likely, this phenomenon can be explained

by the lack of the mass balance determination (further explained in sections 10.2.2 and 10.2.4) or by the contribution of the pyrolysis of the hemicellulose component of the wood. The general increase in the mass fraction of hydrogen in the product gas over the temperature range for all biomass feedstocks, can simply be explained in terms of the increase in cracking severity with increasing temperature.

10.3 MOLAR RATIO OF PRODUCT GASES

10.3.1 Carbon Monoxide to Carbon Dioxide

As illustrated in Figure 34, the molar ratio of carbon monoxide to carbon dioxide increased with temperature and then levelled off for all biomass feedstocks. For ULTRAPYROLYSIS conditions, where there was little steam produced from the feedstock moisture and no steam in the carrier gas, the predominance of CO over CO_2 at high temperatures is predicted by the literature (23). The production of CO_2 from CO and steam by the water gas shift reaction, is **kinetically** favoured at elevated temperatures, but is limited by the availability of steam. However, the reverse step (i.e. the production of CO from CO_2 and H_2) is **thermodynamically** favoured at elevated temperatures.

10.3.2 Hydrogen to Carbon Monoxide

The molar ratio of hydrogen to carbon monoxide for any gas mixture can be used to give a clear indication of its utility as a synthesis gas. In methanol synthesis, for example, the ideal ratio is 2 to 1. During the ULTRAPYROLYSIS test period, the highest H_2/CO ratio was 0.42, and occurred

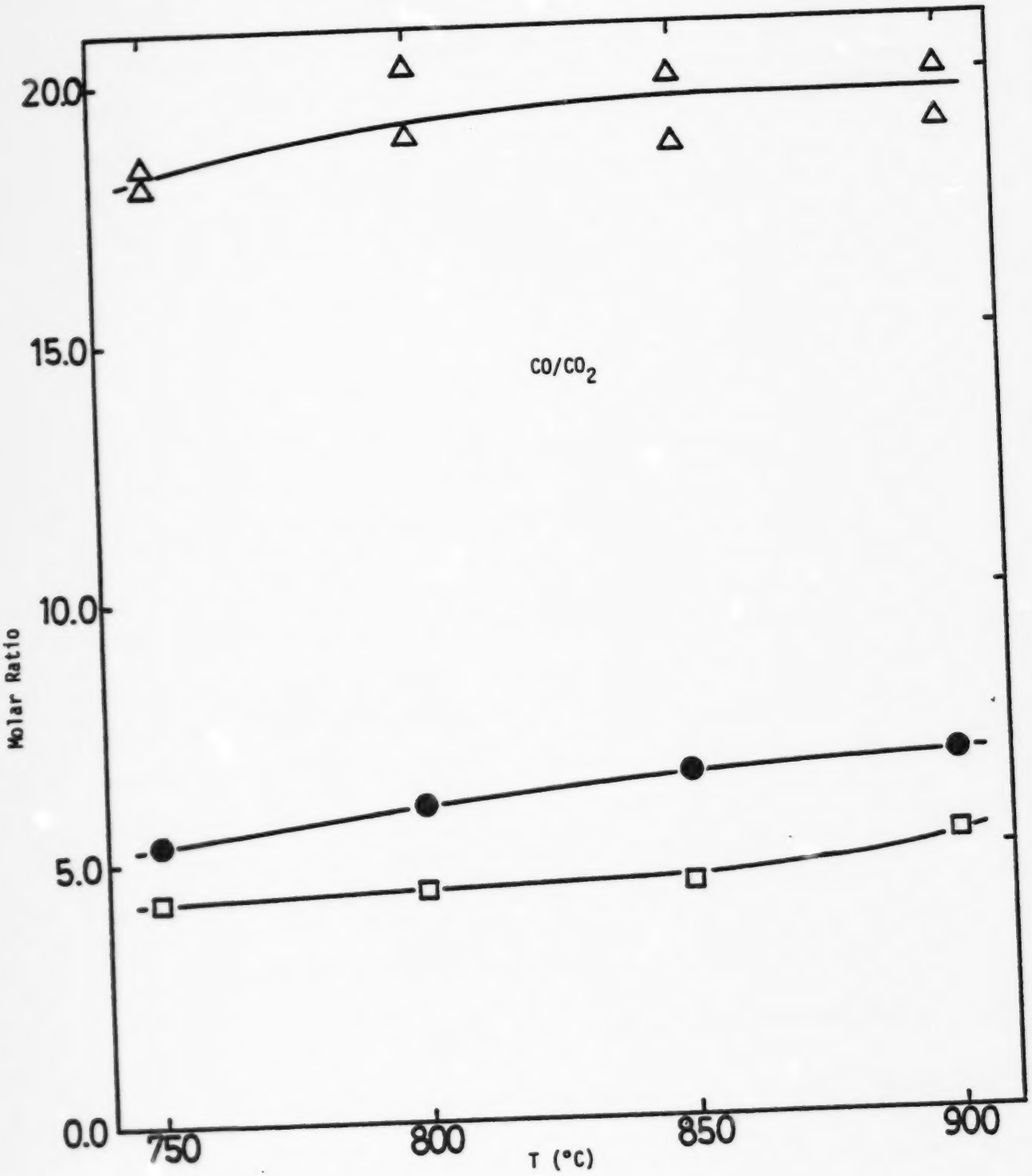

Figure 34 - Molar Ratio of Carbon Monoxide To Carbon Dioxide In The Product Gas At Various Temperatures.

△ Cellulose ● Birch Wood □ Lignin

during the lignin trials at 800°C (Figure 35). The corresponding values for cellulose and birch wood were lower. With the addition of steam at extended residence times (i.e. by allowing equilibrium to be reached),this ratio could have been substantially increased by "shifting" the carbon monoxide to carbon dioxide, thus producing additional hydrogen. Birch wood experiments gave lower ratios than either of its major constituents (lignin and cellulose), which was probably due to synergistic effects or to the contribution of the pyrolysis of its third major component, hemicellulose.

Another significant consideration can be related to all of the comparisons between birch wood and its representative major components, lignin and cellulose. This consideration deals with the chemical nature of lignin which varies significantly from species to species (also within the species, and within the individual tree!), even though all lignin structures have the phenyl-propane unit in common. Therefore, it is perhaps unsuitable to attempt to explain the behaviour of the birch flour pyrolysis in terms of commercially prepared non-birch lignin and cellulose products.

10.3.3 Ethylene to Ethane

The higher ULTRAPYROLYSIS temperatures tended to favour two-carbon unsaturates (i.e. ethylene and acetylene) over the aliphatic ethane molecules (Figure 36). The exponential increase of the ratio of ethylene to ethane with an increase in temperature might be explained in terms of the ethane cracking severity. Figure 33 seems to confirm this conclusion by

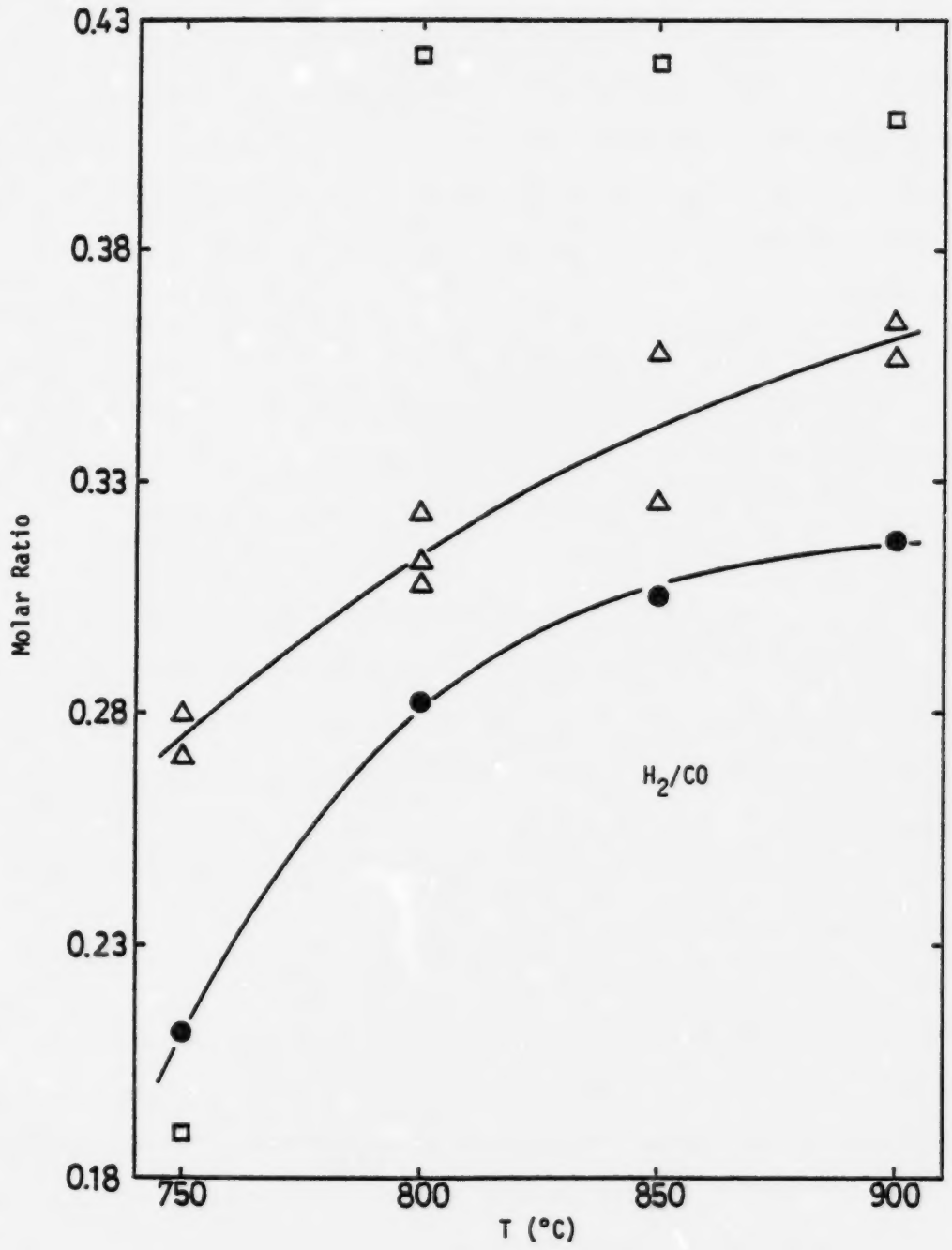

Figure 35 - Molar Ratio of Hydrogen To Carbon Monoxide In The Product Gas At Various Temperatures.

△ Cellulose ● Birch Wood □ Lignin

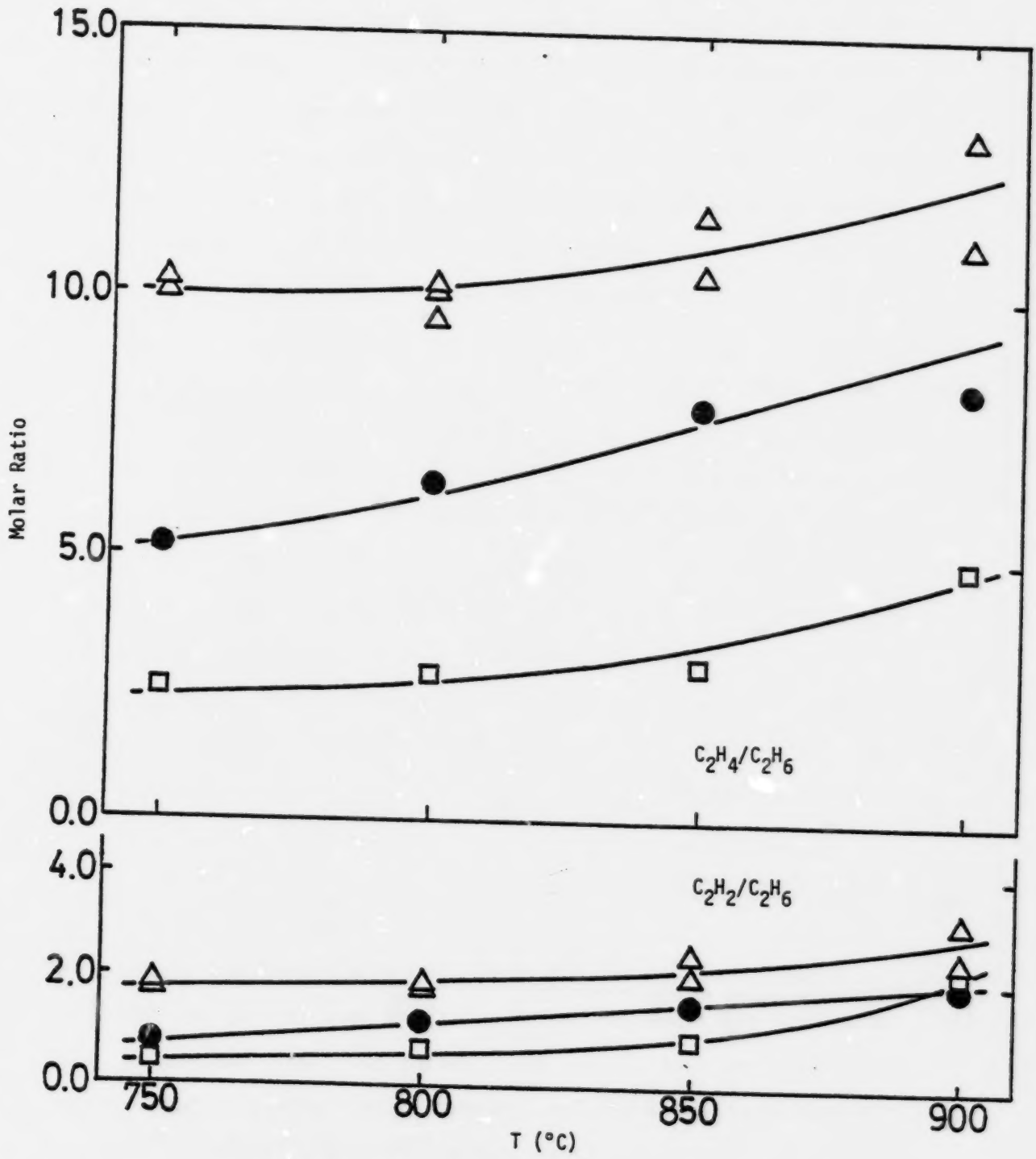

Figure 36 - Molar Ratios of Ethylene And Acetylene To Ethane In The Product Gas At Various Temperatures.

△ Cellulose ● Birch Wood □ Lignin

illustrating a drop in the ethane yield and an increase in ethylene production with increasing temperature. However, the fact that increased ethylene production eventually outstripped the corresponding drop in ethane would seem to suggest that additional ethylene is produced directly from parent molecules at elevated temperatures. The literature (23) indicates that as the temperature is further increased beyond 1000°C, the ethylene production should level off due to its disappearance and conversion to acetylene by additional cracking.

10.3.4 Acetylene to Ethane

As was the case in the ethylene to ethane ratio, the molar ratio of acetylene to ethane also increased exponentially with temperature (Figure 36). In addition, the increase in acetylene production eventually outstripped the corresponding decrease in the ethane. The explanation of this trend for acetylene is similar to that for ethylene. Not only was ethane apparently being cracked to acetylene, but heavier parent hydrocarbons were simultaneously being cracked to form additional acetylene molecules.

10.3.5 Propylene to Ethane

As the temperature was increased, the ratio of propylene to ethane in the product gas decreased for cellulose and wood trials, yet increased when lignin was used (Figure 37). During the lignin experiments, the propylene could have arisen from the cracking of the propane chains of the phenyl-propane lignin structure. However, it is more likely that it was a product of the destruction of the benzene ring units. There is a theoretical basis for this assumption (23):

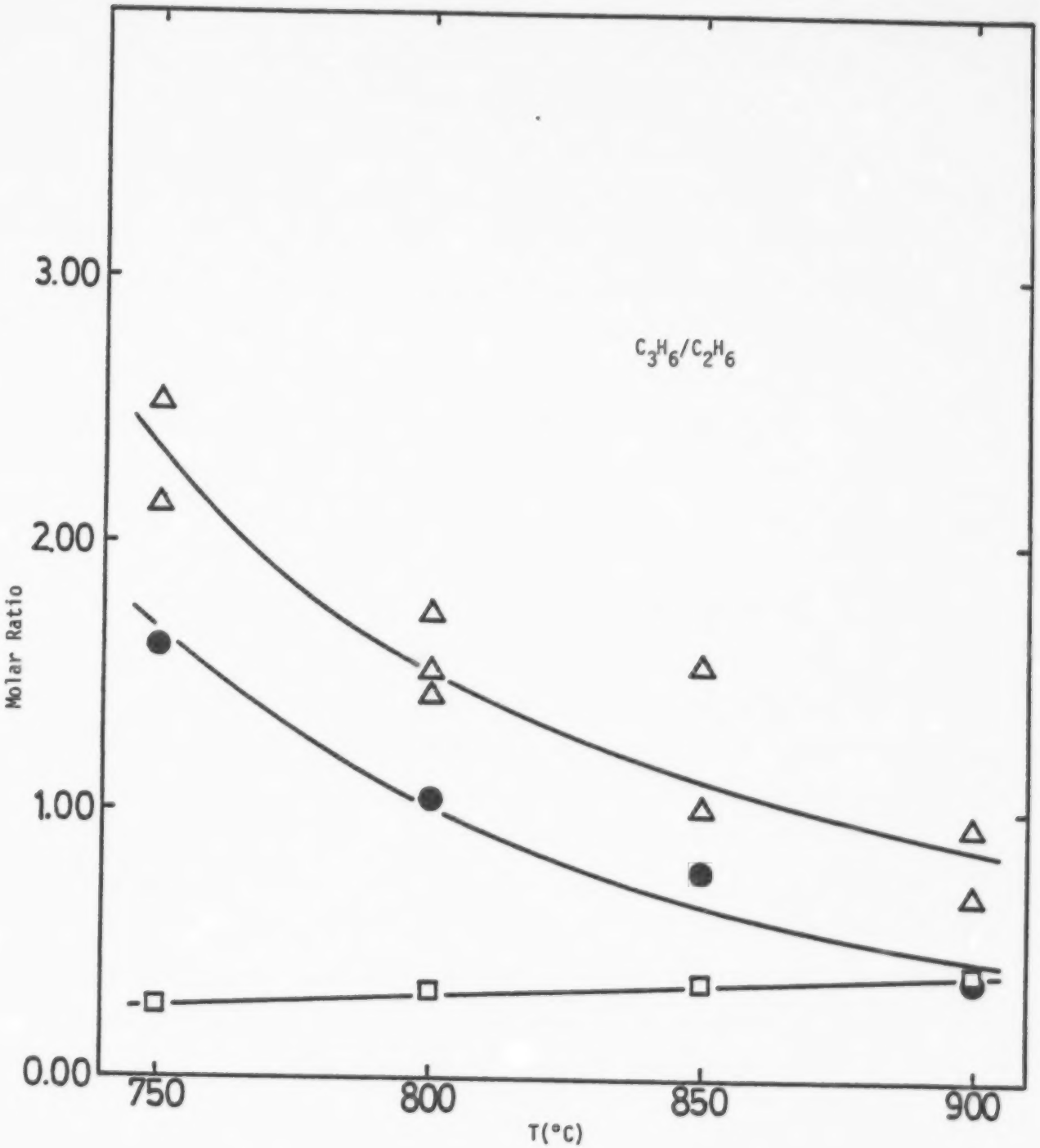

Figure 37 - Molar Ratio Of Propylene To Ethane In The Product Gas At Various Temperatures.

△ Cellulose ● Birch Wood □ Lignin

(i) The propane chains are rapidly cracked to lighter fragments at relatively low temperature (700°C).

(ii) Any propylene which is formed from propane or hydrocarbon molecules, are also rapidly cracked at relatively low temperatures.

(iii) The benzene rings in the lignin molecules are more thermally stable than non-aromatic molecules. Therefore, at higher temperatures, the ring may eventually be cracked to form acetylene and other unsaturates. However, the unsaturates may be quenched before additional cracking can occur, and are thereby preserved in the product gas.

10.3.6 C_2's to Methane

The molar ratio of all two carbon species to methane in the product is illustrated in Figure 38, and was less than unity for all biomass feedstocks over the entire experimental temperature range. This indicated the predominance of methane over the C_2's (expressed as molar fraction of the product gas). For trials with lignin, the ratio rose exponentially with temperature, reflecting the exponential rise in acetylene coupled with a gradual linear drop in methane. The other C_2's offset each other since the fraction of ethane dropped moderately and that of ethylene rose moderately, with a corresponding increase in temperature (see Figures 32 and 33).

The molar ratio of C_2's to methane dropped with an increase in temperature. This reflected an increase in the mass fraction of methane

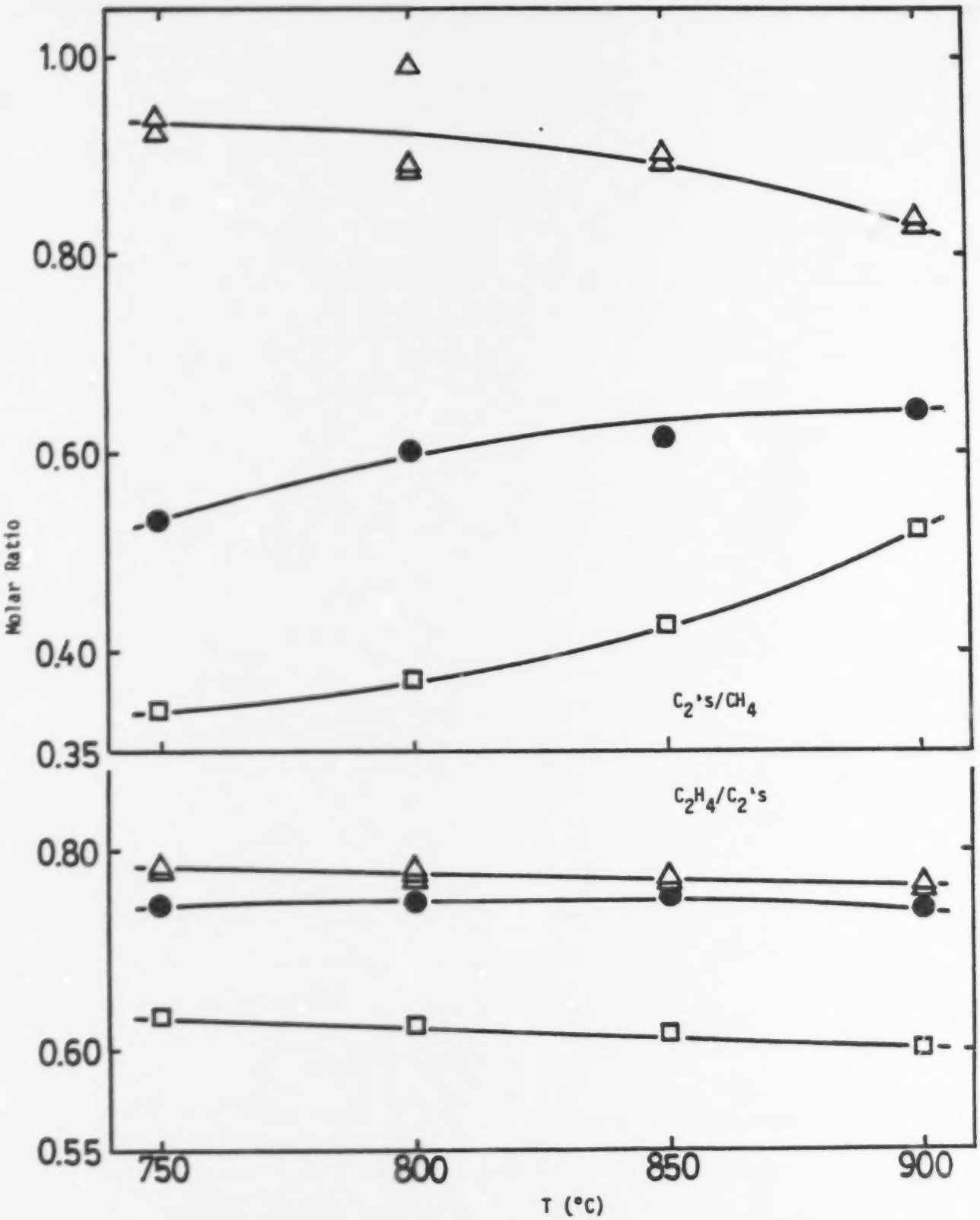

Figure 38 - Molar Ratios of C_2's To Methane And Ethylene To C_2's In The Product Gas At Various Temperatures.

△ Cellulose ● Birch Wood □ Lignin

in the product gas (Figure 33) coupled with relatively constant mass fractions of ethylene, ethane and acetylene in the product gas over the range of experimental temperatures (Figure 32). The molar ratio of C_2's to methane for wood flour trials was consistently between the corresponding values for lignin and cellulose. Although this apparently indicated the individual contribution of lignin and cellulose pyrolysis to the "whole" biomass pyrolysis, the reader is cautioned that the results may be misleading. The Indulin lignin used in this study, was most likely disimilar to the birch lignin. In addition product yields were expressed as a fraction of the product gas, not as a fraction of the biomass feedstock. Therefore, comparisons of the **absolute** yields of the individual products were not made.

10.3.7 Ethylene to C_2's

Ethylene constituted between 60 and 80 mole percent of all of the two carbon species, and was thus the major C_2 component. Cellulose trials gave the highest ratio of ethylene followed by wood and lignin trials, respectively (Figure 38). The ratio remained relatively constant over the range of experimental temperatures for all biomass feedstocks, indicating perhaps that all of the C_2's were formed in a common chemical mechanism.

10.4 Hydrocarbons

As illustrated in Figure 39, lignin pyrolysis clearly gave the highest yelds of total hydrocarbons expressed as a mass fraction of the product gas. At 900°C, the hydrocarbon content of the product gas was

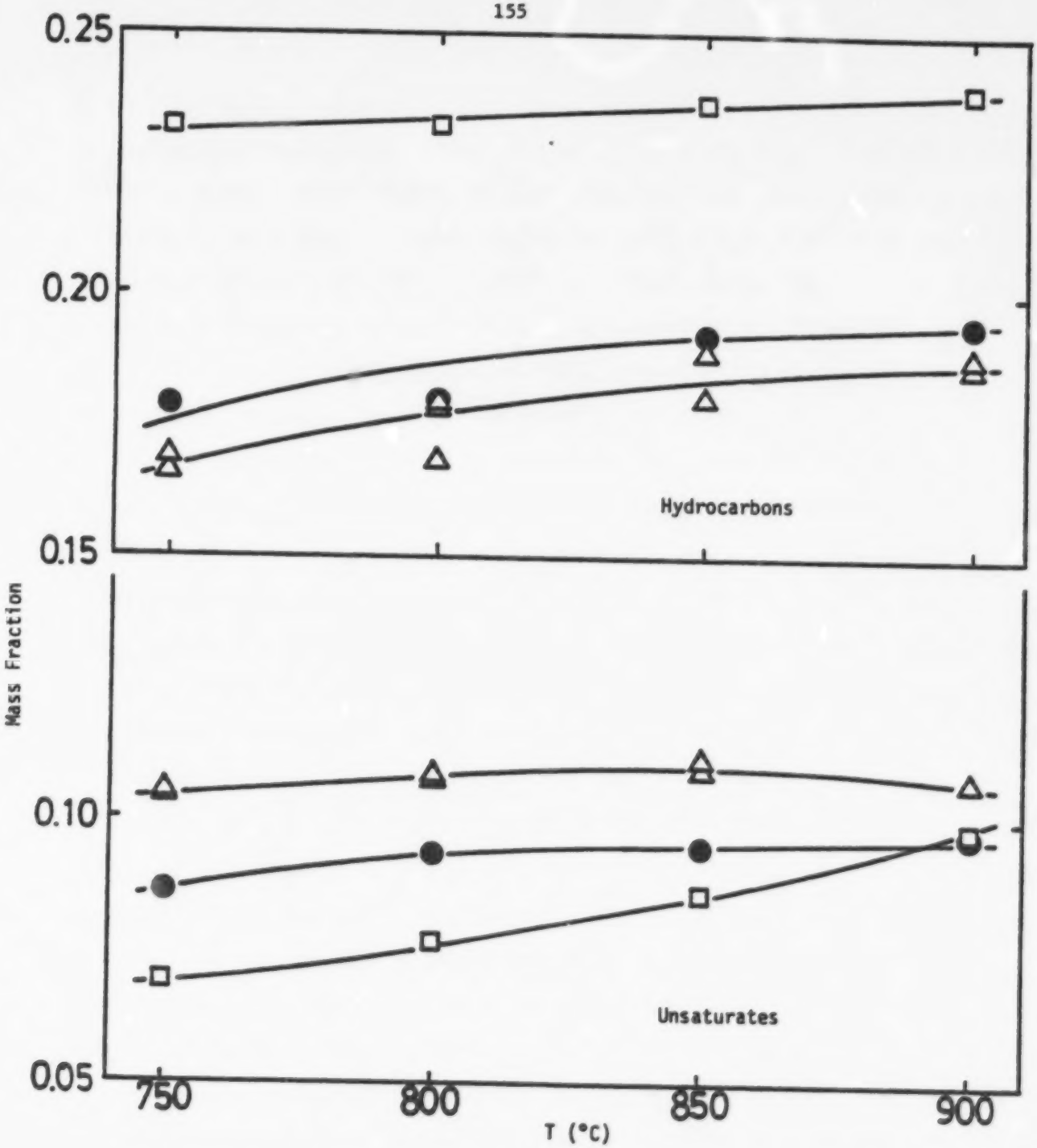

Figure 39 - Mass Fraction Of Total Hydrocarbons And Unsaturates In The Product Gas At Various Temperatures.

△ Cellulose ● Birch Wood □ Lignin

approximately 24 percent (by mass) for lignin trials. The corresponding values were 19.4 and 18.7 percent (by mass) for birch flour and cellulose runs respectively, at 900°C. The hydrocarbon yields tended to level off after moderate increases during the pyrolysis of cellulose and birch wood (as the temperature was increased), while the hydrocarbon yield rose linearly with temperature during lignin pyrolysis. Once again, the values for the wood pyrolysis hydrocarbon yields were consistently between the corresponding values for cellulose and lignin pyrolysis.

Since the unsaturated hydrocarbons (i.e. alkenes and alkynes) are of particular commercial interest in the petrochemical industry, the yields of these valuable chemicals were singled out and expressed as a mass fraction of the product gas (Figure 39). The unsaturates represented between 7 and 11 percent of the product gas during the pyrolysis of wood, cellulose, and lignin at temperatures of 750 to 900°C.

Cellulose generated the highest fraction of unsaturates compared to the other feedstocks, but the yields tended to level off at temperatures exceeding 850°C. The yield of unsaturates from lignin rose exponentially with temperature reflecting the thermal resistance of the aromatic units which tend to crack at higher temperatures (the aliphatic side chains crack at lower temperatures yielding lesser amounts of unsaturates). The behavior of wood with respect to hydrocarbon yields apparently reflected the sum of the pyrolysis of its major components since its yield curve (Figure 39) lies between those for cellulose and lignin trials

The unsaturated portion of the total hydrocarbons in the product gas are reported in Figure 40. This fraction will probably have utility as a "gas quality index" for eventual commercial operation since the non-hydrocarbon gases will most likely be separated out and used as the system transport gas (leaving only hydrocarbons in the product gas). Since unsaturates are of greater comercial significance than saturates, a ratio (i.e. unsaturates/total hydrocarbons) which approaches unity will indicate a high quality gas.

Cellulose consistently produced a higher unsaturate to total hydrocarbon ratio than the other feedstocks over the experimental temperature range. However, this ratio dropped linearly with an increase in temperature. the trend was the opposite for trials with lignin, which gave the lowest unsaturate to hydrocarbon ratio of all feedstocks (yet the ratio increased linearly with temperature). The pyrolysis of wood was once again approximately the sum of the pyrolysis of its cellulose and lignin components (i.e. Figure 40 illustrates that the wood data are generally between those for cellulose and lignin). The average yields of unsaturates in the hydrocarbon content of the product gas were 60, 50 and 35 percent (by mass) for cellulose wood and lignin, respectively.

As illustrated in Figure 41, ethane constituted between 9 and 13 percent of the total mass of the saturated hydrocarbons in the product gas over the range of experimental temperatures (the balance was primarily methane). This mass ratio was similar for all of the biomass feedstocks, and decreased linearly with an increase in temperature. The decrease was probably due to the cracking of ethane to ethylene and acetylene as the temperature was increased.

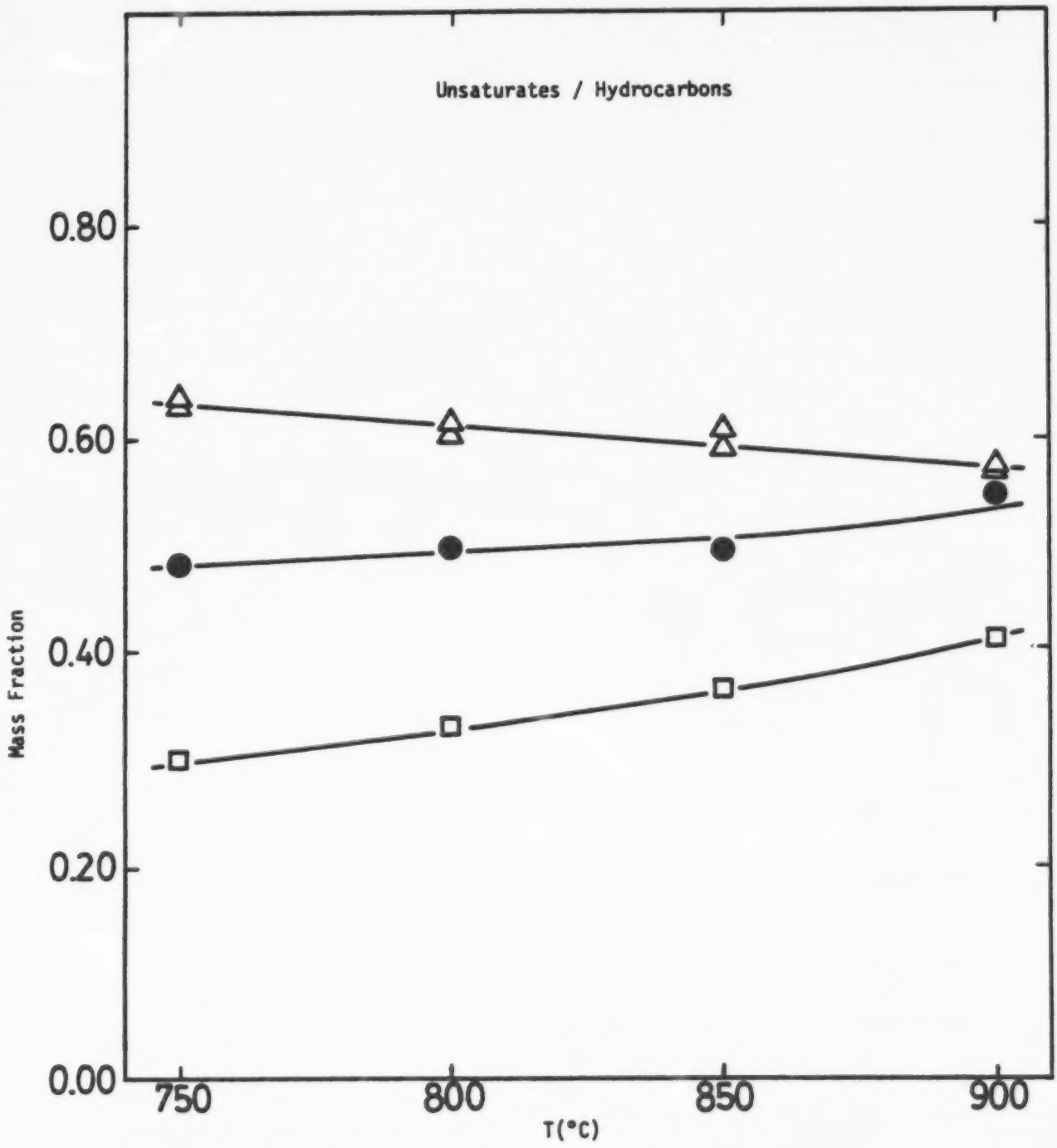

Figure 40 - Mass Fraction Of Unsaturates In The Hydrocarbon Content Of The Product Gas At Various Temperatures.

△ Cellulose ● Birch Wood □ Lignin

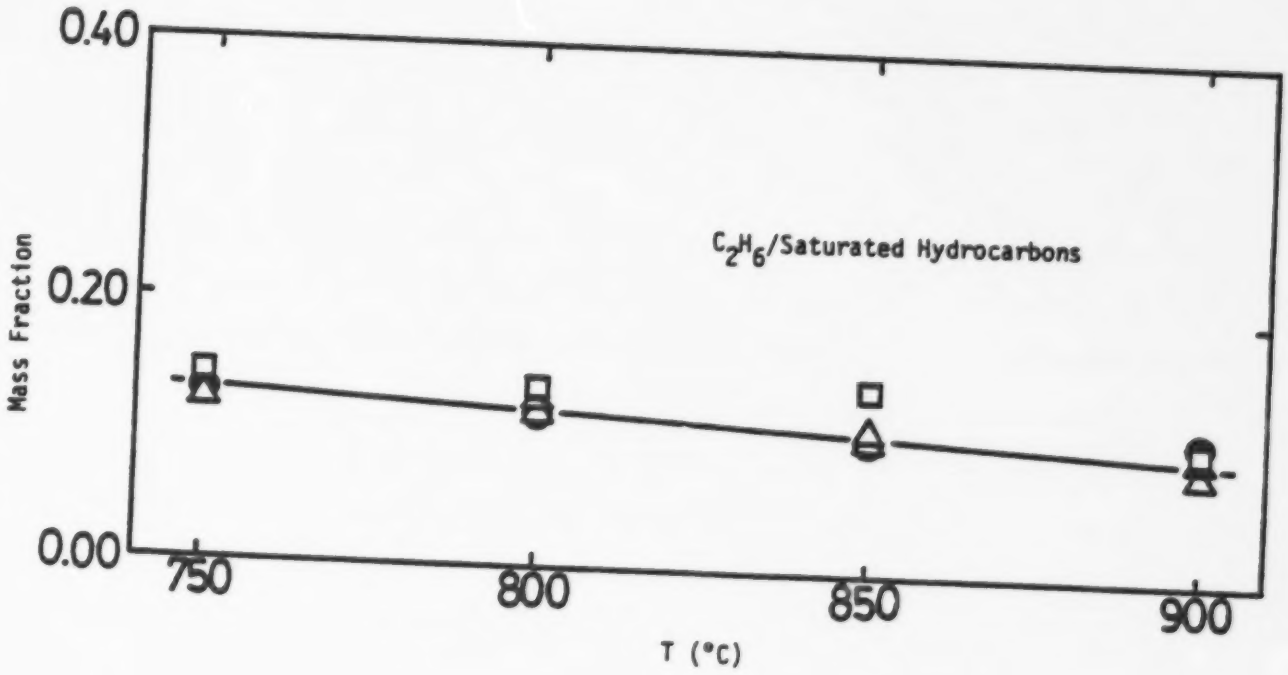

Figure 41 - Mass Fraction Of Ethane In The Saturated Hydrocarbon Content Of The Product Gas At Various Temperatures.

△ Cellulose ● Birch Wood □ Lignin

Figure 42 indicates the yield of methane expressed as a fraction of the total mass of hydrocarbons in the product gas. This yield remained relatively constant over the temperature range for wood pyrolysis. There was, however, a slight increase in the fraction of methane for cellulose trials, and a moderate decrease for lignin trials, as the temperature was increased.

If the two sets of curves in figure 42 are compared, it is evident that for lignin pyrolysis, the fraction of methane in the total hydrocarbon content of the product gas was significantly greater than the corresponding C_2 fraction over the entire experimental temperature range. However, this trend was reversed for cellulose pyrolysis, and the C_2 mass fraction in the total hydrocarbons was significantly greater than the fraction of methane. For wood trials, the methane and C_2 fractions were roughly equal at 750°C; although the C_2 fraction predominated slightly as the temperature was increased. Figure 42 also indicates that the results from wood pyrolysis (i.e. for methane and C_2 contents in the hydrocarbon content of the product gas) were explicable in terms of the behaviour of the sum of the pyrolysis of the lignin and cellulose components.

The fractions of the various individual unsaturated species (ethylene, acetylene and propylene) in the total unsaturated portion of the product gas are presented in Figure 43. Ethylene was clearly the major unsaturated species between 750 and 900°C for all feedstocks. However, this fractional ethylene yield levelled off or actually decreased (depending on the feedstock) as the temperature was increased while the fractional acetylene yield rose linearly or exponentially (depending on

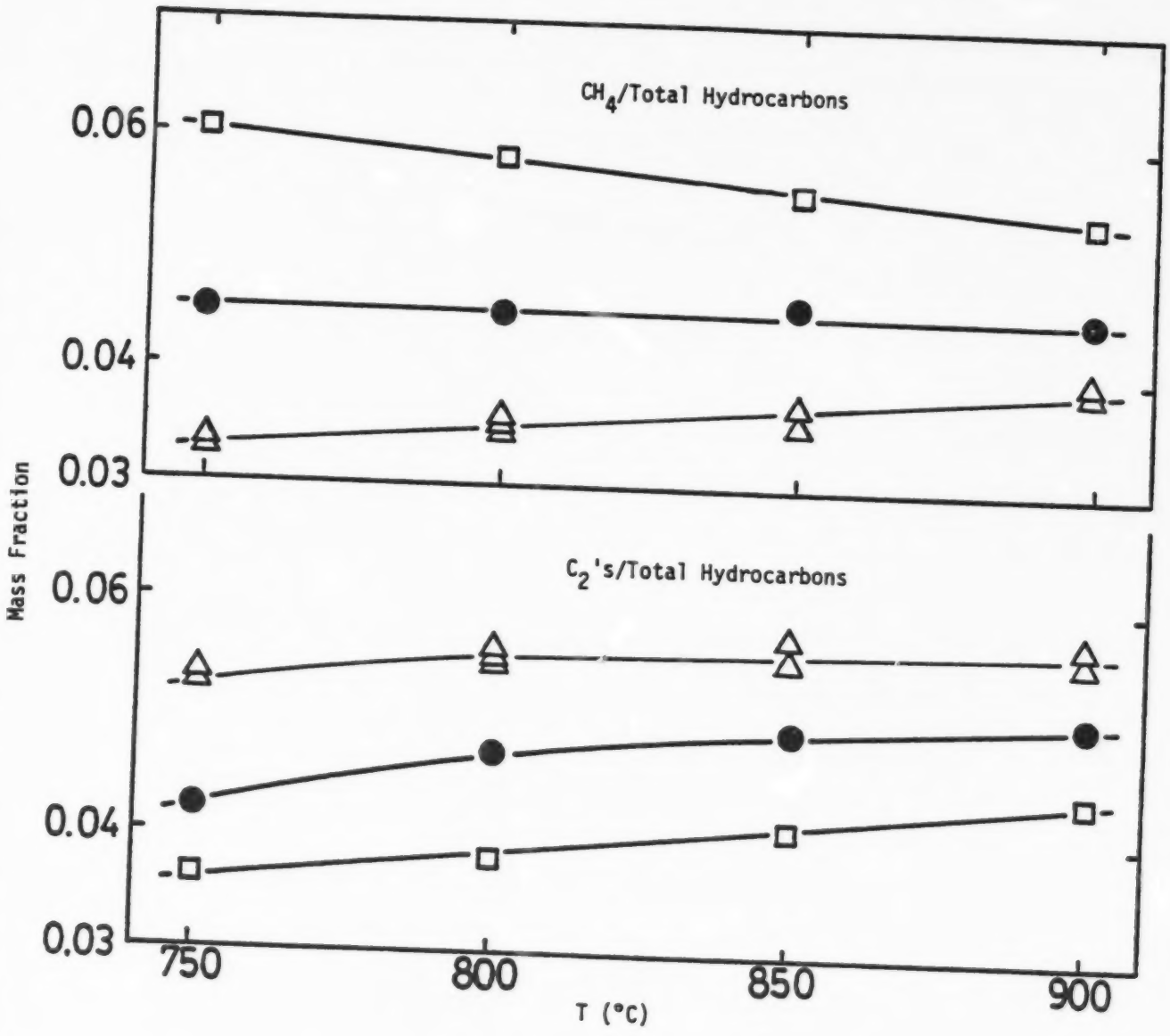

Figure 42 - Mass Fraction Of Methane And C_2's In The Total Hydrocarbon Content Of The Product Gas At Various Temperatures.

△ Cellulose ● Birch Wood □ Lignin

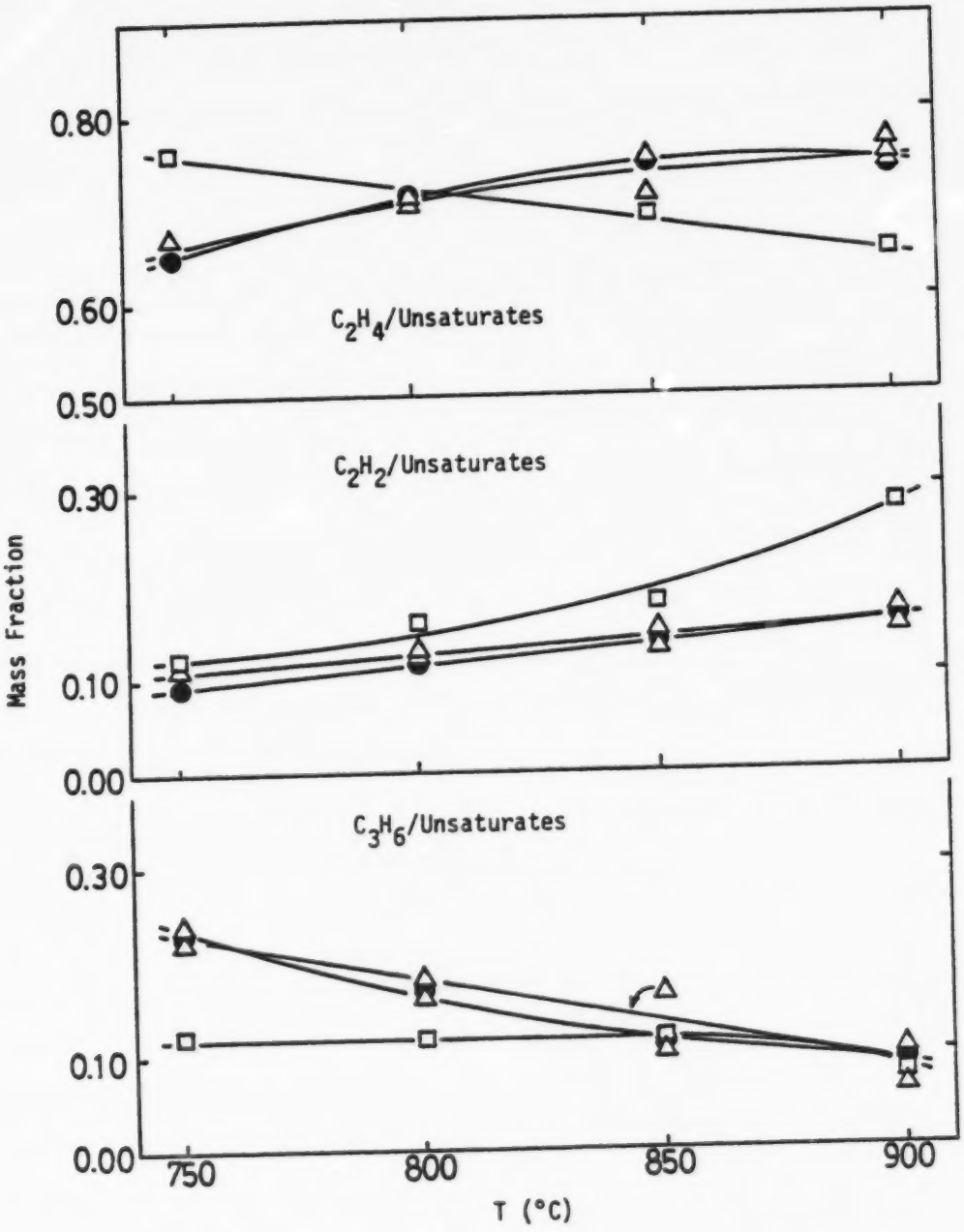

Figure 43 - Mass Fraction Of Ethylene, Acetylene And Propylene In The Unsaturated Content Of The Product Gas At Various Temperatures.

△ Cellulose ● Birch Wood □ Lignin

the feedstock). The fractional propylene yield dropped linearly for cellulose trials with an increase in temperature, dropped moderately at lower temperatures and eventually levelled off at higher temperatures for wood trials, and remained relatively constant at lower temperatures but dropped off at elevated temperatures for lignin trials (Figure 43).

All of the above trends have a clear theoretical basis. Propylene is more rapidly cracked at lower temperatures than ethylene or acetylene and therefore is expected to decrease in favour of ethylene and acetylene as the temperature is increased. This, in fact, was the case for the ULTRAPYROLYSIS cellulose and wood experiments. The aromatic units in lignin were cracked at higher temperatures (i.e. they are more thermally stable than both the cellulose monomers and the aliphatic lignin side chains. Therefore, the decrease in the yield of propylene (i.e. the propylene derived from lignin side chain cracking) which was expected due to its cracking to acetylene and ethylene as temperatures were incresed, was eclipsed by the production of additional propylene from the cracking of the aromatic lignin units moderately high temperatures. The propylene, thus formed, did not have time to completely crack and therefore persisted in the final gas product. At 900°C, the aromatic-derived propylene was exposed to extremely severe cracking conditions and once again the downward trend is evident. At elevated temperatures (for all feedstocks) the fractional ethylene yield levelled off, or actually dropped, as the mechanisms of acetylene formation (i.e. from ethylene cracking) began to take over. The exponential increase in the fractional acetylene yield from lignin as temperature was increased, was probably due to the cracking of the aromatic units.

It is interesting to note that the fractional yields for all unsaturate species, during the pyrolysis of wood, more closely resembled the corresponding yields for cellulose trials rather than those for lignin trials (Figure 43). This can be partially explained in terms of the fundamental theory of biomass pyrolysis. At lower temperatures, the cellulose component and the lignin side chain components of wood readily pyrolyze. The resulting primary pyrolysis products are then rapidly cracked to produce olefins and other unsaturates. The aromatic units of the lignin component are not pyrolyzed and cracked to unsaturates as quickly as the cellulose-derived primary tars unless exposed to higher temperatures. Therefore, one would expect similar trends for wood and cellulose pyrolysis at lower temperatures (i.e. approx. 700°C).

However, at higher temperatures, one would expect the unsaturate yields from wood pyrolysis to reflect the combined pyrolysis of both the lignin aromatic units, and the partially cracked cellulose-derived hydrocarbons. This was not apparently observed in the actual ULTRAPYROLYSIS results as illustrated in Figure 43. As a matter of fact, the fractional yields of acetylene and ethylene from wood pyrolysis continued to resemble the corresponding acetylene and ethylene yields from cellulose pyrolysis, at elevated temperatures. It appears that some synergistic effects were operating during the pyrolysis of wood, which caused the lignin component to favour higher fractional yields of ethylene at the expense of acetylene yields (whereas the opposite behaviour was exhibited during the pyrolysis of pure lignin).

10.5 Heating Value of the Product Gas

It is clear that the nature of the carrier gas used in the ULTRAPYROLYSIS process will affect both the higher heating value (HHV) and the final composition of the product gas. In a commercial application, it is likely that steam will be used as the carrier gas since it can be readily separated from the product gas by condensation (thus reducing product dilution) and since it is considered to be chemically inert under fast pyrolysis conditions (23). Therefore, the dry nitrogen-free higher heating values of the ULTRAPYROLYSIS product gas, as reported in Figure 44, are likely similar to those higher heating values which will occur in a commercial operation.

The higher heating value of the product gas dropped with an increase in temperature from 750 to 800°C for all biomass feedstocks (Figure 44). However, from 800 to 900°C, these values remained relatively constant and were estimated (from the cumulative energy content of the individual gas components) to be 15.9, 16.1 and 18.1 megajoules per normal cubic meter (MJ/Nm^3) for cellulose, wood and lignin trials, respectively (expressed in the more familiar British units, the corresponding values are 403, 410 and 460 Btu/scf). The energy content of the lignin pyrolysis product gas was higher per unit volume than the energy contents of wood and cellulose porduct gases. This was due to the presence of a relatively large molar fraction of hydrocarbons (see Table 20) which have a higher energy "density" than lighter components such as carbon monoxide. Cellulose and wood pyrolysis gas products had larger molar fractions of carbon monoxide which tended to reduce the overall energy density (relative to the energy content for lignin trials).

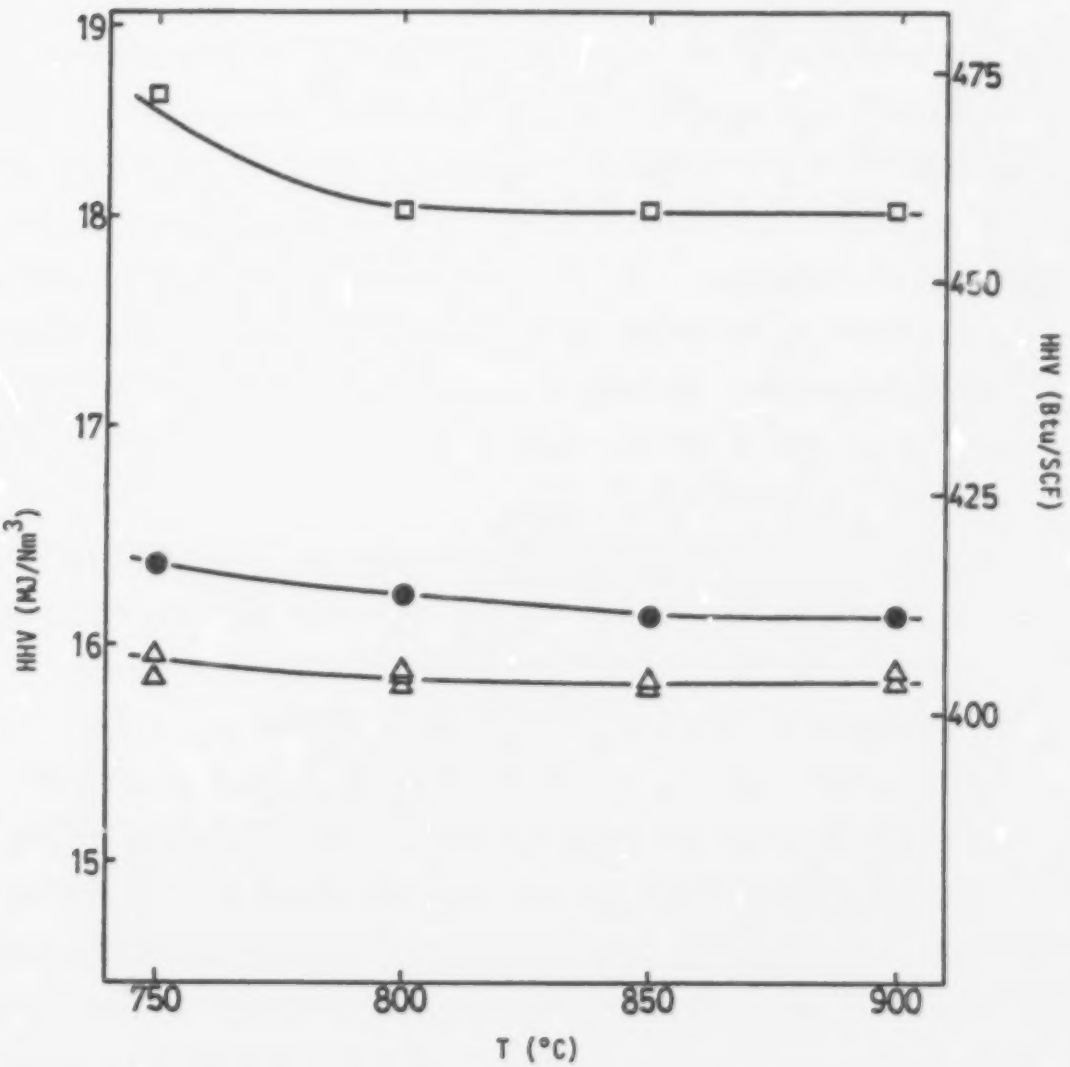

Figure 44 - Higher Heating Values Of The Product Gas Over The Range Of Reaction Temperatures.

△ Cellulose ● Birch Wood □ Lignin

10.6 Molecular Weight of the Product Gas

The average molecular weight of the product gas is given as a function of temperature, for the various biomass feedstocks, in Figure 45. For all biomass feedstocks, the average molecular weight of the product gas decreased with an increase in temperature and tended to level off at 900°C. This general decrease of molecular weight with increasing temperature was due to a corresponding increase in cracking severity, (i.e. heavier hydrocarbons are increasingly cracked to lighter fragments).

The highest value for the product gas molecular weight was 25.4 kg per kg-mole, and occurred during the birch wood experiments at 750°C. The lowest value was 21.7 kg per kg-mole, and occurred for cellulose trials at 900°C. The cellulose pyrolysis gas molecular weight was relatively low due to the presence of a higher molar fraction of light hydrogen and carbon monoxide molecules (i.e. relative to the lignin and wood product gases).

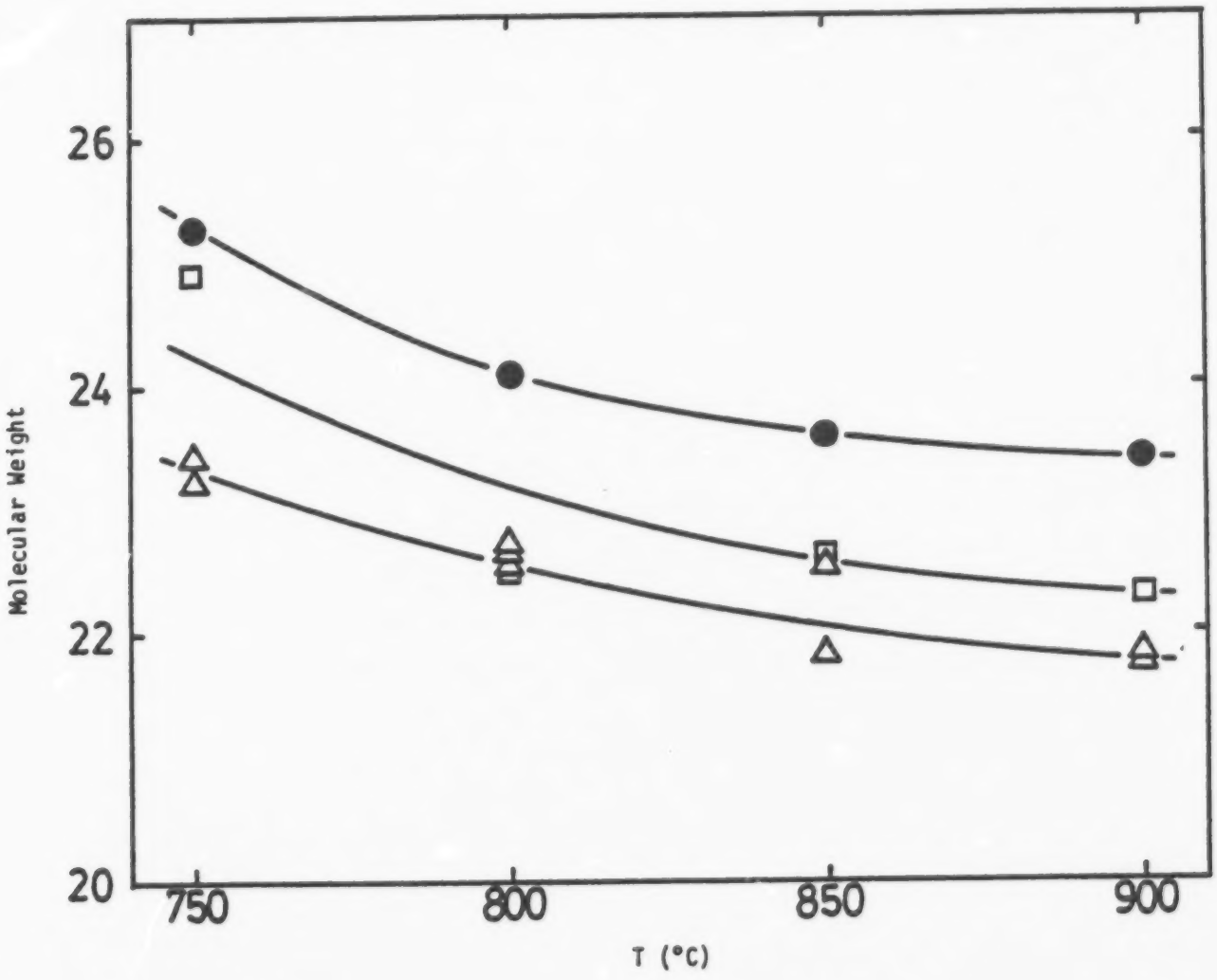

Figure 45 - Molecular Weight Of The Product Gas At Various Temperatures.

△ Cellulose ● Birch Wood □ Lignin

11.0 CONCLUSIONS

The major accomplishment of the ULTRAPYROLYSIS project was the demonstration of the chemistry of fast pyrolysis in equipment that could be used as a conceptual basis for eventual commercial scale-up. In addition, a new reactor design was developed in order to accommodate the high heating rates, rapid thorough mixing, and extremely fast residence times which are required to successfully accomplish fast pyrolysis of biomass. This reactor concept has the potential for other commercial applications which are not necessarily related to pyrolysis.

Preliminary results were extremely encouraging with respect to yields of valuable chemical intermediates and total hydrocarbons. Maximum ethylene yields, expressed as a mass fraction of the product gas, were 8.2, 7.3 and 6.3 percent for cellulose, wood and lignin trials, respectively, at 900°C. Total unsaturated hydrocarbon yields, also expressed as a mass fraction of the product gas, were 10.7, 9.7 and 9.8 percent for cellulose, wood and lignin experiments, respectively, at 900°C. The corresponding yields of total hydrocarbons in the product gas from the pyrolysis of cellulose, wood and lignin, were 18.8, 19.4, and 23.9 percent by mass, respectively, at 900°C.

In general, the pyrolysis of wood was explicable in terms of the pyrolysis of its two major components, cellulose and lignin. However, exceptions to this generalization were evident in some of the results which suggested one or more of the following phenomenon:

(i) Synergistic effects were prevalent during wood pyrolysis (i.e. the interaction of the cellulose, lignin and hemicellulose exhibited an effect whch was not simply the sum of the pyrolysis of the individual components).

(ii) The representative pure lignin sample (i.e. Indulin AT) was chemically disimilar in some significant manner, to the actual birch lignin component.

(iii) Experimental analytical errors were committed.

It was difficult to independently examine the effects of temperature and residence time without affecting the various solids loadings (i.e. for biomass THERMOFOR and CRYOFOR solids) and also the THERMOFOR to biomass mass ratio. This lack of independent control was due to the fixed reactor volume (which prevented manipulation of the residence times without changing the various suspension flow rates or reactor temperatures), and also due to the behaviour of the fluidized bed feeders which delivered a given solids mass flowrate as a function of transport line gas flowrate and downstream system pressure. Incorporation of a mechanical biomass feeder design (which allows independent control of solids loading and transport gas flowrate) and the intended use of reactor tube inserts to manipulate reactor volume, will allow better isolation of the effects of individual variables in the next phase of the work.

12.0 ACKNOWLEDGEMENTS

The generous funding of this project by the Enfor Program (Environment Canada/Energy Mines and Resources Canada), and the excellent cooperation and advice of Dr. D.P.C. Fung and Dr. R.P. Overend are greatly appreciated by the entire ULTRAPYROLYSIS research team.

The following staff members in the Faculty of Engineering Science at the University of Western Ontario deserve mention for their kind assistance during the course of the project; Mr. R. Kager, Mr. H. Cook and Mr. R. Stuart (Engineering Shop); Mr. E. Price and Mr. A. Dieroff (Engineering Stores); Mrs. A. Leitch, Mrs. C. Reid and Mrs. C. Brown (Secretarial Services). The following professional colleagues contributed valuable expertise: Mr. G. Babaz, Mr. P. Galtier, Mr. W. Twarog, Mr. T. Cederberg, Mr. J.P. Gibeault, Mr. M. Nadeau, Mr. S. Duffin, Mr. D. Braun and Mr. M. Schmidt.

Several companies provided goods and services gratis during the course of the project:

FMC, Philadelphia PA (Avicel Cellulose)	Mr. R. Barfoot
IOTECH, Ottawa, Ont. (Lignin)	Mr. G. Noble
W.R. GRACE CO., Valleyfield, P.Q. (Cracking Catalyst)	Mr. Gagné
WESTVACO, Charleston Heights, SC. (Birch Flour)	Mr. T. Diamond
UNIVERSITY OF SHERBROOKE, Sherbrooke, P.Q. (Analytical Services)	Dr. C. Roy

13.0 REFERENCES

1. Soltes, E.J. and T.J. Elder. 1978. "Thermal Degradation Routes to Chemicals from Wood." Proceedings of the 8th World Forestry Congress Proceedings. Jakarta, Indonesia. October.

2. Soltes, E.J. and T.J. Elder. 1981. "Pyrolysis". In Organic Chemicals from Biomass. I.S. Goldstein, Editor. CRC Press. Boca Raton, FL.

3. Soltes, E.J., Wiley, Allen T., and S.C. Kenny Lin. 1981. "Biomass Pyrolysis. Towards an Understanding of its Versatility and Potentials." 3rd Symposium on Biotechnology in Energy Production and Conservation. Gatlinburg, TN. May 12-15. Sponsored by the U.S. Department of Energy. Washington, D.C.

4. Shafizadeh, F. 1968. "Pyrolysis and Combustion of Cellulosic Materials." Advances in Carbohydrate Chemistry 23:419-465.

5. Shafizadeh, F. "Introduction to Biomass Pyrolysis." Proceedings of the Specialists' Workshop on Fast Pyrolysis of Biomass. Copper Mountain, CO. October 19-22. Sponsored by the Solar Energy Research Institute. Golden, CO.

6. Broido, A. 1976. "Kinetics of Solid Phase Cellulose Pyrolysis". In Thermal Uses and Properties of Carbohydrates and Lignins. F. Shafizadeh, Editor. Academic Press, N.Y.

7. Lewellen, P.C., Peters, W.A., and J.B. Howard. 1977. "Cellulosic Pyrolysis Kinetics and Char Formation Mechanism." 16th International Symposium on Combustion. The Combustion Institute. Pittsburgh, PA.

8. Milne, T.A. 1979. "Pyrolysis - Thrmal Behaviour of Biomass Below 600°C." In A Survey of Biomass Gasification. Volume II. Principles of Gasification. Solar Energy Research Institute. Golden, CO.

9. Milne, T.A. and M. Soltys. 1981. "Kinetics and Mechanisms of Fast Pyrolysis." Proceedings of the 12th Thermochemical Conversion Contractor's Review Meeting. Washington, D.C. March 18-19. Sponsored by the United States Department of Energy.

10. Milne, T.A. and M. Soltys. 1982. "Fundamental Pyrolysis Studies." Quarterly Report. October-December 1981. SERI/PR-234-1537. Solar Energy Research Institute. Golden, CO.

11. SERI. 1980. "Specialists' Workshop on Fast Pyrolysis of Biomass." SERI/CP-622-1096. Solar Energy Research Institute. Golden, CO.

12. Diebold, James and John Scahill. 1981. "October 1981 Update on the Progress in the Entrained Flow, Fast Ablative Pyrolysis of Biomass." Proceedings of the 13th Biomass Thermochemical Conversion Contractors' Meeting. Arlington, VA. October 27-29. Sponsored by the Pacific Northwest Laboratory, Batelle Memorial Institute. Richland, WA.

13. Reed, T.B., Diebold, J.P. and R. Desrosiers. 1981. "Biomass Gasification for Production of Gaseous and Liquid Fuels". Proceedings of the 3rd Symposium on Biotechnology in Energy Production and Conservation. Gatlinburg, TN. May 12-15. Sponsored by the United States Department of Energy. Washington, D.C.

14. Bergougnou, M.A., de Lasa, H., Mok, L.K., Graham, R. and J. Hazlett. 1981. "High Intensity Flash Pyrolysis of Wood Using Solid Heat Carriers (Ultrapyrolysis)." Bioenergy R&D Seminar, Otttawa, March 23-25. Sponsored by the National Research Council of Canada. Ottawa, Canada.

15. Mok, L.K., Graham, R.G., Bergougnou, M.A., and H.I. de Lasa. 1982. "Continuous Ultra-Flash Pyrolysis of Wood Using Soilid Heat Carriers and Vortical Contactors (Ultrapyrolysis)." Proceedings of the Industrial Wood Energy Forum '82 Conference. Washington, D.C. March 8-10. Sponsored by the Forest Products Research Society. Madison, WI.

16. Deglise, X., Richard, C., Rolin, A. and H. Francois. 1980. "Fast Pyrolysis/Gasification of Lignocellulosic Materials at Short Residence Time." Energy from Biomass Conference. Brighton, England.

17. Hajaligol, M.R., Peters, W.A., Howard, J.B. and J.P. Longwell. 1980. "Product Comositions and Kinetics for Rapid Pyrolysis of Cellulose." Proceedings of the Specialists' Workshop on Fast Pyrolysis of Biomass. Copper Mountain, CO October 19-22. Sponsored by the Solar Energy Research Institute, Golden, CO.

18. Reed, T.B. 1980. "Perspectives in Heat Transfer Requirements and Mechanisms for Fast Pyrolysis." Proceedings of the Specialists' Workshop on Fast Pyrolysis of Biomass. Copper Mountain, CO. October 19-22. Sponsored by the Solar Energy Research Institute. Golden, CO.

19. Roberts, J. 1983. WESTVACO (Charleston Heights,SC). PRIVATE COMMUNICATION.

20. Diamond, T. 1983. COMPOSITION MATERIALS INC. (Stamford, CT) PRIVATE COMMUNICATION.

21. de Lasa, H. and G. Gau. 1973. "Influence des Agregats sur le Rendement d'un Réacteur a Transport Pneumatique". Chemical Engineering Science 23:1875.

22. Goheen, David, W. 1980. "High Temperature Electric Arc RF Energy and Combustion Gas Heated Pyrolysis of Powdered Biomass." Proceedings of the Specialists' Workshop on Fast Pyrolysis of Biomass. Copper Mountain, CO. October 19-22. Sponsored by the Solar Energy Research Institute. Golden, CO.

23. Graham, R.G., Bergougnou, M.A. and R.P. Overend. 1983. "Fast Pyrolysis of biomass." Report to the National Research Council of Canada. DSS Contract Number 05SU.32255-2-2647. Ottawa, Canada.

24. Antal, Michael Jerry. 1982. "A Review of the Vapor Phase Pyrolysis of Biomass Derived Volatile Matter." Proceedings of the International Conference on Fundamentals of Thermochemical Biomass Conversion. Estes Park, CO. October 18-22. Sponsored by the Solar Energy Research Institute. Golden, CO.

25. Graham, R.G., Bergougnou, M.A., Mok, L.K. and H.I. de Lasa. 1982. "Fast Pyrolysis (ULTRAPYROLYSIS) of Biomass Using Solid Heat Carriers." Proceedings of the International Conference on Fundamentals of Thermochemical Biomass Conversion. Estes Park, CO. October 18-22. Sponsored by the Solar Energy Research Institute. Golden, CO.

14.0 APPENDIX: Summary of Initial Cellulose Pyrolysis Experiments using Silica Sand as the THERMOFOR

During the initial stages of experimentation, particulate solids (i.e. silica sand) were used as the THERMOFOR to carry heat to the THERMOVORTACTOR. However, partial blocking of the preheater coils occurred and the solids were replaced by nitrogen carrier gas alone (to carry heat to the reacting biomass). This blocking was probably caused by fusion and deposition of THERMOFOR sand impurities or by the oxidation of the Inconel coil.

The initial experiments were conducted at 800 and 900°C, and are summarized in Table 24. Load cells had not yet been procured and therefore no attempt was made to close the mass balance. A comparison of the results which are reported in Table 24 (i.el the silica sand THERMOFOR experiments) with the results of the tests which did not use silica sand as the THERMOFOR (Tables 21 and 22), clearly indicated that there were no significant differences. This apparent lack of significance of the effect of THERMOFOR solids in the ULTRAPYROLYSIS process was probably due to the small size of the equipment. The relatively small THERMOVORTACTOR and reactor diameters permitted a high surface area to volume ratio, resulting in significant heat wall effects and a sufficiently rapid heat transfer rate to the biomass. Thus, the conditions required for fast pyrolysis were met even without the use of solids to carry and transfer heat. However, in large commercial-scale equipment where wall effects are diminished, the required heat transfer rates could not be achieved by a gaseous THERMOFOR alone, and the use of solids is therefore essential. A more complete discussion of these concepts is given in Section 9.0.

TABLE 24 Results of Initial celulose Experiments Using silica Sand as the THERMOFOR

RUN NO.	REACTOR TEMP. (°C)	RESIDENCE TIME (m/s)	PRODUCT GAS COMPOSITION*											
			H_2		C_2H_4		C_2H_6		C_2H_2		CO		CO_2		CH_4	
6†	700	700	17.5	(1.5)	4.5	(5.3)	1.0	(1.3)	0.4	(0.5)	64.6	(78.4)	3.7	(7.1)	8.3	(5.8)
7	900	600	18.6	(1.7)	6.3	(8.0)	0.4	(0.5)	1.0	(1.2)	58.1	(73.5)	3.0	(6.0)	12.7	(9.2)
8	800	230	21.1	(1.9)	6.0	(7.7)	0.6	(0.8)	1.1	(1.3)	59.1	(75.5)	3.1	(6.2)	8.9	(6.5)
9	900	200	22	(2.1)	6.5	(8.5)	0.4	(0.6)	1.2	(1.5)	56.8	(74.1)	2.7	(5.5)	10.4	(7.8)
10	900	200	21.8	(2.0)	6.4	(8.4)	0.5	(0.7)	1.2	(1.5)	56.9	(74.2)	2.7	(5.5)	10.4	(7.8)
11	900	170	22.3	(2.1)	6.5	(8.5)	0.5	(0.7)	1.6	(1.9)	56.6	(73.9)	2.7	(5.5)	9.8	(7.3)

* % by volume

(% by mass)

† trace amount of propane was detected

POOR

QUALITY

ORIGINAL